UNIVERSIDAD NACIONAL AUTÓNOMA DE MÉXICO

PROGRAMA DE POSGRADO EN ASTROFÍSICA

INSTITUTO DE ASTRONOMÍA

"ACTIVIDAD NUCLEAR EN GALAXIAS INDUCIDA POR INTERACCIÓN GRAVITACIONAL"

TESIS

QUE PARA OPTAR POR EL GRADO DE:

DOCTOR EN CIENCIAS (ASTRONOMÍA)

PRESENTA:

FRANCISCO JAVIER HERNÁNDEZ IBARRA

TUTORES:

DRA. DEBORAH DULTZIN KESSLER
INSTITUTO DE ASTRONOMÍA
DR. YAIR EMMANUEL KRONGOLD HERRERA
INSTITUTO DE ASTRONOMÍA

MÉXICO, D.F. AGOSTO DE 2013

Agradecimientos

Esta tesis, es el resultado de el trabajo y sacrificio de mi familia. Quiero agradecer inmensamente a mi esposa, Vicenta Janette Aldana Quezada su apoyo, trabajo y sacrificio incondicional durante todo este tiempo. Ha sido un largo camino desde la maestría el que hemos recorrido juntos. Yo me encargo Vice de que haya valido la pena para nosotros. También quiero agradecer a mis padres Francisco Hernández y Ofelia Ibarra, quienes siempre han estado apoyándome en todo y a quienes además de la vida les debo inconmensurable gratitud.

A mis tutores por supuesto Deborah Dultzin y Yair Krongold, quiero agradecer la guía y paciencia en estos años, que al final se tornaron un poco difíciles por todos aquellos problemitas de carácter administrativo/burocrático.

Por último pero no menos importante, quiero decir gracias a todos y cada uno de mis compañeros del IA con quienes he convivido todo este tiempo, nunca antes compañeros había hecho tantos amigos "con todo el sentido de la palabra" hasta que llegue a este instituto.

Para Vicenta, Victoria y Valentina.

Quienes han sacrificado esposo y padre, para ver realizado este trabajo.

Índice General

Índice de Figuras

Índice de Tablas

Resumen

En este trabajo de tesis, se analizaron alrededor de 900 espectros de galaxias cercanas (0.01 < z < 0.05). Estos espectros se obtuvieron del catastro del Sloan Digital Sky Survey (SDSS) en su versión Data Release 7 (DR7) (Abazajian et al. 2009). Los espectros se obtuvieron a partir de observar con fibras ópticas que permiten obtener la información de la parte interior de las galaxias. Estas fibras abarcan 3 segundos de arco en el cielo, por lo que permite analizar Ã¡reas en el núcleo de las galaxias que van desde 1 y hasta 2 Kpc en diámetro de acuerdo a la distancia de nuestros objetos.

Con el objetivo de estudiar la incidencia de la actividad AGN en galaxias debido a interacciones gravitacionales y analizar como afecta el ambiente circungaláctico a este fenómeno, se escogieron tres muestras de galaxias. Dos de estas muestras corresponden a galaxias aisladas y una a galaxias en pares aislados.

El primer catálogo de galaxias aisladas de Karachentseva (1973) contiene 1051 galaxias de las cuales hemos recopilado y analizado los espectros de 413 objetos. En esta muestra las galaxias son consideradas aisladas cuando no tienen una galaxia vecina de tamaño similar (diámetro $> \frac{1}{4}$ de la galaxia a considerar aislada) dentro de un radio de 20 veces el diámetro de la galaxia. El criterio de aislamiento para estas galaxias garantiza que no han experimentado una fusión de masas similares los últimos 3 Gaños. El segundo catálogo de galaxias aisladas. Es la muestra de galaxias de disco de Varela (2004) que contiene originalmente 203 objetos, 100 de ellos hemos analizado en este trabajo. El criterio para denotar galaxias aisladas esta basado en un cociente logarítmico f, entre fuerzas de marea internas y externas que experimentan las galaxias. Las galaxias con f $\leq$ -4.5 son consideradas como aisladas ya que no presentan signos de alguna perturbación. Se estima que las galaxias en esta muestra no han sido perturbadas al menos en los últimos 2 Gaños. El catálogo de pares de galaxias de Karachentsev se define con velocidades de recesión menores que 1200 Km/s entre sus componentes, así como con separaciones menores que 100 Kpc entre los pares. Hemos separado estos pares en tempranos (E+E) considerando elípticas y esferoidales, en mixtos elíptica + espiral (E+S) y en espirales (S+S) para estudiarlas por tipo morfológico.

El estudio realizado en esta tesis fue hecho de manera homogénea y auto consistente; esto quiere decir que el procedimiento para sustraer el espectro estelar de la galaxia anfitriona y medir sus líneas en emisión fue el mismo para los espectros de galaxias en las tres diferentes muestras. Esto, con la finalidad de evitar sesgos en la forma de escoger las muestras, ya que resultados anteriores en la literatura condujeron a conclusiones contradictorias (p.ej. Stauffer 1982a,b y Koulouridis et al. 2006a,b).

Para sustraer la parte del espectro que pertenece a la contribución estelar de la galaxia anfitriona, se utilizó un programa llamado Principal Component Analysis (PCA, por sus siglas en inglés) siguiendo el método de Hao et al. (2005). Esta técnica utiliza una combinación lineal de 8 espectros de galaxias con solo líneas de absorción, un espectro típico de estrellas tipo A para tomar en cuenta la emisión de la población estelar joven y una ley de potencia para ajustar la posible existencia de algún componente no-térmico de la forma $f(\lambda) \propto \lambda^{-1.5}$. Una vez ajustado el espectro de la galaxia anfitriona, éste es restado del espectro original y se obtiene un espectro con puras líneas en emisión donde los componentes en absorción y el continuo estelar han sido removidos.

Después de medir el flujo de las líneas en emisión, usamos diagramas de diagnóstico (Baldwin et al., 1981; Veilleux & Osterbrock, 1987) para separar la actividad AGN de posibles galaxias Starburst o simplemente galaxias con núcleos cuyos cocientes en intensidades de líneas se asemejan a regiones H II. También, mediante los diagramas de diagnóstico pudimos diferenciar entre la actividad nuclear Seyfert y LINER (del inglés Low Ionization Nuclear Emission Region).

Nuestros resultados muestran para las galaxias aisladas de Karachentseva y Varela, la actividad AGN presenta una incidencia del $43\% \pm 5\%$ y $31\% \pm 11\%$ respectivamente. Nuestros resultados también muestran que la incidencia de la actividad AGN decrece gradualmente hacia tipos morfológicos tardíos pasando de un $70\% \pm 15\%$ de incidencia AGN en galaxias elípticas hasta un $10\% \pm 16\%$ en galaxias tipo Magallanes Sm. Confirmamos que existe una correlación muy fuerte entre la morfología de tipo temprano y la incidencia de AGN. Donde la mayoría de los objetos son de tipo LINER.

Observamos también que esta correlación se aplana si se consideran objetos que no tienen líneas en emisión y que necesariamente deben de contabilizarse como galaxias que no tienen AGN. El hecho anterior no ha sido considerado ya que otros autores (Varela et al. (2004); Coziol et al. (2011); Sabater et al. (2012)) no tuvieron el suficiente número de objetos de tipo temprano para considerar tal efecto. Este aplanamiento se manifiesta dado que alrededor de la mitad de las galaxias de tipo temprano no presenta líneas en emisión.

Un resultado muy importante es que la actividad nuclear de tipo 1 (AGN con líneas an-

chas) esta casi completamente ausente en las dos muestra de galaxias aisladas. Incluso las pocas galaxias que presentan líneas anchas, ($< 3\,\% \pm 2\,\%$ de las muestras) pueden clasificarse como intermedias de tipo 1.5-1.9. Lo anterior dista mucho de poder explicarse con un modelo unificado ya que se esperaría que en una muestra de AGN habría alrededor de la mitad de galaxias con líneas anchas. Incluso si se argumenta que el toro de polvo es grumoso y/o combado, el hecho de no encontrar una galaxia AGN de tipo 1 entre 175 galaxias probablemente sea indicativo que el medio aislado en donde se encuentran sea un factor a considerar.

En este trabajo encontramos una gran fracción de galaxias tipo AGN en las muestras aisladas ($43\,\% \pm 5\,\%$ y $31\,\% \pm 11\,\%$). Dado que la inmensa mayoría de nuestras galaxias son representativas de los AGN de baja luminosidad, la tasa a la cual el hoyo negro acreta masa sería del orden de entre 10^{-5}-10^{-3} $M_{\odot}$/año (Ho 2003). De lo anterior, es probable que los procesos de evolución secular como fusiones menores o perturbaciones gravitacionales de un potencial asimétrico en las galaxias podrían ser los causantes de la actividad AGN de baja luminosidad. Si las AGN en ambientes aislados presentan bajas tasas de acreción, bajas luminosidades y la ausencia casi completa de líneas anchas en sus espectros, es probable que la región de líneas anchas no sea capaz de formarse en estas circunstancias (Nicastro 2000;Elitzur & Ho 2009).

Para la muestra de galaxias en pares, se analizaron 385 espectros. La incidencia de la actividad nuclear es de un $41\,\% \pm 6\,\%$ muy comparable con la muestra de galaxias aisladas con números de objetos similares en cada tipo morfológico. Los tipos tempranos de galaxias muestran de nuevo esta tendencia de presentar mayor incidencia de AGN en galaxias elípticas y esferoidales ($\sim 74\,\% \pm 4\,\%$) mostrando una posible correlación que puede tener la actividad nuclear con la morfología galáctica.

Al comparar la incidencia de actividad AGN por tipo morfológico, solo las galaxias con de tipo Sb tienen mayor incidencia en la muestra de galaxias en pares mixtos ($62\,\% \pm 9\,\%$) comparada con la muestra de aisladas de Karachentseva ($45\,\% \pm 1\,\%$) que podría ser estadísticamente significativa. Esto puede ser debido a la interacción o perturbación a la cual puede estar sujeta una galaxia espiral por una elíptica. Las galaxias AGN de tipo 1 de nuevo están casi ausentes y parece no poder ser explicado por un modelo AGN unificado.

Con todo esto, la evolución secular de las galaxias parece ser suficiente para detonar el fenómeno del AGN aunque se presente de baja luminosidad. El hecho de que el medio de estas muestras no influya en la incidencia de actividad sino más bien la morfología así lo sugiere. Otros trabajos han encontrado relación entre pares de galaxias y una intensa formación estelar (Rogers et al. 2009), incluso entre pares y actividad nuclear (Ellison et al. 2010,2011), pero

estos pares tienden a estar muy cercanos entre si (< 30 Kpc) y simulaciones númericas han mostrado que la incidencia de la actividad nuclear y/o Starburst se incrementa en diferentes episodios de choque entre galaxias. Mientras no haya un choque directo entre galaxias, la evolución secular puede mantener la actividad AGN considerando la morfología de la galaxia.

Introducción General

En la astronomía contemporánea se ha estudiado mucho el fenómeno de núcleo activo de galaxia o AGN. Uno de los principales retos es llegar a comprender como y por que procesos se alimenta el hoyo negro supermasivo. A lo largo de muchos años estos estudios se han enfocado en investigar el medio ambiente de los AGN basados en muestras conocidas de AGN vs no-AGN. Los sesgos introducidos por efectos de selección en las muestras habían producido resultados contradictorios.

En esta tesis, abordamos el estudio de la incidencia de la actividad nuclear en una manera complementaria; es decir, primero definimos las muestras de galaxias a comparar y luego estudiamos la actividad nuclear en ellas. El propósito es comparar muestras que contengan galaxias de todos los tipos morfológicos con criterios de selección equivalentes, tanto en la muestra de galaxias aisladas como en la de pares aislados. Esto, con el fin de llevar a cabo un estudio auto consistente y estadísticamente significativo sobre el rol que tienen las interacciones gravitacionales y la morfología en el proceso de AGN.

Por primera vez en este trabajo, tenemos suficientes objetos en todos los tipos morfológicos para hacer un estudio estadístico de la actividad nuclear y comparar entre muestras. Encontramos que la incidencia en la actividad nuclear es más alta en tipos morfológicos tempranos y desciende conforme consideramos tipos morfológicos tardíos. Aunque sin cuantificar esta tendencia ya se conocía; Sin embargo, vemos por primera vez que si incluimos en las muestras las galaxias sin líneas de emisión esta relación entre la incidencia AGN y el tipo morfológico se puede aplanar para galaxias elípticas, esferoidales y espirales tempranas.

También, hemos encontrado que los AGN de tipo 1 o de líneas en emisión anchas permitidas están casi por completo ausentes en las muestras. Este es un dato significativo que no favorece al modelo unificado (incluso si se considera un toroide de gas grumoso o distorsionado) dado que las de tipo 1 apenas si representan un $3\% \pm 2\%$. En este $\sim 3\%$ consideramos galaxias con una componente ancha en las líneas y la componente más prominente corresponde a una galaxia Seyfert 1.5.

En este trabajo hemos señalado que bajo condiciones de una tasa de acreción baja resulta factible pensar que el AGN presenta baja luminosidad y que la región de líneas anchas no logra formarse. Estas pueden ser las condiciones prevalecientes en las galaxias aisladas dado que nosotros hemos encontrado estas características en ellas.

En el primer capítulo presento una introducción básica a los núcleos activos de galaxias, donde el enfoque reside en describir la estructura de los mismos, sobre todo para dos tipos particulares de AGN: Las galaxias tipo Seyfert y LINER. En la sección 1.7 se describe brevemente el modelo unificado para las galaxias con núcleo activo, modelo que será revisado a la

par de nuestros resultados.

Dado que el estudio de esta tesis esta enfocado en los núcleos activos y su medio ambiente, el segundo capítulo esta dedicado a describir en resumen los posibles detonantes tanto internos como externos de la actividad nuclear. Uno de los objetivos de este trabajo radica en poder discernir que procesos (externos y/o internos) son más importantes para la activación del núcleo activo de galaxia.

El capítulo tercero es el primer resultado de este trabajo. Encontrar la incidencia de la actividad nuclear en galaxias aisladas resulta determinante para tener una muestra de control donde por lo menos se asegure que la galaxia no ha tenido ningún tipo de interacción/fusión en un tiempo considerable. De esta manera los resultados en la incidencia de AGN tenderían a ser explicados en forma natural por una evolución secular en la galaxia misma.

Al tener resultados de una muestra de control en la actividad nuclear de galaxias aisladas, resulta natural comparar esta muestra con cualquier otra donde las galaxias estén en ambientes más densos. Esto lo hacemos en el cuarto capítulo, en el que comparamos la incidencia de la actividad AGN en una muestra de galaxias en pares aisladas cercanas y de masas similares. Hemos analizado pares de tres tipos: tempranos (E+E), mixtos (E+S) y espirales (S+S). Es importante mencionar que esta comparación es auto consistente y homogénea puesto que los métodos de selección y reducción de datos han sido los mismos para las muestras.

En el capítulo quinto se presenta un trabajo sobre cuásares y líneas de absorción anchas. Trabajo que surge de analizar espectros de tipo cuásar obtenidos con una diferencia de alrededor de 26 años. El capítulo sexto se presentan las conclusiones generales de este trabajo.

Capítulo 1

Introducción a los Núcleos Activos de Galaxias

En el Universo, los denominados Núcleos Activos de Galaxias (NAGs o más comúnmente AGN por sus siglas en ingles Active Galactic Nuclei) tienen luminosidades bolométricas en sus galaxias anfitrionas de hasta diez mil veces mayores que las galaxias que no poseen núcleo activo. La fuente de energía es una de las más poderosas junto con los estallidos de rayos gamma (GRB's del ingles Gamma Ray Bursts) que se observan actualmente en la astronomía moderna.

La explicación de la fuente de energía en núcleos activos de galaxias radica en el paradigma de que un hoyo negro supermasivo (SMBH del ingles Super Massive Black Hole) en el centro de estas galaxias esta acretando materia y parte de ella se esta convirtiendo en la radiación observada. La emisión de estos objetos se explica mediante procesos no térmicos, ya que los procesos térmicos no son capaces de reproducir la radiación y/o luminosidades observadas en todo el espectro electromagnético.

El estudio de los procesos físicos que se presentan en los AGN, ha tenido sobre todo en los últimos años un gran progreso en la carrera por descubrir, analizar y modelar los diferentes componentes de los núcleos activos. Aunque aún se dista de tener un modelo auto consistente y satisfactorio que nos explique todas las facetas de la actividad AGN. El mero proceso de alimentar el hoyo negro supermasivo de las galaxias y la relación que juega el AGN con su galaxia anfitriona esta lejos todavía de ser entendido completamente.

1.1.　El paradigma Hoyo Negro.

La pregunta fundamental acerca de los AGN es: ¿Cómo es generada la energía que se detecta?. En esencia, el problema radica en explicar que procesos producen las luminosidades detectadas en los AGN ($L_{bol} \sim 10^{42-47}$ erg s^{-1}) en una región significativamente pequeña tanto como un parsec cúbico. El paradigma actual consiste en una fuente central que contiene un disco de acreción extremadamente caliente alrededor de una hoyo negro supermasivo. La energía es generada por material que cae en el disco luego en el hoyo negro mediante procesos que pueden convertir la materia en energía.

Las propiedades básicas de los hoyos negros se pueden expresar usando su radio gravitacional (r_g) y el radio de Schwarzschild (r_s) donde:

$$r_g = \frac{GM}{C^2}, r_s = 2r_g. \tag{1.1}$$

También, se puede definir el momento angular s de un hoyo negro

$$s \sim I\Omega \simeq Mr_g{}^2\frac{v}{r} \simeq Mr_gc, \tag{1.2}$$

donde Ω es la velocidad angular y el momento angular específico (por unidad de masa),

$$s/M \equiv r_gc \sim 5x10^{23}M_8cm^2s^{-1}, \tag{1.3}$$

donde M_8 esta dada en unidades de 10^8 $M_\odot$. Considerando un hoyo negro supermasivo en un núcleo de galaxia, s/M a una escala galáctica (r=1 kpc, v=300 km s^{-1}) es varios ordenes de magnitud mayor que r_gc determinado en trabajos como Shakura & Sunyaev (127). De esta manera, para hoyos negros que crezcan sustancialmente en tiempos de escala de evolución galáctica, debe existir un mecanismo eficiente para deshacerse del exceso de momento angular del gas acretado y llevarlo hacia el centro.

Las partículas de gas muy cercanas al centro ($r_g \sim 1000$) están sujetas a diferentes tipos de fuerzas, un balance típicamente entre las fuerzas de gravedad y radiación nos permite hacer un análisis más detallado de los procesos internos en el hoyo negro antes de que el material caiga dentro del horizonte de eventos y la información se pierda.

1.1.1. La Luminosidad de Eddington

Suponga una fuente central de masa M que emite luz monocromática L_ν. La presión de radiación que actúa sobre las partículas de gas desde una distancia r estaría dada por:

$$f_{rad} = \frac{N_e \sigma_T}{4\pi r^2 c} \int_0^\infty L_\nu d\nu = \frac{N_e \sigma_T}{4\pi r^2 c} L \tag{1.4}$$

donde L es la luminosidad total integrada, N_e es la densidad electrónica y σ_T la sección eficaz de Thompson. La fuerza de gravedad esta dada por:

$$f_g = \frac{GM\mu m_p N_e}{r^2} \tag{1.5}$$

donde ahora μ peso molecular promedio (~ 1.17 para un gas solar completamente ionizado). Para una acreción de tipo esférica de este gas $f_g \leq f_{rad}$. Pero al igualar las fuerzas $f_g = f_{rad}$ obtenemos la luminosidad de Eddington,

$$L_{Edd} = \frac{4\pi cGM\mu m_p}{\sigma_T} \simeq 1.5 \times 10^{38}(M/M_\odot) ergs^{-1}, \tag{1.6}$$

la cual representa la máxima luminosidad permitida de una fuente de masa M la cual es abastecida por acreción esférica. Aunque esquemas más realistas pueden considerar gas parcialmente neutro y por ende mayor opacidad. De esta manera la L_{Edd} puede ser menor que el valor presentado en la ecuación 1.6.

La ecuación 1.6 también es conocida como el limite de Eddington, y puede ser usada para establecer una masa mínima M_E para una luminosidad en particular. En unidades apropiadas para un AGN, se puede escribir como:

$$M_E = 8 \times 10^5 L_{44} M_\odot, \tag{1.7}$$

de donde L_{44} es la luminosidad de la fuente central en unidades de $10^{44} ergs^{-1}$, la cual es

característica de un galaxia tipo Seyfert proporcionando una masa mínima de Eddington de $\sim 10^6 M_\odot$ y para un cuásar típico de $L \approx 10^{46} ergs^{-1}$ de $\sim 10^8 M_\odot$.

De la definición de tasa de acreción $\dot{M} = L/\eta c^2$, donde η es la eficiencia de convertir la energía potencial gravitacional en radiación electromagnética, en ello se pueden definir como la tasa de acreción de Eddington $\dot{M}_{Edd}$ requerida para producir un L_{Edd}.

$$\dot{M}_{Edd} = \frac{L_{Edd}}{\eta c^2} \simeq 3M_8 \left[\frac{\eta}{0.1}\right]^{-1} M_\odot a\tilde{n}o^{-1}, \tag{1.8}$$

y un tiempo de Eddington t_{Edd} como el tiempo típico asociado a esta tasa de acreción y esta dado por

$$t_{Edd} = \frac{M}{\dot{M}} \simeq 4 \times 10^8 \eta a\tilde{n}o. \tag{1.9}$$

de esta manera se puede expresar la tasa de acreción relativa (tasa de acreción por unidad de masa de hoyo negro) de la siguiente manera:

$$\frac{L}{L_{Edd}} \propto \frac{\dot{M}}{\dot{M}_{Edd}} \propto \frac{\dot{M}}{M}. \tag{1.10}$$

ver (111).

1.2. Clasificación de los AGN.

La clasificación de los núcleos activos de galaxias se ha caracterizado de acuerdo a los resultados observacionales en las diferentes bandas del espectro electromagnético. Rasgos como las líneas en los espectros, relativos excesos de emisión en radio, rayos-X, Ultravioleta, Infrarrojo, y variabilidad en su fuente de emisión, han llevado a considerar todo una gama de objetos como AGN. Hoy en día, la astronomía considera como núcleos activos de galaxias a los cuasares, blazares que se dividen en objetos tipo BL Lacertae y OVV (del inglés Optical Violent Variables), radio galaxias, galaxias IRAS (del InfraRed Astronomical satellite), galaxias Seyfert y muy probablemente los LINERs.

Diferencias entre tipos de galaxias activas y galaxias normales										
Tipo de Galaxia	Núcleo Activo	Líneas en Emisión		Rayos-X	Exceso de		Emisión en Radio	Jets	Variabilidad	Radio Fuerte
		Angostas	Anchas		UV	Lejano-IR				
Normal	No	Débil	No	Débil	Ninguna	Ninguna	Ninguna	Ninguna	No	No
Starburst	No	Si	No	Algunos	No	Si	Algunos	No	No	No
LINERs	?	Si	Si	Algunos	Algunos	Algunos	No	No	Si	No
Seyfert 1	Si	Si	Si	Algunas	Algunas	Si	No	No	Si	No
Seyfert 2	Si	Si	No	Algunas	Algunas	Si	No	Si	Si	No
Quasar	Si	Si	Si	Algunos	Si	Si	Algunos	Algunos	Si	10%
Blazar	Si	No	Algunos	Si	Si	No	Si	Si	Si	Si
BL Lac	Si	No	Débiles	Si	Si	No	Si	Si	Si	Si
OVV	Si	No	Más intensas que BL Lac	Si	Si	No	Si	Si	Si	Si
Radio galaxia	Si	Algunas	Algunas	Algunas	Algunas	Si	Si	Si	Si	Si

Tabla 1.1: *Características espectrales de los AGN.*

Los AGN comparten una fenomenología en común. Propiedades básicas como una mayor luminosidad bolométrica comparada con galaxias "normales", núcleos muy brillantes que no se pueden resolver espacialmente, radiación sincrotrón y además, líneas anchas en emisión permitidas con anchos a potencia media (o FWHM de Full Width High Maximun) de miles de kms^{-1}, y/o líneas angostas permitidas y prohibidas con cientos de kms^{-1} en sus FWHM.

1.3.   Estructura de los AGN.

Aunque el área del núcleo activo en las galaxias se concentra en una región central muy pequeña, los procesos del núcleo activo pueden cubrir un intervalo de radio bastante grande como para tener repercusión en la galaxia entera. En los AGN se observan líneas en emisión de alta ionización que suelen ser producidas por fotoionización o ionización colisonal mediante choques. Esto sugiere que la fuente de energía de los núcleos activos viene de un proceso no térmico que se presenta como un continuo ionizante que en la radiación ultravioleta sigue una ley de potencias de la forma $f_\nu = C\nu^{-n}$, donde n es el índice espectral con un valor de ~ 1.2.

A continuación presentamos algunas estructuras y propiedades de los AGN.

1.3.1.   La Región de Líneas Anchas (BLR).

La región de líneas anchas llamada BLR (Broad Line Region) por sus siglas en inglés. Se considera una zona con apenas alrededor de entre 0.01-1 pc ($L/4\pi r^2 \sim 10^9$ ergs^{-1} cm^{-2}) de radio desde el mismo centro del hoyo negro. Sus densidades columnares se estiman en $\sim 10^{22-24}$ cm^{-2} y densidades de gas en nubes de entre 10^9-10^{11} cm^{-3}. Los tiempos dinámicos en estas nubes se estiman de algunos centenares de años y tienen factores de cobertura de apenas el 10 %. Se cree que las nubes se encuentran ligadas y que la gravedad domina completamente sobre la fuerza que ejerce la presión de radiación. Las nubes pueden alcanzar velocidades que pueden ir desde 1000 hasta 15000 kms^{-1} según sea el caso del AGN. La velocidad y dirección del gas virializado tiene como resultado un ensanchamiento Doppler con las velocidades mencionadas anteriormente, produciéndose así en esta región líneas anchas.

Las condiciones físicas en esta región son tales que el hidrógeno se encuentra en una proporción de 10^{-2}. Con las altas densidades columnares en esta zona, se puede inferir que solo la superficie iluminada en las nubes esta altamente ionizada y su interior neutro. Aún con lo anterior, la densidad no suele ser demasiado alta para suprimir líneas semi-prohibidas como C III] $\lambda 1909$ y O III] $\lambda 1663$. Como se ha dicho, una gran parte de estas nubes debe ser neutra ya que solo la emisión de rayos-X parece penetrar en esta región. Estas partes producen fuertes líneas de H I, Mg II y Fe II. En esta parte del AGN, la densidad electrónica mínima es de alrededor de 10^8 cm^{-3} y al observarse líneas de Fe II sugiere que una temperatura inferior a 3500 K ya que para temperaturas mayores deberíamos ver Fe III ionizado colisionalmente.

1.3.2.   La Región de Líneas Angostas (NLR).

La siguiente zona que consideramos se encuentra situada entre 100 y 1Kpc del centro ($L/4\pi r^2 \sim 10^2$ ergs^{-1} cm^{-2}). Sus densidades columnares se estiman en $\sim 10^{20-21}$ cm^{-2}, con nubes de baja densidad ($\sim 10^4$ cm^{-3}) y temperaturas de $\sim 10^4$K. También se cree que el factor de cobertura es menor que en la BLR. Las condiciones físicas en este lugar son considerablemente diferentes que aquellas que se presentan la BLR a pesar de que el nivel de ionización sea muy similar. Aquí, debido a la baja densidad que presentan sus nubes, la presión de radiación y los perfiles de línea pueden incluir objetos no ligados gravitacionalmente.

En la NLR son emitidas líneas angostas prohibidas y permitidas (velocidades de cientos de kms^{-1}) por la baja densidad. Los cocientes de líneas para iones distintos suelen proporcionar distintas temperaturas y densidades para esta región, por lo cual se infiere un NLR estratificado.

1.3.3.   El Toroide de Polvo.

El toro de polvo se encuentra en una región según estimaciones de entre 1 y 100 pc de radio a partir del centro de la galaxia anfitriona, localizado alrededor del hoyo negro en forma de toroide tiene densidades del orden de 10^{4-6} cm^{-3} y densidades columnares extremadamente grandes, 10^{45} cm^{-2} e incluso mayores (ver Figura 1.1).

Dado que esta estructura toroidal es muy grande en radio se espera contenga diversas zonas estratificadas con diferentes condiciones físicas. Lejos del centro del AGN, a 10 o incluso 100 pc, el gas es ópticamente grueso con muy bajas temperaturas. Solo los rayos-X duros pueden penetrar esas regiones. Tales regiones tienen cantidades exorbitantes de polvo que se ven reflejadas en espectros con emisión en el infrarrojo y líneas en absorción debidas a diferentes tipos de polvo como algunos silicatos e hidrocarburos aromáticos policíclicos.

1.3.4.   Regiones de Brotes Violentos de Formación Estelar.

Las regiones de brotes violentos de formación estelar son conocidas en la literatura como "Starburst". Estas regiones son consideradas normalmente como un componente diferente en los AGN. Radios típicos de estas regiones pueden alcanzar varios Kpc y densidades de 10^{0-3} cm^{-3}. En estas zonas de las galaxias, las estrellas pueden desarrollar vientos largamente extendidos o envolventes como resultado de la interacción de sus atmósferas con el campo
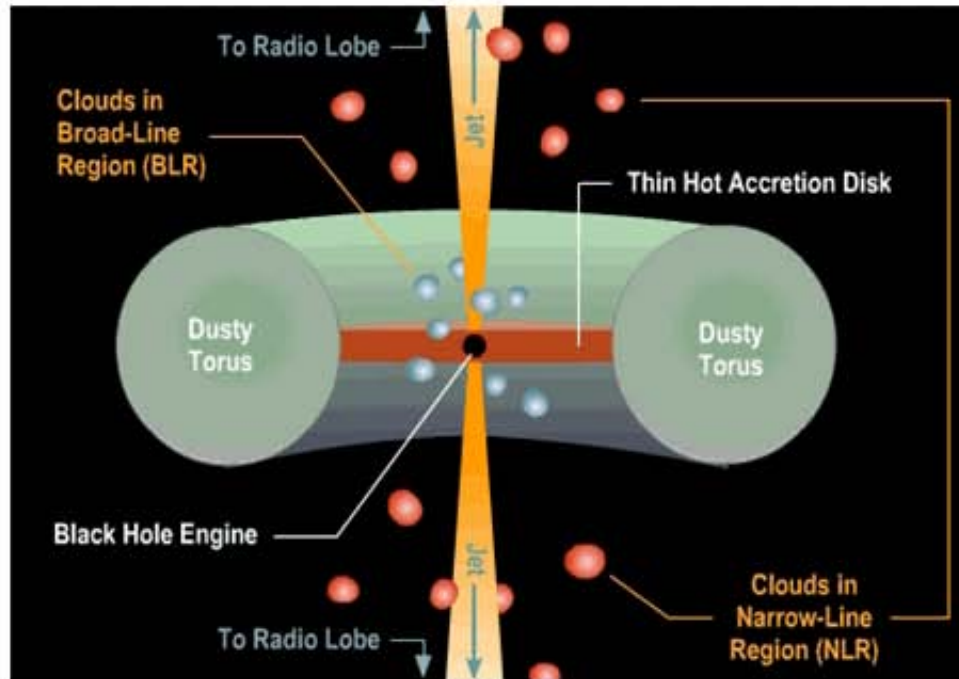
Figura 1.1: *Estructura del AGN. Tomada de www.astro.ufl.edu.*

de radiación externo. Estas estrellas son denominadas "bloated" (hinchadas o expandidas) y muestran espectros típicos de BLR y NLR según el radio al cual se observe la zona. Por otra parte, tales vientos suelen tener grandes gradientes en densidad que, lo suficientemente lejos de las estrellas puede observarse gas altamente ionizado. De esta manera, la presencia de estas estrellas pueden cerrar la brecha entre varios componentes observados en los AGN con diferentes densidades (2; 3).

Los rasgos típicos espectrales de rayos-X en regiones de Starburst muestran líneas en emisión excitadas colisionalmente. En la Figura 1.2 se muestra el espectro en rayos-X de la galaxia Starburst M82.

Una zona de starburst lo suficientemente cercana a la fuente central puede tener un parámetro de ionización tan alto que puede cambiar el balance de ionización y presentar espectros que pueden diferir de los que se presentan en regiones más lejanas del campo de radiación.
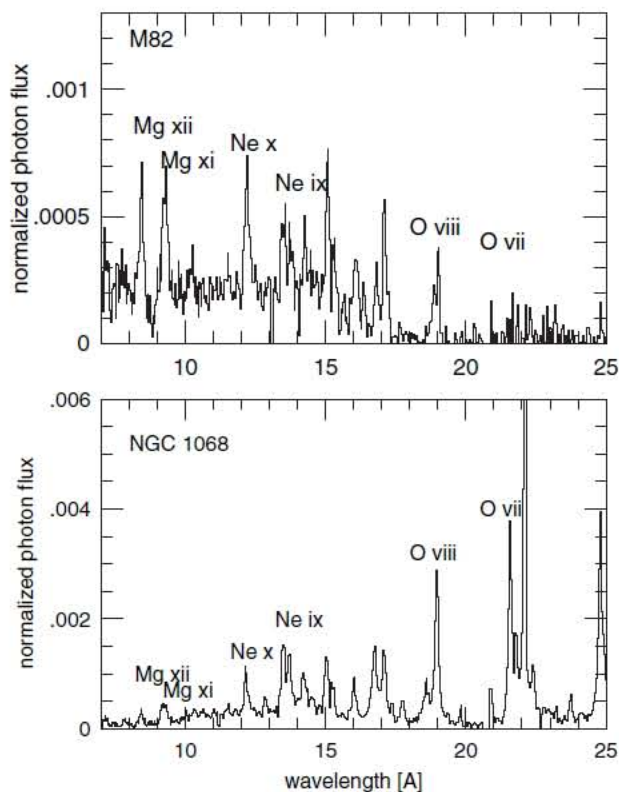
Figura 1.2: *Comparación entre los espectros en rayos-X para una típica galaxia Starburst M82 y un galaxia AGN de tipo II (NGC1068) con nebulosidad extendida de rayos-X. Imágenes de archivo XMM-Newton.*

1.3.5. El Disco de Acreción.

El disco de acreción central es un objeto de alta densidad y gran densidad columnar en el gas entre 10-1000 r_s el cual puede estar expuesto a la fuente del continuo ionizante. Uno de los posibles escenarios involucra tres regiones como se muestran en la Figura 1.3. Dentro de los primeros 1000 r_s desde el centro, la presión de radiación es mayor que la del gas, resultando en un disco grueso y caliente. Lo anterior podría explicar el origen de la llamada gran joroba azul vista así en los espectros ópticos. Hacia 10^5 r_s ($\sim$1pc), es un disco delgado soportado por presión de radiación que se hace más grueso conforme aumenta el radio. La superficie cóncava del disco exterior puede ser irradiada tanto por la fuente central como por la porción de disco interno resultando en flujos de material hacia al exterior de los discos. Finalmente más allá de 10^5 r_s el disco exterior puede romperse en numerosas nubes debido al colapso gravitacional.

En estas condiciones, el espectro del continuo puede mostrar líneas de emisión y/o absorción dependiendo de la geometría y la línea de visión. El disco mismo es considerado como la fuente emisora de la parte óptica y ultravioleta pero debemos considerar que solo recibe una proporción de la radiación principal. Algunos modelos consideran la posibilidad de que la emisión de rayos-X viene de una corona que se encuentra envolviendo el disco de acreción. Luego, al fotoionizar este medio con radiación UV puede llevar a los fotones a alcanzar energías tan altas como para emitir en estas longitudes de onda mediante el proceso de efecto Compton inverso (46).
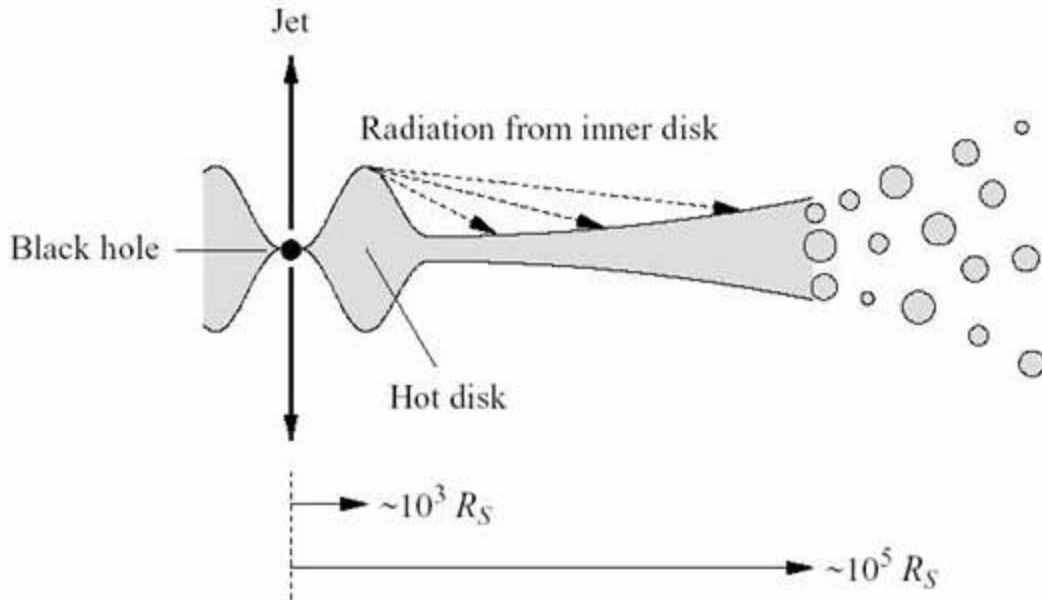
Figura 1.3: *Estructura del disco de acreción (Carroll & Ostlie 1996, Modern Astrophysics.)*

Dado que la geometría entre disco y fuente principal es desconocida, y que, además, la viscosidad del disco depende de un parámetro α muy incierto, el rango de parámetros que pueden aceptarse es grande. De aquí que se pueden visualizar dos escenarios:

1.- Para un estado en el cual se tienen parámetros que denotan baja ionización. Las rasgos espectrales principales serán de líneas de elementos neutros con un fuerte continuo en rayos-X. Las líneas más fuertes serán debidas a FeI-XVII, alrededor de 6.4 Kev, por que la combinación de abundancia y fluorescencia es producida por tales iones.

2.- Por otro lado. Si se tiene parámetros de alta ionización, la parte interior del disco

estará ionizada y será fuente de alta excitación y ionización para líneas de rayos-X. Se predice que las líneas más probables en esta región serán aquellas de transiciones resonantes. Además, tales líneas se espera que estén ensanchadas por el campo gravitacional y por la velocidad rotacional del gas, dado que están lo suficientemente cerca del hoyo negro supermasivo.

1.4. Galaxias Seyfert.

Las galaxias Seyfert (nombradas así por el astrónomo que las descubrió Carl K. Seyfert en 1943), son galaxias en su mayoría espirales que presentan un núcleo tan brillante en apariencia puntual que da origen a líneas espectrales en emisión de gas altamente ionizado. Estas galaxias suelen ser los objetos más cercanos y por ende los mejor estudiados con un núcleo activo o AGN como lo hemos venido llamando.

Las galaxias Seyfert se caracterizan básicamente por el ancho e intensidad de sus líneas en emisión. Por ejemplo, las galaxias denominadas Seyfert de tipo 1, contienen es su espectro óptico líneas en emisión que incluyen tanto líneas permitidas como prohibidas. Las líneas permitidas son anchas con velocidades de varios miles de kms^{-1} en su FWHM. Entre las líneas que se observan están HI, HeI, HeII y FeII. Las líneas prohibidas son angostas con anchos característicos en su FWHM de apenas algunos cientos de kms^{-1}. Aquí se encuentran entre las líneas más intensas [O III], [N II], [S II], [O II] y [O I] por mencionar algunas (ver Figura 1.4).
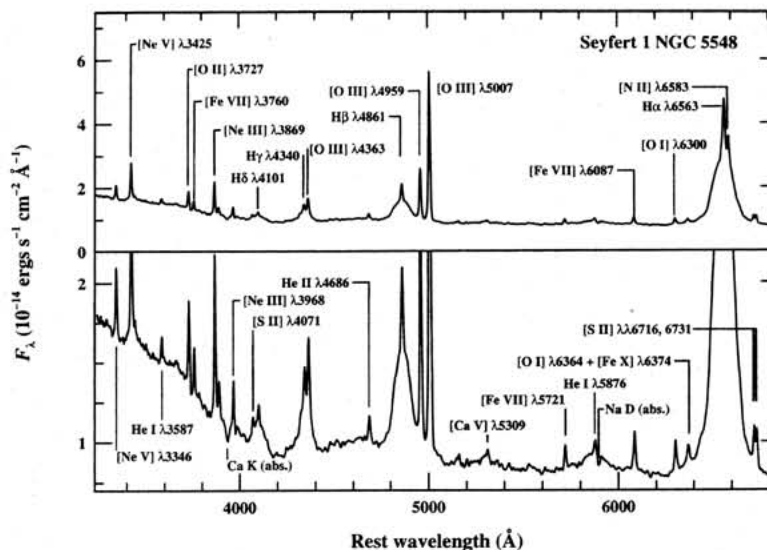
Figura 1.4: *El espectro óptico de la galaxia Seyfert 1 NGC1275. Cortesia de A. V. Filippenko.*

Para las galaxias nombradas como Seyfert tipo 2, ambos conjuntos de líneas (permitidas y prohibidas) tienen anchos angostos de algunos cientos de kms^{-1} en su FWHM (ver Figure 1.5).
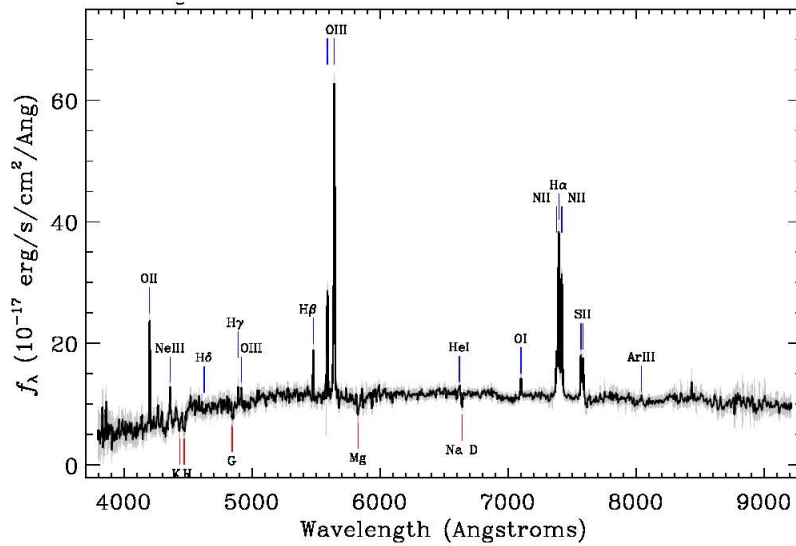
Figura 1.5: *El espectro óptico típico de una galaxia Seyfert 2. Imagen tomada del SDSS.*

En general existen propiedades entre estos dos tipos de galaxias que son un poco diferentes como por ejemplo la luminosidad en el óptico que tiende a ser más intensa en los objetos de tipo 1. También existen estudios de en otras longitudes de onda donde las galaxias de tipo 1 presentan emisión de rayos-X duros mientras las de tipo 2 no (Elvis et al. 1978). Ambos tipos presentan exceso de emisión en el infrarrojo (1-10μm) aunque las de tipo 2 presentan una distribución espectral de energía (SED del ingles Spectral Energy Distribution) más baja en la zona de 0.1-1μm. Lo cual, se interpreta como la absorción por parte de el toro de polvo en esas longitudes de onda.

1.5. La Secuencia de Lick.

Las diferencias encontradas entre las galaxias de tipo 1 y tipo 2 clasificadas así por los anchos de sus líneas en emisión, pronto no fue suficiente. Algunas galaxias mostraban componentes anchas menos intensas o muy débiles y muchas de las veces solo algunas líneas permitidas mostraban ensanchamiento. Entonces fue necesario hacer una clasificación mas
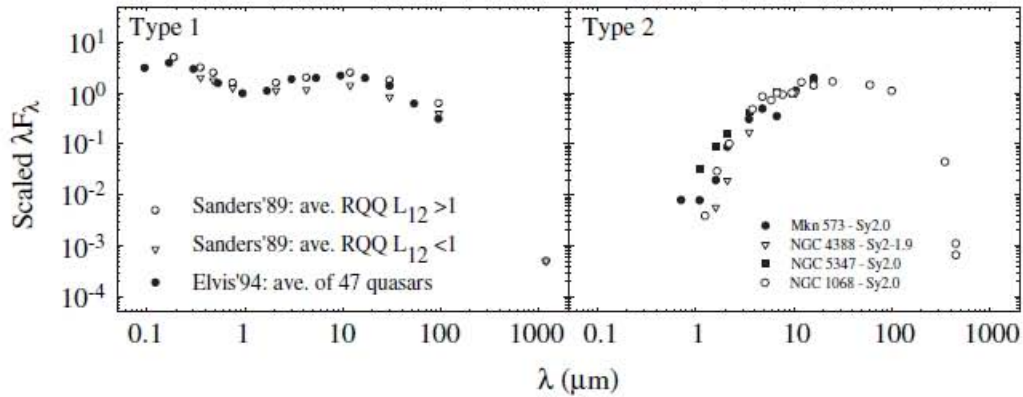
Figura 1.6: *Compilación de SED para AGN de tipo 1 y 2 respectivamente (Alonso-Herrero et al. 2003).*

fina a manera de poder incluir estas nuevas galaxias con propiedades distintas. La secuencia de Lick (nombrada así por haber sido propuesto por astrónomos del observatorio del mismo nombre) toma en cuenta tipo intermedios de galaxias en las que se observan líneas permitidas en emisión que presentan un doble perfil (ancho y angosto). La clasificación se muestra a continuación.

♦ Las galaxias Seyfert 1 son aquellas en las cuales todas sus líneas permitidas muestran ensanchamientos de varios miles de kms^{-1}.

♦ Las galaxias Seyfert 1.5 son aquellas donde se puede apreciar en sus líneas permitidas el perfil doble de componentes anchas y angostas.

♦ Las galaxias Seyfert 1.8 las componentes anchas en las líneas permitidas Hα y Hβ se muestran debilitadas o tenues comparadas con sus componentes delgadas.

♦ Las galaxias Seyfert 1.9 muestran solo una componente ancha muy tenue en Hα, y en Hβ ya no se distingue.

Algunos autores por ejemplo Winkler (1992), han aprovechado esta perspectiva para desarrollar una clasificación cuantitativa de acuerdo a los cocientes de línea de las galaxias Seyfert. En este trabajo seguimos esta clasificación para nombrar nuestros propios objetos. Esta clasificación se determina de la siguiente manera:

Winkler maneja un término R para denotar el tipo de galaxia Seyfert. El termino R se define a continuación:

$$R = \frac{F(H\beta)}{F([OIII]\lambda 5007\text{Å})} \qquad (1.11)$$

Esto es, el cociente de los flujos de Hβ y [O III] y se puede resumir como sigue:

$R < 5$ Galaxia Seyfert 1.

$2 < R < 5$ Galaxia Seyfert 1.2

$0.33 < R < 2$ Galaxia Seyfert 1.5

$R < 0.33$ Galaxia Seyfert 1.8 (Componentes anchos débiles)

Galaxia Seyfert 1.9 (Componente ancho visible en Hα pero no en Hβ)

Galaxia Seyfert 2 (Componentes anchos no visibles)

Como podemos intuir, tal parece que estos objetos vienen de un mismo proceso mediante el cual, la velocidad y luminosidad desciende conforme llegamos a galaxias con menores velocidades en sus FWHM. Tal pareciese que forman una secuencia (Osterbrock 1984). Algunos autores han considerado la posibilidad de que la cantidad de gas en la BLR sea la culpable (Osterbrock 1978). De esta manera si la BLR tiene grandes cantidades de gas, la emisión de líneas permitidas serían de tipo ancho, lo que daría lugar a una galaxia AGN de tipo 1, luego, conforme vaya disminuyendo la cantidad de gas aparecerían los tipos intermedios y si la BLR no tiene gas, entonces no hay líneas anchas y el resultado es el de una galaxia AGN de tipo 2.

1.6.   LINERs.

Los LINERs (acrónimo del ingles Low Ionization Nuclear Emision) son regiones nucleares de las galaxias que presentan líneas en emisión de baja ionización a luminosidades menores comparadas con las galaxias Seyfert. Estos objetos fueron definidos por primera vez por Heckman (1980) y presentan anchos típicos en sus líneas de entre 200-400 kms^{-1}, menores que en las galaxias Seyfert y comparables con las velocidades rotacionales de las estrellas en los

núcleos de las galaxias. Aunque hoy en día se reconoce que también existen líneas anchas permitidas y por ende se les clasifica como LINER de tipo 1 y de tipo 2, en analogía con la clasificación de galaxias Seyfert.

Los LINERs están considerados como los núcleos activos de galaxias de baja luminosidad pero al mismo tiempo son los más comunes en el Universo conocido. Al menos un 30 % de las galaxias espirales muestran este fenómeno y la fracción puede ser incluso mayor considerando galaxias elípticas.

El nivel de baja ionización que presentan los LINERs en sus líneas se ha propuesto con respecto a la emisión de galaxias Seyfert y se define de forma cuantitativa mediante dos condiciones para los cocientes de intensidad de líneas:

$$1.\text{-} \ [\text{O II}]\lambda 3727\text{Å} \geq [\text{O III}]\lambda 5007\text{Å}$$
$$2.\text{-} \ [\text{O I}]\lambda 6300\text{Å} \geq 0.33[\text{O III}]\lambda 5007\text{Å}$$

El cociente típico [O II]λ3727Å/[O III]λ5007Åpara los LINERs es de alrededor de 1, mientras que para las galaxias Seyfert 1 es $\sim$0.5. La línea de [O I]λ6300Å es fuerte en estos objetos mientras las líneas de alta ionización como [Ne V] y [Fe VII] no son observadas (ver Figura 1.7).
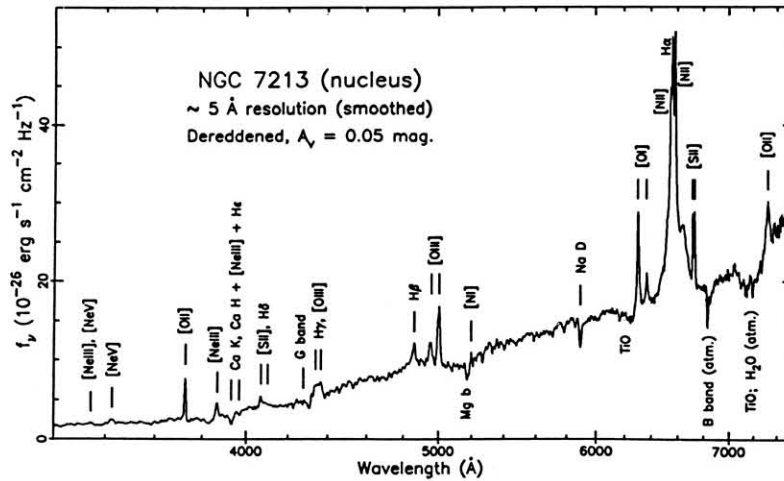
Figura 1.7: *Espectro LINER de la región central de NGC7213 (Filippenko y Halpern 1986).*

Entre los LINERs el cociente de líneas [N II]λ6583Å/Hα es alto ($\geq$0.6) y puesto que estas líneas yacen en una región muy accesible del espectro óptico, además de que son muy cercanas en longitud de onda, algunos autores han utilizado únicamente este cociente para

identificar LINERs. La utilización de diferentes cocientes para definir LINERs han conducido a inconsistencias por que no todos los objetos cumplen con la definición estricta de Heckman.

Hoy en día, muchos investigadores están convencidos de que los objetos tipo LINER representan el extremo de baja luminosidad de los AGN. Existe evidencia contundente de que muchos LINER albergan una fuente de radiación no térmica (es decir, una fuerte emisión de continuo dominado por una ley de potencias y no por una emisión de cuerpo negro como sucede en los procesos térmicos) como las observaciones de rayos-X. El problema con los LINERs es que representan (debido a sus líneas de baja ionización y luminosidad) la frontera entre galaxias AGN y galaxias con gran formación estelar en sus núcleos. Como se puede apreciar en la Figura 1.8, los espectros de LINER y galaxia "normal" son muy semejantes excepto por una sutil diferencia entre las intensidades de algunas líneas.
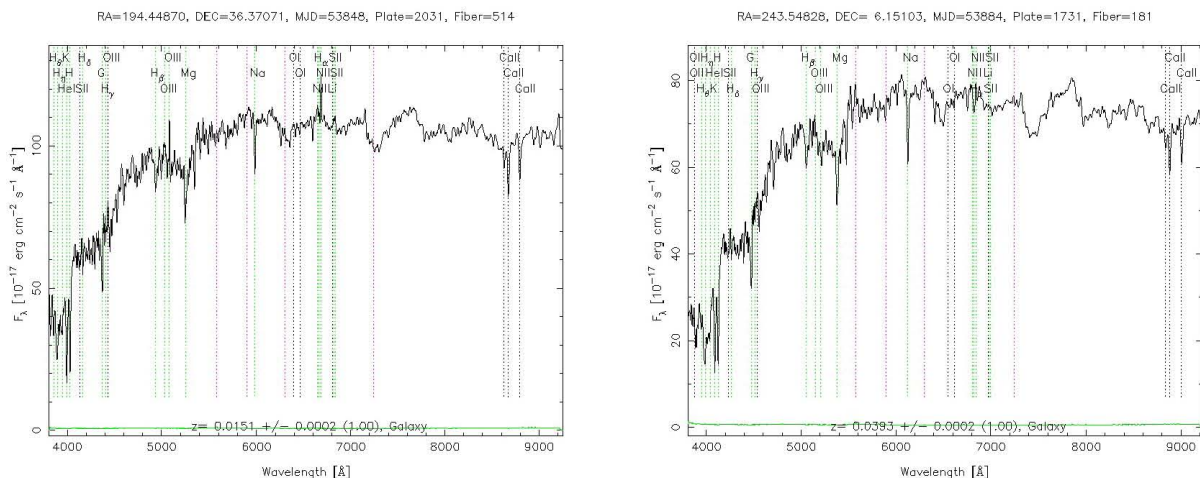
Figura 1.8: Comparación entre un espectro LINER (izquierda) y una galaxia "normal"(derecha). Imágenes de tomadas de SDSS, λ en Å.

Esto ha llevado a que algunos LINERs se puedan explicar por grandes choques de material ionizado en los centros de las galaxias (Fosbury et al, 1978, Dultzin-Hacyan & Ruano 1996, Veilleux et al. 1999). Otros autores creen que pueden ser el resultado de fotoionización por fuentes térmicas (Filippenko & Terlevich 1992, Binette 1994, Cid fernandez 2011 etc.) en el entendido de que una población estelar muy grande de estrellas post-AGB en el centro de las galaxias pueden llevar a ionizar lo suficientemente como para alcanzar la intensidad de los cocientes de líneas requeridos y clasificarlos como LINERs.

1.7.   El Modelo Unificado para los AGN.

Como se puede apreciar en la Tabla 1.1, los diferentes tipos de AGN comparten ciertas características por lo que los procesos físicos que se invocan para explicar los AGN pueden conjuntarse y explicar este fenómeno como un proceso evolutivo en las galaxias. De esta manera la forma de ver los núcleos activos resulta en diversas manifestaciones de los mismos procesos físicos que se diferencia en si por el momento, distancia, luminosidad, orientación y medio ambiente en el que los observamos.

Al día de hoy, se sabe de muchos objetos en los que la clasificación sugerida ha cambiado con el paso del tiempo. Esto pone de manifiesto el carácter evolutivo o al menos cambiante en los objetos con núcleo activo. Precisamente en este trabajo hemos encontrado ejemplos de galaxias que no pueden ser clasificadas como en la literatura astronómica dadas sus nuevas propiedades en observaciones recientes.

Algunos autores han considerado la posibilidad de que los AGN sean un mismo objeto visto desde diferentes líneas de visión. Observaciones espectro-polarimétricas han descubierto que algunas galaxias Seyfert tipo 2 muestran ensanchamiento de líneas con las que se clasifican las Seyfert de tipo 1. Antonucci & Miller en 1985, observaron líneas anchas de Balmer y Fe II en una galaxia clasificada Seyfert tipo 2 en luz polarizada. Como solo en luz polarizada las líneas permitidas se ensanchaban, la dispersión de la luz parecía ser un ingrediente fundamental para ello, luego entonces esta dispersión podría mostrar la BLR de las galaxias. Al comparar los vectores de polarización con los ángulos posicionales de la estructura nuclear en radio frecuencias, Antonucci en 1993, encontró que la polarización tiende a ser paralela en los núcleos de tipo 1 y perpendicular en los de tipo 2. Este hecho sugiere en si mismo que las galaxias AGN de tipo 2 tienen también una BLR que solo de puede ver en luz polarizada y las galaxias Seyfert tipo 1 y tipo 2 son en realidad una misma, vista con diferente orientación (ver Figura 1.9). Las consideraciones sobre la línea de visión son dos:

1.- Si se observa el núcleo activo paralelamente al eje del toro en dirección perpendicular al disco de acreción de la galaxia. Entonces se podrá observar directamente la región de líneas anchas de la galaxia y por ende se clasificará como un objeto de tipo 1.

2.- Si por el contrario, la línea de visión con que se observa la galaxia esta perpendicular al eje del toro o paralelo al disco de acreción, el toro de polvo del AGN no permitirá ver la región donde se ensanchan las líneas (BLR) y solo se observan líneas angostas dando como resultado la clasificación de una galaxia de tipo 2.

El Modelo Unificado explica entonces el porque de las líneas anchas y angostas mediante
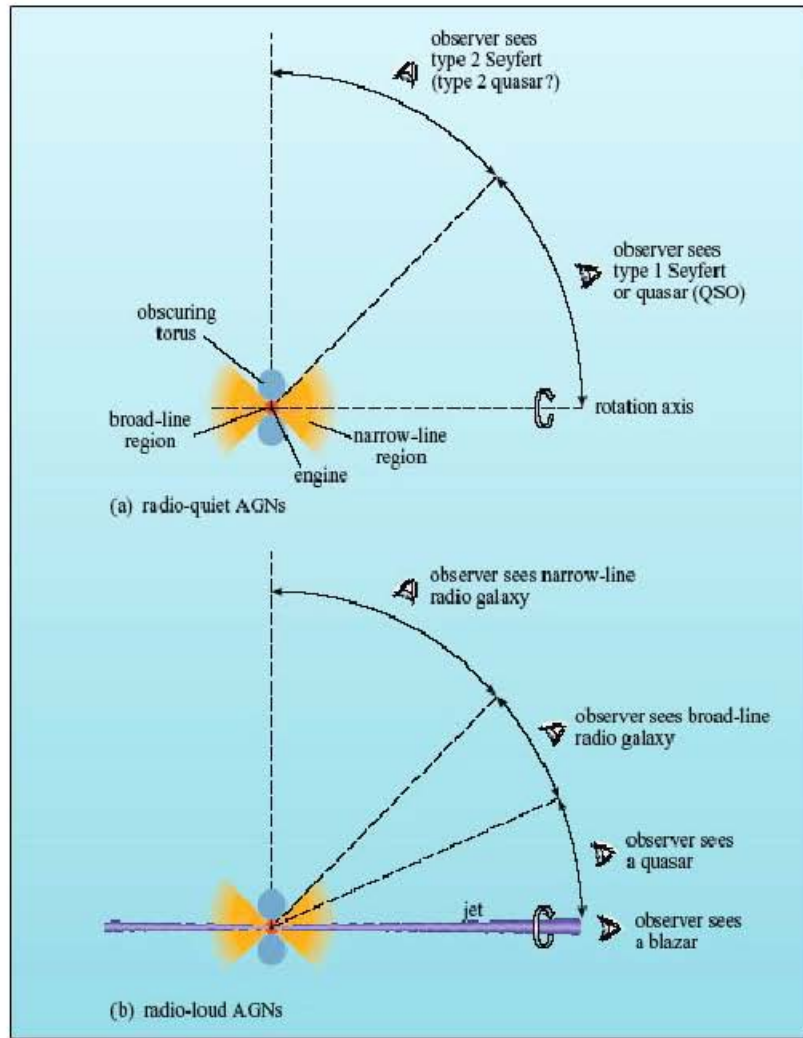
Figura 1.9: *Esquema del Modelo Unificado. (a) Para las galaxias radio calladas y (b) para las galaxias radio ruidosas.*

la orientación de nuestra línea de visión hacia el núcleo de la galaxia. El problema vino cuando mediante muchas más observaciones espectro-polarimétricas no todas las galaxias de tipo 2 mostraban líneas anchas (Ver trabajos de Barth, Filippenko & Moran 1999 a, b y Tran 2003a, b). Esto aunado a que las galaxias huésped presentan diferentes funciones de luminosidad y la emisión de rayos-X duros solo en las galaxias Seyfert 1 ponen en duda la capacidad del modelo.

Otros estudios de AGN en cuanto a su medio circundante pone de manifiesto que las galaxias de tipo 2 están frecuentemente más acompañadas por otras galaxias que las de tipo 1 (Dultzin-Hacyan et al. 1999; Krongold et al. 2001, 2002) lo que parecería no estar de acuerdo con el modelo unificado. Más aún, este modelo tampoco explica la ausencia casi total de

galaxias con líneas anchas en grupos compactos de galaxias (Martínez et al. 2010), de galaxias pares y aisladas (Hernández-Ibarra et al. 2011,2013).

Capítulo 2

Detonantes Internos y Externos de los AGN

La búsqueda de una esquema coherente para explicar la actividad nuclear ha sido muy fructífera en las últimas décadas. Por mucho tiempo, la idea de que la acreción de material en un objeto supermasivo u hoyo negro supermasivo (SMBH $> 10^6$ M$_\odot$) puede subministrar el material para que la actividad nuclear se lleve a cabo se ha venido consolidando. En los últimos años, las evidencias dinámicas sugieren que en la inmensa mayoría de las galaxias alberga un SMBH. El reto ahora es explicar como es alimentado el SMBH y como evoluciona, además de dilucidar la relación del hoyo negro con su galaxia anfitriona en los contextos local y cosmológico.

Los estudios sobre los núcleos activos de galaxias se han diversificado para entender mejor este fenómeno. Los posibles detonantes de esta actividad se han dividido en internos y externos. Los internos se refieren a propiedades intrínsecas de las galaxias anfitrionas como pueden ser tipo morfológico, color, potenciales no-axisimétricos etc. Los externos son considerados como el entorno intergaláctico entre galaxias y sus interacciones. La conexión entre estos dos factores resulta de vital importancia para entender el proceso evolutivo de las galaxias y por ende el del Universo mismo.

2.1. La Correlación SMBH-Bulbo.

Las observaciones de gas en alta resolución de la dinámica estelar (Kormendy & Richstone et al. 1995) y observaciones del telescopio espacial Hubble (Harms et al. 1994;Ferrarese et al. 1996; van der Marel & van den Bosch 1998; Ferrarese & Ford 99; Gebhardt et al. 2000) han

provisto evidencia de que algunas decenas de galaxias albergan en su núcleo lo que parece ser un SMBH. Las mediciones más confiables de la dinámica son las que logran resolver el radio de influencia R_{g-bh} dentro del cual la fuerza gravitacional del SMBH supera las de estrellas cercanas con dispersión de velocidad σ a saber de,

$$R_{g-bh} = \frac{GM_{bh}}{\sigma^2} = 11.2pc \left(\frac{M_{bh}}{10^8 M_\odot}\right)\left(\frac{\sigma}{200kms^{-1}}\right)^{-2} \tag{2.1}$$

Sin embargo, las escalas que estos radios representan están todavía muy por arriba del radio de Schwarzschild (10^{5-6} R_{s-bh}) dado por:

$$R_{s-bh} = \frac{2GM_{bh}}{c^2} = 5 \times 10^{-4}pc \left(\frac{M_{bh}}{10^8 M_\odot}\right) \tag{2.2}$$

Aunque la mayoría de las galaxias donde se ha podido medir estos radios ha sido en galaxias elípticas y algunas espirales (tipo Sa-Sbc). El hacer este tipo de mediciones en galaxias de tipo tardío y enanas representa un reto y no existen mediciones confiables para masas de hoyos negros menores que 10^6 $M_\odot$.
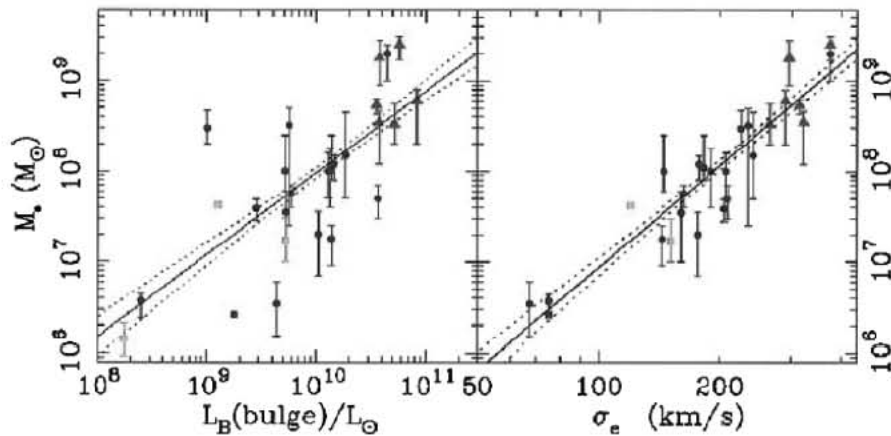
Figura 2.1: *Izquierda: Masa del hoyo negro vs luminosidad del bulbo. Derecha: Correlación entre SMBH-σ. Los cuadros denotan galaxias con detección de máseres, triángulos con cinemática de gas y círculos con cinemática estelar. Las líneas sólida y punteada son los mejores ajustes (tomado de Gebhardt et al. 2000).*

2.2.   Abasteciendo El AGN y El Starbusrt.

2.2.1.   Tasas de Acreción.

Para los disco de acreción en hoyos negros con una eficiencia de conversión ϵ entre materia y energía, la luminosidad bolométrica radiada L_{bol} esta relacionada con la tasa de acreción ($\dot{M}_{bh}$).

$$\dot{M}_{bh} = 0.15 M_\odot yr^{-1} \left(\frac{\epsilon}{0.1}\right) \left(\frac{L_{bol}}{10^{45} erg s^{-1}}\right) \tag{2.3}$$

En la Tabla 2.1 se presentan luminosidades bolométricas y tasas de acreción para ciertos cuásares y AGN cercanas. El intervalo completo en L_{bol} para galaxias Seyferts y LINER fue tomado de Ho, Filippenko y Sargent 1997a, b, mientras que para los cuásares fueron tomados como en la literatura; b. La $\dot{M}_{bh}$ (columna 4) típica es derivada de los valores de la columna 3 suponiendo una eficiencia radiativa de $\epsilon \sim 0.1$.

Type of AGN (1)	L_{bol}[a] (ergs s^{-1}) (2)	Typical L_{bol} (ergs s^{-1}) (3)	Typical $\dot{M}_{bh}$[b] (M$_\odot$ yr^{-1}) (4)
QSOs	10^{46}–10^{48}	10^{47}–10^{48}	10–100
Seyferts	10^{40}–10^{45}	10^{43}–10^{44}	10^{-3}–10^{-2}
LINERs	10^{39}–$10^{43.5}$	10^{41}–10^{42}	10^{-5}–10^{-4}

Tabla 2.1: $\dot{M}_{bh}$ y L_{bol} típicos de cuásares y AGN cercanos.

2.2.2.   El Problema del Momento Angular.

El problema más importante en suministrar material al hoyo negro es el momento angular del material más que el material en si. El momento angular específico del material en la última orbita estable antes de caer al hoyo negro es $10^{24} M_8 cm^2 s^{-1}$ donde $M_8 = 10^8 M_\odot$. En contraste, a un radio de 200 pc del hoyo negro el momento angular es ~ 1000 veces mayor que en la zona de la última orbita estable. Debido a ello, encontrar los mecanismos que puedan reducir el momento angular en un 99.99 % resulta primordial en la investigación de los AGN.

Los mecanismos regularmente requeridos para remover el momento angular y llevar el material a escalas menores para abastecer ya sea un Starburst u hoyo negro suelen ser: torques

gravitacionales, fricción dinámica, torques hidrodinámicos (choques) por mencionar algunos. Estos diferentes procesos en las galaxias suponen una importancia relativa conforme nos encontremos a diferentes distancias del centro galáctico y en diferentes medios intergalácticos como fusiones, pares, grupos o galaxias aisladas.

Los torques gravitacionales operan a tiempos de escala (t_{grav}) comparables a los tiempos orbitales y proveen así, el modo más eficiente de reducir el momento angular a lo largo de escalas intermedias (de varios Kpc a cientos de pc). Esto se puede mostrar comparando t_{grav} con los tiempos de escala para la fricción dinámica t_{df} y torques viscosos t_{vis} para una masa M (Tabla 2.2). La fricción dinámica de una nube con masa M y velocidad v a un radio R operan en tiempos de escala $\propto (R^2\ v/M \ln \Lambda)$, donde $\ln \Lambda$ es el logaritmo de Coulomb (Binney & tremaine 1987). De esta manera, una nube de gas con $10^7\ M_\odot$ a un Kpc de radio del centro de una galaxia espiral, tendrá un t_{df} un orden de magnitud mayor que t_{gra}. Sin embargo, para cúmulos masivos de gas a radios cercanos, la fricción dinámica se torna importante: podría llevar una nube de $10^8\ M_\odot$ de un radio de 200 pc a $\sim$10 pc en pocas decenas de millones de años.

R (pc) (1)	M (M$_\odot$) (2)	t_{gra} (Myr) (3)	t_{df} (Myr) (4)	t_{visc} (Myr) (5)
1000	1e7	20	1020	1000
200	1e7	4	60	–

Tabla 2.2: *Escalas de tiempo para torques gravitacionales, fricción dinámica y torques viscosos.*

En una galaxia aislada, los torques gravitacionales son necesariamente provocados por potenciales no-axisimétricos como barras a diferentes escalas. Mientras barras de gran escala (de kpc de diámetro) pueden llevar material del disco exterior a un radio de un kpc, para después apilarse alrededor de unos cientos de pc debido a la resonancia interior de Lindblad. De aquí, la fricción dinámica puede llevar ese material hacia el centro de la galaxia a unos cuantos decenas de pc. Finalmente, procesos como el feedback, explosiones de supernova y barras nucleares pueden remover energía y momento angular de una fracción del gas circundante. En escalas de decenas de pc, los torques de marea provocados por el hoyo negro en si, pueden disolver cúmulos de gas y estrellas llevándolos hacia el disco de acreción. Subsecuentemente, ya en escalas de pc o sub-pc, los torques viscosos y flujos hidromagnéticos en el AGN pueden ser importantes para que el material caiga al disco de acreción del SMBH.

Las simulaciones sugieren que el ritmo al cual se llevan a cabo estos procesos depende de la historia de acreción que hayan tenido las galaxias. En galaxias con fusiones mayores (razones de masa 1:1) los tiempos de coalescencia son de $\sim$ 1 Gaño e incluso menores. Esto perturba el

sistema de tal modo que se detona un período de relajación violenta donde el gas experimenta fuertes y variantes torques gravitacionales, perdiendo grandes cantidades de momento angular y llevando material hacia el hoyo negro a una tasa $\gg 1$ $M_\odot$ año^{-1} en tiempos realmente cortos. Por otro lado, si las razones de masa entre las fusiones de galaxias son menores (razones de $\sim 1{:}20$) los tiempos de coalescencia son de entre 3 y 5 Gaños, dejando así a los torques gravitacionales, fricción dinámica y torques viscosos como los posibles responsables de llevar material hacia el núcleo galáctico.

## 2.2.3.	La Conexión Starbusrt-AGN

En los últimos años en la literatura astronómica, se ha diferenciado entre los fenómenos de Starbusrt y AGN. El primero tiene origen en una detonación de formación estelar muy probablemente debido a un tipo de fusión entre galaxias o a alguna perturbación de tamaño considerable dentro del núcleo galáctico. El segundo se cree que la radiación emitida es el resultado de procesos en un disco de acreción alrededor de un hoyo negro supermasivo. Sin embargo, los dos fenómenos presentan características similares, ya que ambos procesos son capaces de producir emisión de rayos-X térmicos, radiación ionizante, emisión infrarroja, emisión no térmica en radio y demás. Por lo tanto, es muy probable que estos dos procesos estén relacionados e incluso en muchos de los casos se puedan confundir.

Uno de los problemas más emblemáticos tratando de discernir entre un proceso y otro se presenta en las galaxias AGN de baja luminosidad llamados LINER. Algunos autores han mostrado que un buen número de estrellas POST-AGB pueden ionizar el medio circumnuclear al grado de obtener cocientes de líneas que califican para una clasificación de LINER. Esto, aunado al hecho de que muchos LINER se encuentran en galaxias de tipo elíptico y presentan una población de estrellas muy evolucionadas. lo anterior ha llevado a considerar lo que ahora llaman falsos AGN (ver cid Fernandes et al. 2011). A pesar de ello, muchos autores consideran que son procesos muy diferentes y que el fenómeno del Starbusrt no puede explicar (fuera de los AGN de baja luminosidad) la actividad nuclear en AGN como Seyfert, radio galaxias y la familia de cuasares. Por otra parte, hay autores que consideran que algunos de los LINER si son AGN por que comparten características más propias de los núcleos activos que de las galaxias con un Starbusrt.

Una cosa segura es que, aún si la actividad nuclear no es el resultado directo de un proceso de Starbusrt o de brotes estelares intensos, estos pueden contribuir a que se desencadene una AGN. De hecho, la actividad nuclear puede ser el resultado de este proceso en diferentes magnitudes para los diferentes tipos de AGN. Si regiones de formación estelar intensa en el

centro de las galaxias pueden llegar a mover material hacia los centros galácticos y con ello alcanzar el disco de acreción, sería una forma de alimentar el hoyo negro supermasivo.

2.2.4. Actividad Nuclear Inducida por Interacción Entre Galaxias.

A fines de los años 80 y 90's. Se había establecido una correlación estadísticamente significativa entre fuertes interacciones galácticas y el fenómeno de AGN. Esta correlación se reportó solo para sistemas con alta tasa de acreción (≥ 10 $M_\odot$ año^{-1}) tales como cuasares muy luminosos, galaxias radio-ruidosas (Hutchings 1987; Yates et al. 1989;Disney et al. 1995; Bahcall et al. 1997 y Kirhakos et al. 1999). Otros trabajos muestran que la actividad nuclear se ve inducida por interacciones de marea entre galaxias (Hernández-Toledo 2000, Ellison et al. 2010,2011).

Para galaxias Seyfert, LINER e incluso algunos cuasares de moderada luminosidad, la correlación mencionada antes no esta presente. Esto simplemente puede deberse a que en estos objetos las tasas de acreción son mucho menores que en los cuasares más luminosos. Una $\dot{M}$ de baja intensidad (10^{-2}-10^{-3}) puede estarse llevando a cabo por procesos menos energéticos en el gas circumnuclear.

Se conoce que un hoyo negro puede consumir entre 1 y 10 $M_\odot$ por año. Dado esto, entonces los tiempos en que un hoyo negro puede estar acretando material estarían dados en función de la cantidad de gas que llegue a consumir. En este sentido, la masa requerida para alimentar el hoyo negro es muy pequeña comparada con la masa del gas presente en el medio interestelar cercano al centro. Así, el problema se reduce básicamente a explicar como llega la materia hasta el hoyo negro para ser acretada.

Como hemos mencionado anteriormente, se requiere de varios mecanismos a diferentes escalas para llevar materia hasta el hoyo negro. El reto es llegar hasta aproximadamente 100 veces el radio de Schwarzschild (~ 0.001 pc). Para lograr lo anterior, es necesario remover casi en su totalidad el momento angular del gas y es posible que un mecanismo como una colisión entre galaxias de masas similares pueda conseguirlo debido a las violentas fuerzas de marea, torcas gravitacionales y fricción dinámica que son capaces de remover el momento angular a diferentes escalas de la galaxia.

2.2.5.   Tipos de Interacción Galáctica

Dado que en las interacciones entre galaxias existen muchos parámetros (masas de las galaxias, velocidad, dirección, parámetro de impacto, spin, tipo morfológico, etc) que tenemos que tomar en cuenta para cuantificar el grado de interacción. Con el afán de clasificar estas interacciones de manera que no resulte subjetiva, Dultzin-Hacyan (1997) propuso una clasificación de las interacciones en tres tipos principales con base en la distancia entre galaxias y la perturbación que se produce en el encuentro.

1.- **Interacciones Débiles.** Se refiere a galaxias que se encuentran en pares físicos que solo llegan a experimentar fuerzas de marea gravitacionales entre ellas. Las fuerzas de marea pueden llegar a ser importantes al grado de inducir actividad nuclear sobre todo en los sistemas pares que se componen de una galaxia elíptica y una espiral con mucho gas.

2.- **Interacciones Fuertes.** Se presenta cuando hay un colisión directa entre las galaxias pero no quedan ligadas, solo existe un traslape y siguen su camino. En esta interacción se producen distorsiones dramáticas en la morfología de ambas galaxias y pueden producir anillos galácticos.

3.- **Fusión Galáctica.** Este tipo de interacción es completa. Las galaxias terminan por fusionarse y llegar a la coalescencia. Este es el fenómeno más drástico entre las interacciones y da como resultado una galaxia elíptica altamente perturbada independientemente de la morfología que hayan tenido las galaxias anteriormente (si son galaxias de masas comparables).

Capítulo 3

Nuclear Activity In Isolated Galaxies

En este artículo, presentamos un estudio espectroscópico sobre la incidencia de la actividad nuclear específicamente en dos muestras de galaxias aisladas. En total, tomamos 513 espectros disponibles en SDSS (DR7) para estas muestras. Analizamos 413 espectros del catálogo de galaxias aisladas de Karachentseva (CIG) y 100 de la muestra de galaxias espirales aisladas de Varela. En estas muestras, hicimos un análisis de la clasificación morfológica para corroborar e incluso corregir aquellas galaxias que presentan errores en su clasificación.

Hemos puesto especial cuidado a la hora de sustraer la contribución espectral de las estrellas de fondo y medir las líneas en emisión. Con la medición de líneas construimos diagramas BPT que nos permiten discernir entre galaxias con o sin actividad nuclear y el tipo de la misma. En este trabajo se ha considerado a las llamadas galaxias compuestas o en transición como galaxias con núcleo activo o actividad AGN.

Por primera vez se cuenta con una muestra de galaxias aisladas que presenta un número estadísticamente significativo en todos los tipos morfológicos. La incidencia de actividad nuclear en las muestras llega a ser del $43\% \pm 5\%$ y $41\% \pm 5\%$ para galaxias con líneas de emisión. Además, esta incidencia es mayor en galaxias del tipo temprano en comparación con las galaxias espirales de tipo tardío.

Al considerar galaxias que no presentan líneas en emisión en las muestras notamos que, la incidencia AGN decrece en los tipos tempranos y puede equipararse con la incidencia en galaxias Sa y Sb. Este último resultado se pudo obtener dado la mayor cantidad de galaxias de tipo temprano en una de las muestras comparada con otras muestras de galaxias aisladas.

Otro resultado importante es la ausencia tan marcada ($< 3\% \pm 2\%$) de la actividad nuclear de tipo 1 de entre 175 AGN. Esta ausencia no favorece la explicación mediante la orientación y oscurecimiento (modelo unificado) de los tipos 1 y 2 de AGN.

Dada la alta incidencia de AGN en galaxias aisladas, interpretamos este resultado mediante la existencia de una evolución secular que considera incluso fusiones menores entre galaxias.

Artículo aceptado en la revista Monthly Notices of the Royal Astronomical Society. Junio 6, 2013.

Nuclear Activity in Isolated Galaxies

Francisco J. Hernández-Ibarra[1][*], Deborah Dultzin[1], Yair Krongold[1],
Ascensión del Olmo[2], Jaime Perea[2] and Jesús González[1]

[1] *Instituto de Astronomía, Universidad Nacional Autónoma de México, Apartado Postal 70-264, 04510 México DF, México.*
[2] *Instituto de Astrofísica de Andalucía (C.S.I.C.) Apartado 3004, 18080 Granada, Spain.*

ABSTRACT

We present a spectroscopic study of the incidence of AGN nuclear activity in two samples of isolated galaxies (Karachentseva, V.E. & Varela, J.). Our results show that the incidence of non-thermal nuclear activity is about 43% and 31% for galaxies with emission lines and for the total sample 40% and 27% respectively. For the first time we have a large number of bona-fide isolated galaxies (513 objects), with statistically significant number of all morphological types. A large fraction ($\sim$70%) of elliptical galaxies or early type spirals have an active galactic nucleus and $\sim$70% of them are LINERs. We find a larger fraction of AGN in early morphological types, as also found in the general population of galaxies. Only 3% of the AGN show the presence of broad lines (not a single one can be classified as type 1 AGN). This is an important result which is at odds with the unified model even if we consider warped or clumpy tori. Finally, we interpret the large fraction of AGN in isolated galaxies as the result of secular accretion.

Key words: galaxies: active - galaxies: evolution - galaxies: interactions

1 INTRODUCTION

Along the last 25 years, many authors have studied the AGN environment (Stauffer 1982a,b; Dahari 1984, 1985; Kennicutt & Keel 1984; de Mello et al. 1995, 1996; Laurikainen & Salo 1995; Dultzin-Hacyan et al. 1999; Krongold et al. 2001, 2002; Schmitt 2001; Sorrentino et al. 2006; Koulouridis et al. 2006a,b; Márquez & Masegosa 2008). The incidence of nuclear activity in galaxies and their environment has become a topic of debate because there are different mechanisms that can possibly trigger nuclear activity depending on the galaxy's environment. Interactions between galaxies are well known to produce enhancement in star formation in galaxies (Lonsdale et al. 1984; Kennicutt et al. 1987; Keel 1993; Krongold et al. 2002; Barton et al. 2000; Woods & Geller 2007; Lin et al. 2007). Others authors also have evidence for a connection between circumnuclear starburst and AGN (Storchi-Bergmann 2008, and references therein). There are also suggestions for a connection between interactions and nuclear no-thermal activity specifically of type 2 (Dultzin-Hacyan et al. 1999; Krongold et al. 2001). Other studies have dealt with the AGN population of compact groups (Martínez et al. 2010) as well as in larger groups like clusters of galaxies (Ruderman & Ebeling 2005; von der Linden et al. 2010; Pimbblet & Jensen 2012; Pimbblet et al. 2013). The general results of these studies show a tendency for AGN to be hosted in massive galaxies, and towards the center of the clusters.

In this paper we study the incidence of activity in isolated galaxies. In a forthcoming paper (Hernández-Ibarra et al. in preparation 2013) we will present the results of a survey of AGN in paired galaxies of similar mass.

It is important to study galaxies in a restricted environment in order to elucidate what mechanisms could be determinant to trigger AGN activity. Isolated galaxies can be defined as those systems that are formed in low galactic density environments, but that evolved without major interactions with other galaxies of similar mass over the last 3 Gyr. In this context, any non-axisymmetric structures in these galaxies such as bars, tails, plumes or stripping material must be the result of secular evolution.

The study of truly isolated galaxies is thus fundamental to benchmark the role of interactions in nuclear activity. Studies of field galaxies (e.g. Ho et al. 1997) cannot provide this information as these samples may include galaxies that have undergone or are undergoing an interaction.

This is the first paper of a series involving a self consistent and homogeneous way to study nuclear activity in galaxies in different environments. In the present work, we study the incidence of nuclear activity in two samples of bona-fide isolated galaxies using an efficient way to extract the stellar contribution (host spectrum). The purpose of this

[*] E-mail:hibarra@astro.unam.mx

2   *F. J. Hernández-Ibarra, D. Dultzin, Y. Krongold, A. Del Olmo, J. Perea, J. González*

work is to have a well defined sample of isolated galaxies with optical spectroscopic characteristics that allow us to classify them according to their type of activity. Studying the incidence of the nuclear activity in isolated galaxies alone is of great value to establish if AGN is a common and/or persistent phenomenon even when strong tidal external perturbations have not been present during the last few Gyr of galaxy evolution. This would indicate that AGN activity can be triggered by secular evolution processes in galaxies. Our results on this sample will be further used as a benchmark to compare the incidence of activity in a sample of isolated pairs of galaxies (Hernández-Ibarra et al. in preparation 2013).

This paper is organized as follows. In §2 we describe our samples. In §3 we present the data analysis and classification. Results are given in §4 and §5 contains the discussion about the possible mechanisms for developing an AGN in isolated galaxies.

2   CHARACTERISTICS OF THE SAMPLES

As stated above the so called "field galaxies" cannot be used as a proper sample in the study of the properties of truly isolated galaxies. Therefore in this study we used two samples of rigorously defined isolated galaxies: The photometric catalogue of isolated galaxies (CIG) by Karachentseva (1973) and the northern isolated disk galaxies compiled by Varela et al. (2004).

We take all available spectra from DR7 of SDSS (Abazajian et al. 2009) for the two samples. The spectra have a wavelength coverage from 3800-9200Å with a resolution power of 1800-2200 and a signal-noise (S/N) >4 per pixel at g=20.2. The SDSS spectra were taken through a fiber aperture of 3 arcsec in diameter (corresponding to 700 pc radius in average for our samples). This means only that central regions of the galaxies were observed. All the objects in both samples have magnitudes in r < 17.77. Thus, according to SDSS spectroscopic limit (r = 17.77), both samples are complete.

The (CIG) catalogue contains 1051 galaxies. It is one of the best sources of isolated objects. The isolation criteria are still used as the basis for new catalogues of isolated galaxies (e.g. Verdes-Montenegro et al. (2005); Karachentseva et al. (2010); Hernández-Toledo et al. (2010); Coziol et al. (2011); Karachentsev et al. (2011)). These isolation criteria guarantee that the galaxies have not experienced a major merger/interaction over the last 3 Gyr.

The catalogue was based on a visual search of northern-sky galaxies ($\delta \geqslant -3^o$) with a magnitude limit of $m_{Zw} \leqslant 15.7$ and a range in z from $\sim$ 0.01 to 0.05. Only objects which have high galactic latitude are considered in order to avoid galactic extinction[1] This sample, is reasonably complete ($\sim$ 90%) in the magnitude range $13.5 \leqslant m_{Zw} \leqslant 15.7$ (Hernández Toledo et al. 1999). In this catalogue a galaxy is considered to be isolated when it does not have a neighbor of similar size (diameter > $\frac{1}{4}$ of the target galaxy) within 20 diameters.

This corresponds to a magnitude difference $\sim$ 3 (excluding any possible AGN luminosity contamination). Considering a "field" velocity of 150 km/s for a galaxy with diameter of 25 kpc, it would require $\sim$ 3 Gigayears for a companion galaxy to abandon the area enclosed in the 20 diameters of isolation criterion. A similar time would be required to erase morphological perturbations due to a merger. This means that these galaxies have been unperturbed on average by at least that time.

The second sample we examined is that of northern isolated disk galaxies compiled by Varela et al. (2004) wich originally contains 203 disk galaxies. This sample considers different criteria for isolation. In particular, it is based on the logarithmic ratio f, between inner and tidal forces acting upon the candidate galaxy by a possible perturber (see Varela et al. 2004, equation 3). Only galaxies with low f ratio (f $\leqslant$ -4.5) are considered as isolated because they do not show signatures of any perturbation. They estimated that the objects in their sample have not been affected by other galaxies during the last 2 Gyr. It is important to consider another sample obtained with different criteria in order to assess the reliability of our results.

We analyzed 413 spectra for the CIG catalogue and 100 for Varela's sample from SDSS DR7. After a meticulous inspection of the SLOAN images, we excluded those spectra which: 1) Do not have the optic fiber in the center of the galaxy (KIG 479 and KIG 237) or incomplete spectra like in KIG 702 and KIG 479, 2) Are Blue Compact/H II Galaxies (6 galaxies in Varela's sample, 1 in CIG), 3) Galaxies showing traces of interaction (tidal tails etc) or present a companion namely: KIG 349, KIG 439, KIG 468, KIG 634 and KIG 687 (Sulentic et al. 2006; Verley et al. 2007) and 4) Galaxies that did not achieve 3 σ detection in all their line intensities (37 galaxies of CIG sample).

A visual inspection was performed for all galaxies to confirm the morphological classification according to NED, SIMBAB and HYPERLEDA. In those few cases where an obvious misclassification was present, the morphology was corrected by us. In addition we found that PGC 33255 could be part of a pair and excluded this galaxy of the sample. Strangely enough, we found two elliptical galaxies with a very blue compact core: PGC29177 and PGC43121 that show typical HII region spectra, and were also excluded from our analysis. With this into account, our spectroscopic sample from CIG consists of 367 galaxies while the spectroscopic sample from Varela consists of 93. Out of these galaxies 18 and 10 respectively do not present emission lines. In Table 1 we show the general statistics for both samples.

We were careful to distinguish between intrinsic no emission and a problem of detectability related to low S/N. For this purpose we set a threshold of 10^{38} erg s^{-1} in Hα luminosity. The galaxies below this threshold are the true no-emission objects with a probability of being an AGN of less than 2% and 4% for the CIG and Varela's samples respectively. The distribution of morphology and Hα luminosity of our samples are presented in Figure 1.

---

[1] We know that our results are insensitive to reddening because we use line emission ratios which cancel this effect.

Table 1. General statistics of both Isolated galaxy samples.

Sample	Total	No Emission	Excluded	Fitted	AGN+Comp	H II	AGN Type 1
CIG	413	18(4%)	47(11%)	348(84%)	150(36%)	198(48%)	12(3%)
VAR	100	10(10%)	7(7%)	83(83%)	26(26%)	57(57%)	1(1%)
TOTAL	513	28(5%)	54(11%)	431(84%)	176(34%)	255(50%)	13(3%)
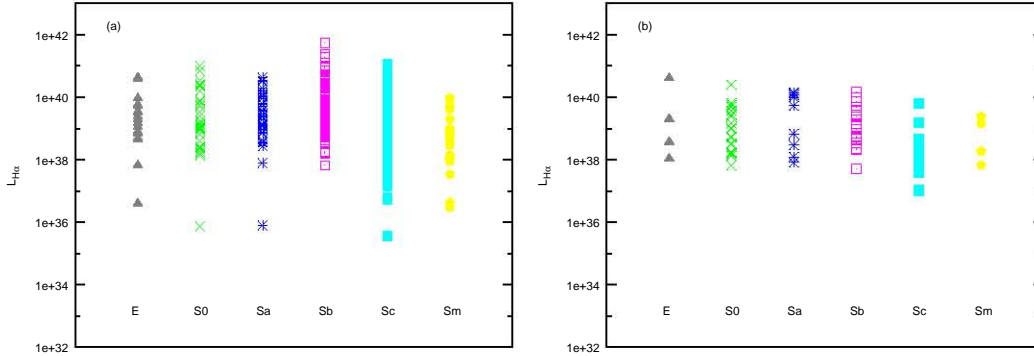
Figure 1. Morphological distribution of Hα luminosity for (a) CIG sample and (b) Varela's sample. Mean values of AGN Hα luminosity for CIG and Varela's samples are $L_{H\alpha} = 9.2 \times 10^{39}\ erg\ s^{-1}$ and $L_{H\alpha} = 1.8 \times 10^{39}\ erg\ s^{-1}$ respectively which correspond to Low Luminosity AGN.

3 DATA ANALYSIS AND NUCLEAR CLASSIFICATION

We examined all of the spectra looking if emission lines were present. Within the spectral range covered by the SDSS spectra we searched for Hβ, [OIII]λ5007Å,[OI]λ6300Å, [NII]λλ6548,6584Å, Hα and the two Sulfur ([SII]λλ6717,6731Å) lines. In many cases the nebular emission is very weak or it can be even diluted in the strong stellar continuum of the galaxy. Since the integrated SDSS spectra are collected through 3 arcsecs fibers, they include not only the nuclear emissions but also the surrounding stellar light coming from the host galaxy. This contamination turns out to be more significant at the central parts of the galaxies and as the spheroidal/bulge component becomes more relevant. In fact it can even mask weak emission lines such as those detected in galaxies with an AGN. Therefore to obtain a reliable nuclear classification based on the emission lines it is mandatory to subtract the stellar contribution. We applied the principal component analysis (PCA) method following Hao et al. (2005) to subtract this contribution. We used their first 8 eigenspectra from their low redshift range. These eigenspectra are the resulting eigenvectors of a PCA analysis applied to a sample of high S/N spectra of non-emission galaxies. In addition, as they pointed out, we included two more components, an A star spectrum accounting for the possible presence of post-starburst features and a power-law to take into account of the possible existence of a non-thermal component. The analysis is performed for all the spectra of our sample and it consists on a multiple regression of each spectrum to a linear combination of the 8 eigenspectra plus the two additional components. Previously to the fit each galaxy spectrum was moved to zero redshift which is the one of the template library. We also masked all those regions where emission lines may appear since the

quality of the fit lies on the matching of the continua. Once the regression is performed, the direct subtraction of the resulting fit to the original (z=0) spectrum provides us with a pure emission line spectrum where all the underlying absorption components and eventually a non thermal component of the continuum are removed.

Line fluxes were calculated with Sherpa software (http://cxc.cfa.harvard.edu/sherpa/) (which comes in the CIAO distribution, http://cxc.harvard.edu/ciao/). Sherpa reads the data and evaluates a given model on this data set. Then, it varies the free parameters to minimize a statistical goodness function to obtain the best set of parameters that fit the data. In our case our model is composed only by Gaussians.

We evaluated two methods to fit the lines. The first one consisted in constraining the width and velocity to the same value in our fits, for two separated groups of lines, forbidden and permitted. Therefore these fits included four free parameters in our models: the width and velocity of the forbidden and the permitted lines. An additional free parameter for each line in the model was the intensity of each emission line. The second method we used was to constrain the width and velocity for all the detected lines (independently on whether they were permitted or forbidden) to have the same value (i.e. only two free parameters to model all lines) plus an additional free parameter for the intensity of each line. Our results show that both methods are equivalent without any substantial difference. We decided to fit the emission lines with the second method since it has less free parameters. For those objects where a broad component was required in addition to the narrow one, an individual broad Gaussian was fitted with fully independent free parameters (see Figure 2 for fit examples).

We have used the Baldwin, Phillips and Terlevich op-

KIG1008   PGC40475
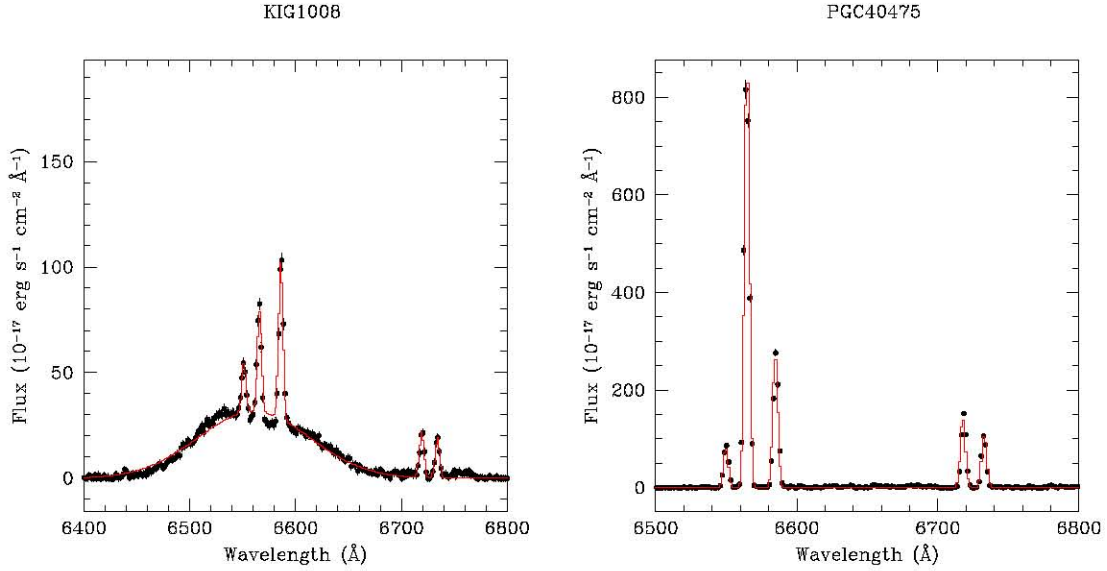
Figure 2. Examples of fits in Hα region for galaxies with and without broad line respectively. Black data points denote the spectrum with the stellar contribution subtracted and the red line shows the fit.

tical diagnostic diagrams (Baldwin et al. 1981; Veilleux & Osterbrock 1987) to separate star-forming galaxies from active galactic nuclei (AGN). Line ratios adopted were ([O III]/Hβ), ([N II]/Hα), ([S II]/Hα) and ([O I]/Hα). With these ratios we produced the ([O III]/Hβ) vs ([N II]/Hα) diagram (hereafter [N II] diagram), the ([O III]/Hβ) vs ([S II]/Hα) [S II] diagram and the ([O III]/Hβ) vs ([O I]/Hα) [O I] diagram. Line ratios with their errors and AGN type are presented in Tables 6 and 7 for CIG and Varela's samples respectively (see the complete Tables at the end of this article version). The last column in these tables gives the nuclear type. We have used the quantitative definition by Winkler (1992) to measure the contribution of a broad component when present, and thus establish the Seyfert type.

We used two demarcations to identify the galaxy type. The first one is the theoretical division line proposed by Kewley et al. (2001) (K01 line hereafter) where objects above this line on the diagrams have nuclear activity. The second one is the empirical line derived by Kauffmann et al. (2003) (K03 line hereafter), this empirical line is based on the location of star-forming galaxies for the SDSS. Galaxies that lie between this two lines are called composite (or transition) objects. This objects need non-thermal processes to produce the line ratios (in addition to star forming processes). Therefore, we will take these objects as AGN in this work. Further support comes from the work done by Trouille et al. (2011) where they found that composite galaxies on BPT [N II] diagram are X-ray hard sources and have a high X-ray luminosity to total infrared luminosity.

We have performed the analysis of the CIG catalogue studying the effects of galactic morphology. Figure 3 shows a histogram of morphological types for both samples and Figure 4 shows the mass distribution for both samples. It is clear from Figure 3 that around 70 % of the galaxies in the CIG have morphologies between Sb and Sc. This result is consistent with a work done by Hernández-Toledo et al.
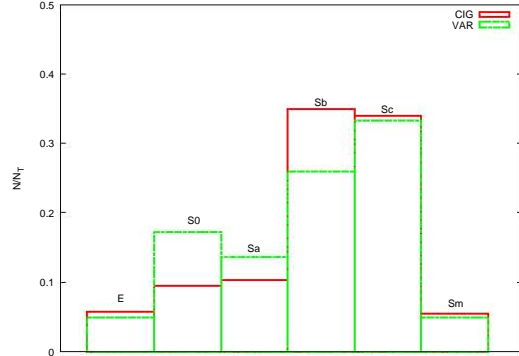
Figure 3. Morphological type distribution of the samples considered in this work. The continuous (red) line corresponds to the CIG sample and the dashed (green) line to the Varela sample.
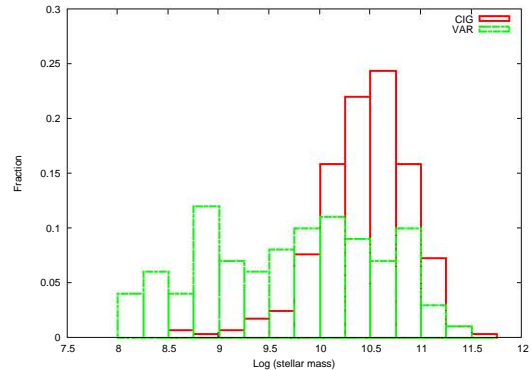
Figure 4. Mass distribution for the two samples. Labels like in Figure 3.
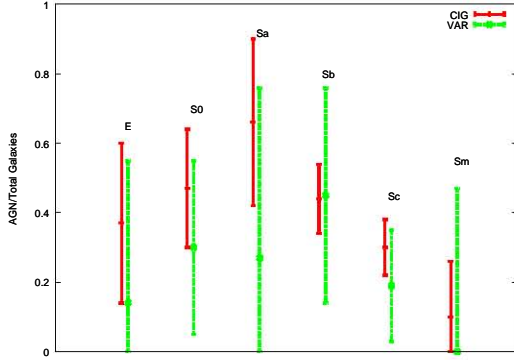
Figure 5. Statistical comparison between isolated samples. Labels like in Figure 3.
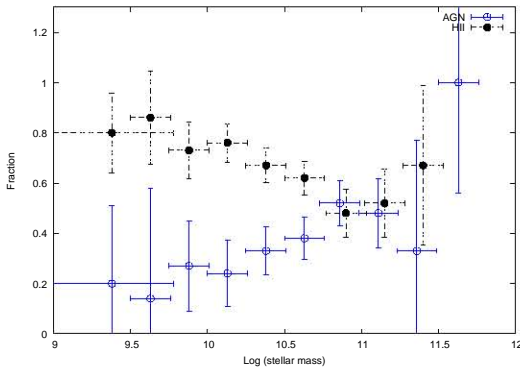
Figure 6. Fraction of AGN and HII galaxies as function of stellar mass. AGN are represented by (blue) empty circles and H II objects by (black) filled circles. Errors in the y-direction are the standard deviation per bin and "errors" in x-direction simply denote the full range of mass in each bin.

(2010) for other isolated galaxy sample. The fraction of AGN for each morphological type in both samples is shown in Figure 5. We can see that within the large statistical errors the comparison is valid.

In Figure 6 we show the mass distribution of galaxies with AGN and H II activity. Considering that the sample is reasonably complete ($\sim 90\%$) we can clearly see a trend were the incidence of AGN is higher for more massive galaxies. Conversely the incidence of strong H II activity is higher for low mass galaxies. This is for masses $< 10^{11} M_\odot$. From the above analysis we can confirm the well know tendency for later type morphology galaxies to be also relatively lower mass galaxies.

4 RESULTS

Our main results are summarized in Tables 2 to 5, and also in Figures 5 to 10.

In Table 2 we show numbers and percentages of activity and morphological classes for the CIG sample. Column 1 presents the morphological type, the total number of galaxies is listed in column 2. Columns 3 and 4 list the number of

galaxies with H II and Composite (hereafter Comp) activity and their percentages, respectively. Column 5 contains the number of galaxies in the AGN+Comp region and their percentages. In column 6 we present the total number of galaxies including those with no-emission lines. Columns 7, 8 and 9 show the number and percentages for H II, Comp and AGN+Comp activity respectively. In Table 3 we present the same data as in Table 2 for Varela's sample.

In Figure 7 we show the [N II] BPT diagram. All galaxies in the composite region are taken as AGN as argued in §3.

We can clearly see that the incidence of nuclear activity is statistically higher in early type galaxies and decreases gradually as we go to late types in this subsample of emission lines galaxies only. The dependence on morphology is quite significant: going from 70 % in E galaxies to 10 % in Sm. The incidence of nuclear starburst activity decreases in the opposite sense: going from 90 % for Sm to 30 % for E. Meanwhile, if we consider the total sample (including galaxies without emission lines) the incidence gives a flatter distribution from E to Sb and decreases only for late types (compare columns 5 and 9 in Tables 2 and 3). This is clearly observed in Figure 5.

In Figure 8, we show the position of our objects in the BPT [N II] diagram for Varela's sample. In this sample there are only 4 ellipticals, whereas the majority (27) are Sc. Considering that early types have a larger incidence of AGN, this can explain the fact that we find a total incidence of AGN of only 31 % as compared to 43 % in the CIG sample.

In Figure 9 we present the [S II] diagnostic diagram for the CIG sample. This diagram is useful to separate between Seyferts and LINERs.

In Figure 10. We show yet another diagram [O I]. This diagram differs only slightly from the one in Figure 9. The main difference is in the relative proportion of Seyferts and LINERS except for ellipticals. We point out that the [O I] line is weaker than the [S II] line and thus the mean error is large.

In Table 4. We quantify the incidence of AGN activity and morphology distribution derived from the [S II] and [O I] diagrams for CIG sample. Columns 1 and 2 are the morphological type and the number of galaxies in each type. In column 3 we list the number of AGN and the percentage in parentheses. The number of Seyfert galaxies and the percentage are listed in column 4. The number of LINERs is in column 5. Columns from 6 to 9 contains the same data of columns of 2 to 5 but this time for the [O I] diagram. Table 5 is the analogous of Table 4 for Varela's sample.

From these Tables we can confirm the result that the incidence of AGN activity is higher for early type galaxies in the sample with emission lines only. When all galaxies are considered the distribution flattens as found before for the CIG sample (see Fig.5). Again, the incidence of Seyfert galaxies is more frequent in morphologies from Sa to Sc, but specially in Sb.

In Tables 4 and 5 we show the data for the [S II] and [O I] diagrams. The AGN fractions are different from those in Tables 2 and 3. The reason is that we do not consider composite nuclei in the [S II] and [O I] diagrams. Unfortunately models by Kauffmann et al. (2003) for these particular diagnostic diagrams ([S II] and [O I]) are not available. In

6   *F. J. Hernández-Ibarra, D. Dultzin, Y. Krongold, A. Del Olmo, J. Perea, J. González*
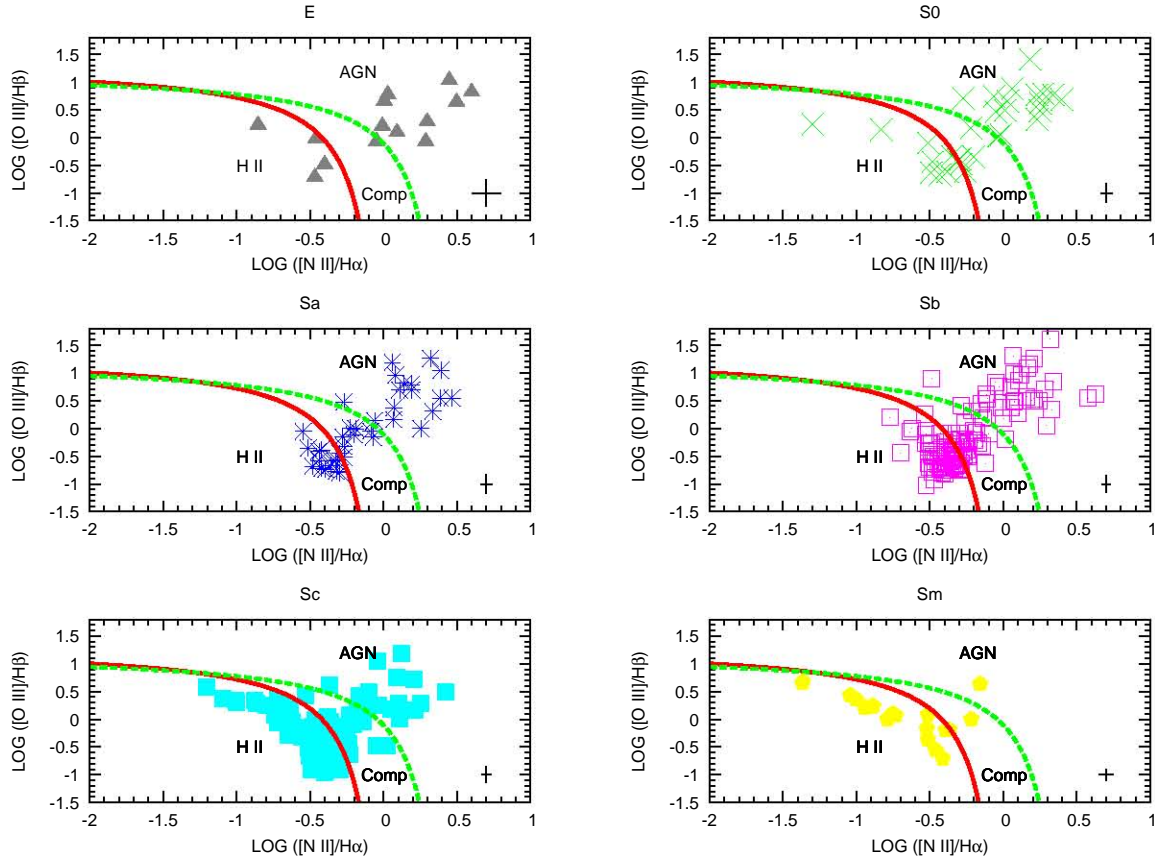
Figure 7. The [N II] diagnostic diagrams for CIG sample with different morphologies. This diagram separates between tree different kind of activity in galaxies like AGN, Composite and H II like region galaxies. The green dashed line (Ke01) separates galaxies with a AGN from Composite (AGN+Starburts activity). Continuous red line (Ka03) divides pure star forming galaxies from AGN-starburts composite objects. Elliptical galaxies are shown as filled gray triangles, lenticular as green crosses, Sa as blue asterisks, Sb as pink empty squares, Sc as filled cyan squares and Sm as filled yellow pentagons. The cross at the lower right part of the diagram is the mean error in the line ratios.
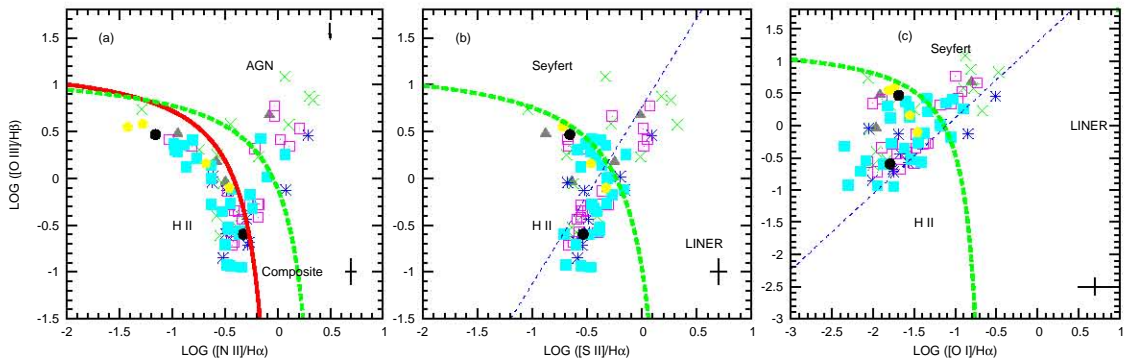
Figure 8. (a) The [N II], (b) [S II] and (c) [O I] diagnostic diagrams for Varela's sample. Labels like in Figure 7. The low incidence of nuclear activity are present on Sc and Sm types. Filled circles represent objects which cannot be classified.

Table 2. Morphology distribution and incidence of nuclear activity for the CIG sample derived from [N II] BPT diagnostic diagram.

M.T.	Galaxies with Emission lines				Total sample			
	Total	H II	Comp	AGN+Comp	Total	H II	Comp	AGN+Comp
E	14	4(29%)	1(7%)	10(71%)	23	4(17%)	1(4%)	10(43%)
S0	30	9(30%)	5(17%)	21(70%)	38	9(24%)	5(13%)	21(55%)
Sa	38	13(34%)	8(21%)	25(66%)	38	13(34%)	8(21%)	25(66%)
Sb	122	67(55%)	20(16%)	55(45%)	124	67(54%)	20(16%)	55(44%)
Sc	124	87(70%)	22(18%)	37(30%)	124	87(70%)	22(18%)	37(30%)
Sm	20	18(90%)	1(5%)	2(10%)	20	18(90%)	1(5%)	2(10%)
Total	348	198(57%)	57(16%)	150(43%)	367	198(54%)	57(16%)	150(41%)
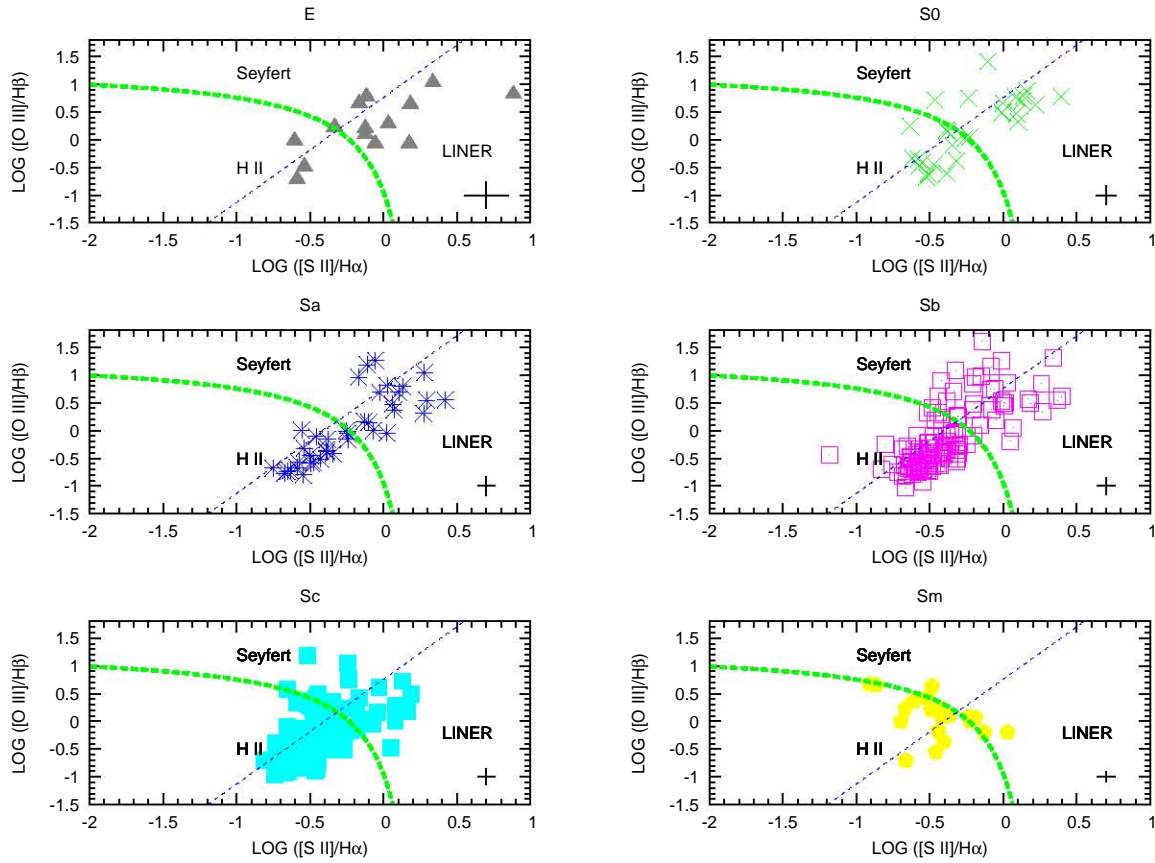
Figure 9. The [S II] diagnostic diagram for CIG sample. Blue dashed line represents Seyfert/LINER line and others labels like in Figure 7.

Table 3. Morphology distribution and incidence of nuclear activity in Varela's sample derived from [N II] BPT diagnostic diagram.

M.T.	Galaxies with Emission lines				Total sample			
	Total	H II	Comp	AGN+Comp	Total	H II	Comp	AGN+Comp
E	4	3(75%)	0(0%)	1(25%)	7	3(43%)	0(0%)	1(14%)
S0	14	8(57%)	1(7%)	6(43%)	20	8(40%)	1(5%)	6(30%)
Sa	11	8(73%)	1(9%)	3(27%)	11	8(73%)	1(9%)	3(27%)
Sb	21	11(52%)	4(19%)	10(48%)	22	11(50%)	4(18%)	10(45%)
Sc	27	22(81%)	3(11%)	5(19%)	27	22(81%)	3(11%)	5(19%)
Sm	4	4(100%)	0(0%)	0(0%)	4	4(100%)	0(0%)	0(0%)
Total	81	56(69%)	9(11%)	25(31%)	91	56(62%)	9(10%)	25(27%)

8   *F. J. Hernández-Ibarra, D. Dultzin, Y. Krongold, A. Del Olmo, J. Perea, J. González*
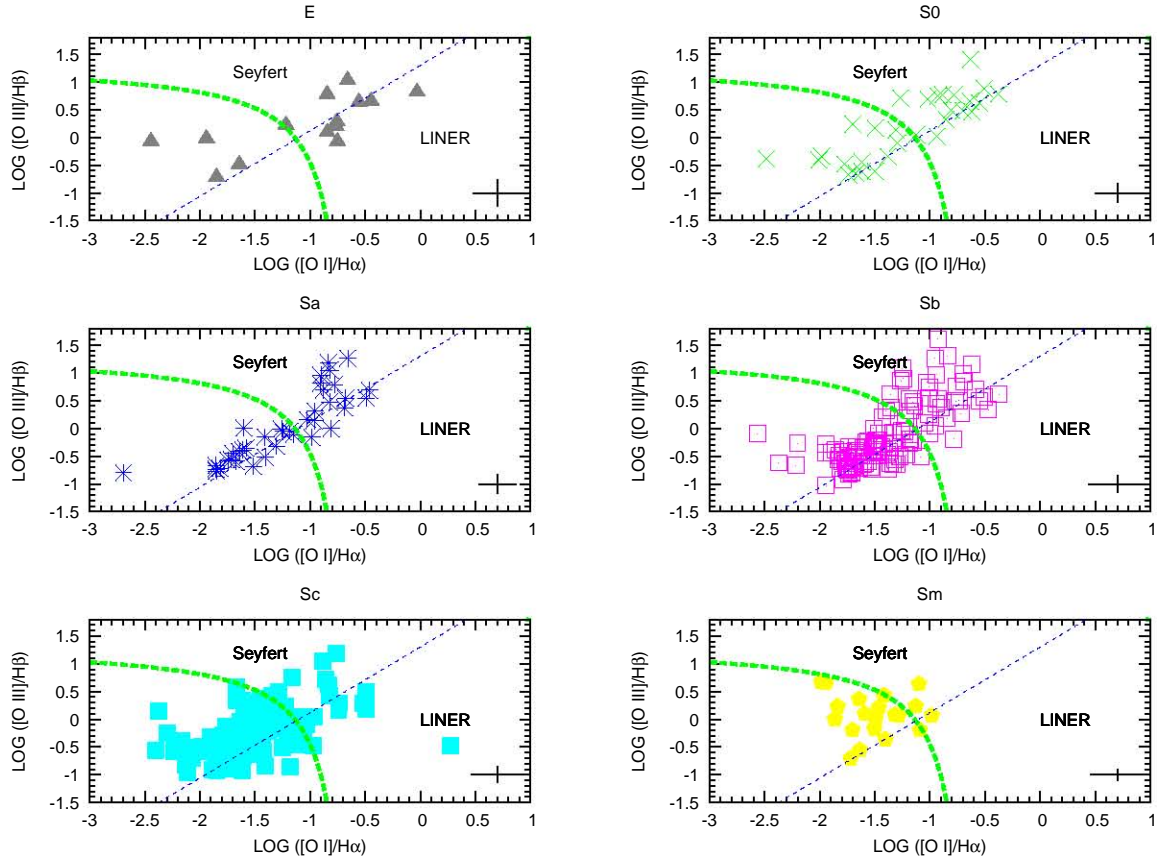
Figure 10. The [O I] diagnostic diagram for CIG sample. Labels like on Figure 7.

Table 4. Incidence type of nuclear activity for different morphologies from [S II] and [O I] diagnostic diagrams for CIG sample.

M.T.	[S II] Diagram				[O I] Diagram			
	Total	AGN	Seyfert	LINER	Total	AGN	Seyfert	LINER
E	14	11(79%)	3(27%)	8(73%)	13	10(77%)	3(30%)	7(70%)
S0	30	15(50%)	3(20%)	12(80%)	28	16(57%)	12(75%)	4(25%)
Sa	38	15(39%)	3(20%)	12(80%)	36	17(47%)	11(65%)	6(35%)
Sb	122	31(27%)	15(48%)	16(52%)	120	39(33%)	30(77%)	9(23%)
Sc	124	21(17%)	8(38%)	13(62%)	123	22(18%)	11(50%)	11(50%)
Sm	20	6(30%)	1(17%)	5(83%)	20	3(15%)	2(67%)	1(33%)
Total	348	99(28%)	33(33%)	66(67%)	340	107(31%)	69(64%)	38(36%)

Table 5. Incidence type of nuclear activity for different morphologies from [S II] and [O I] diagnostic diagrams for Varela's sample.

M.T.	[S II] Diagram				[O I] Diagram			
	Total	AGN	Seyfert	LINER	Total	AGN	Seyfert	LINER
E	4	2(50%)	0(0%)	2(100%)	4	1(25%)	1(100%)	0(0%)
S0	14	6(43%)	2(33%)	4(67%)	14	6(43%)	5(83%)	1(17%)
Sa	11	3(27%)	0(0%)	3(100%)	11	2(18%)	0(0%)	2(100%)
Sb	21	5(24%)	1(20%)	4(80%)	21	6(29%)	6(100%)	0(0%)
Sc	27	5(19%)	3(60%)	2(40%)	27	5(19%)	4(80%)	1(20%)
Sm	4	0(0%)	0(0%)	0(0%)	4	0(0%)	0(0%)	0(0%)
Total	81	21(26%)	6(29%)	15(71%)	81	20(25%)	16(80%)	4(20%)

consequence we only take into account the AGN activity with the Kewley limit for self-consistency.

We want to point out to recent models developed by Stasińska et al. (2006). These models predict lower values for the ratios of [N II]/Hα and [O III]/Hβ for AGN. In a Figure analogous to Fig. 7 the models by Stasińska et al. (2006) would produce an even larger zone of composite objects.

The most notable result is the absence of type 1 AGN in both isolated samples. In the CIG sample there are 12 galaxies which show lines with a broad component. Five of these galaxies (all of them classified as Seyfert nuclei) have a clear broad component, three are Sy 1.5 (KIG 214, KIG 747, KIG 1008), one is Sy 1.8 (KIG 749) and one is Sy 1.9 (KIG 349). Other three objects (KIG 204, KIG 603 and KIG 605) are classified as LINERs. For two additional AGN (KIG 553, KIG 591) a Seyfert/LINER classification was not possible. The remaining two objects are HII galaxies with broad components. Broad components in HII regions are rare but have indeed been found (e.g. Binette et al. 2009).

In Varela's sample there is only one 1.8 type Seyfert galaxy (PGC48521). This object was classified as Sy 1 in SIMBAB and Sy 1.9 in NED. It has been shown that a few galaxies can vary their type with time (e.g. Shapovalova et al. 2008, 2012). Whether this is the case, or this object was misclassified in SIMBAD has little relevance for our general conclusions.

To be conservative, we consider these 13 galaxies as the fraction of possible AGN with broad components (including the two HII galaxies to allow for any possible misclassification). These numbers indicate that the fraction of type 1 objects is $\lesssim 3\%$.

5 DISCUSSION

The large number of galaxies of all morphological types permits us to quantify the link between morphology and nuclear activity. Our results indicate a close link between these two properties. This implies that any result of the incidence of activity without this consideration reflects the particular morphological distribution of the sample and therefore is not reliable. Our sample includes for the first time a statistically significant number of isolated early type galaxies (E+S0).

We found that Elliptical and S0 galaxies have the highest incidence of nuclear activity in isolated environments when only galaxies with emission lines are considered (a similar result was found by Varela et al. (2004); Coziol et al. (2011); Sabater et al. (2012)). However, when the total sample is taken into account (including galaxies without emission lines) these apparent excess disappears and all early types (including Sa and Sb types) have similar fractions (see Fig. 5). This important difference could be found thanks to the large number of elliptical and spheroidal galaxies in our sample. This results are consistent with those found for "field" galaxies (Heckman 1980; Keel 1983; Kauffmann et al. 2003; Miller et al. 2003). Finding the same trend between isolated and field galaxies could be expected if we consider that AGN require SMBHs and black holes are correlated with bulges. However, the large number of AGN among isolated galaxies is of great importance and indicates that secular evolution processes can trigger/maintain low luminosity AGN activity (see below).

We consider as secular evolution the following mechanisms capable of driving gas into the nuclear region: 1) Minor mergers (luminosity ratio larger than 10 in our sample); 2) Dark matter accretion; 3)Non-axisymmetric gravitational perturbations.

With respect to dark matter, Hernandez & Lee (2010) showed from an analytical treatment of the accretion rate that, for the largest black hole masses of quasi-stellar objects ($>10^9$ M$_\odot$), the runaway regime would be reached on time-scales wich are shorter than the lifetimes of the halos in question for central dark matter densities in excess of 250 M$_\odot$/pc^3. This limit scales inversely with the black hole (BH) mass.

The most common non-axisymmetric internal potential is due to the presence of a bar. However in the particular case of barred galaxies it has been shown that most probably bars do not enhance nuclear activity (Moles et al. 1995; Ho et al. 1997c; Lee et al. 2012). The later authors look for the incidence of AGN activity in barred galaxies. Alonso et al. (2013) compare only AGN galaxies with and without bars. They find a trend for higher luminosity in the O [III] line for barred AGN. This effect is more noticeable for the more massive and luminous galaxies.

However the samples used in those studies were not rigorously isolated and thus the effects of the environment cannot be disentangled from those of the bar. The samples used in this work provide the opportunity to perform a rigorous test of the effect of a bar. This can be achieved due to both the selection criteria and the quality of the data. A detailed analysis of the bar fraction requires a deep photometric study. This analysis will be presented in a forthcoming paper (Hernández-Toledo et al. in preparation 2013).

We note that although a large fraction of isolated galaxies are active, their SMBH has not grown significantly over the last 3 Gyr. Given that most of our galaxies are representative of the low luminosity end of AGN, the mass accretion rate should be in the range of $10^{-5} - 10^{-3}$ M$_\odot$/yr, and the radiative efficiency η should be significantly smaller than 10 % (Ho 2003, 2009). Such low efficiencies are predicted for low luminosity AGN (Narayan & McClintock 2008). Assuming the AGN in our sample have accreted at a constant rate over the last 3 Gyr the growth of their SMBH ranges between $10^4 - 10^6$ M$_\odot$. Then, it is clear that isolated galaxies in poor environments have failed to accrete enough material (at least during the last Gyr) to present higher luminosities and significant black hole growth. Thus, our results support a hierarchical scenario in which the environment is crucial to determine properties such as luminosity, mass, and central SMBH mass, fulfilling the expectations of the downsizing for SMBH growth (Pérez-González et al. 2010).

The spiral isolated galaxies will not migrate from the blue to the red sequence since feedback is not efficient in these faint AGN (Krongold et al. 2007). The later result supports again that secular evolution in these galaxies is the important mechanism to establish the bulge-black hole relation. This is in contrast to the case of massive galaxies transitioning from the blue to the red branch of the color-color diagram which require a major merger followed by a substantial feedback in the QSO phase.

On the other hand our isolated ellipticals are already in the red-branch of galaxies that probably have experienced a major merger in the distant past. The fact that essen-

tially all of them are AGN may simply reflect the fact that it is easier to drive gas to the center of spheroidal systems. The remanent inter stellar medium (ISM) in these galaxies is typically in the range (10^6-10^7 M$_\odot$). Therefore, they contain enough gas to power their SMBH over the last 3 Gyr. This does not exclude, however, the possibility of an external supply of material as suggested by several authors (Bertola et al. 1992; Caon et al. 2000; Sarzi et al. 2006). The large fraction of AGN in these galaxies suggests that the presence of a large bulge facilitates the mass in fall to the center. We note, however, that a small fraction of this LINERS could be fake AGN ("retired galaxies", Cid Fernandes et al. (2011)).

All these results indicate that the presence of AGN activity is a common phenomenon. This is an important result as traditionally it has been assumed that an external perturbation is required to induce nuclear activity. Our results indicate that a low luminosity AGN phase is a part of the secular evolution of a large number of galaxies. These findings are consistent with those by Ho et al. (1997a,b); Ho (2002, and references therein). However, in those studies it was impossible to disentangle the environmental effects from those of internal galactic evolution, given that the isolation history was not known a priory in their samples. Our results do not deny the possibility that external perturbations may enhance the frequency of nuclear activity among galaxies, as has been suggested by previous studies (Dultzin-Hacyan et al. 1999; Krongold et al. 2002, 2003; Rogers et al. 2009; Ellison et al. 2010, 2011). The effect of a strong gravitational interaction will be studied in a forthcoming paper where the incidence of AGN in a sample of isolated close pairs of similar mass galaxies will be analyzed.

We note that the absence of type 1 AGN in these samples of isolated galaxies is outstanding. There is not a single type 1.0 AGN among the 175 active galaxies in our samples. The fraction of types 1.5-1.9 is less than 3 % in both isolated galaxy samples. There have been indications in the past for very low fractions of type 1 activity in physical pairs of galaxies (Dultzin et al. 2008), and in compact groups (Martínez et al. 2010). These results are at odds with a simple interpretation of the unified model (UM), and suggest that an additional evolutionary trend is at work. The appearance of a type 1 nucleus may be delayed by as much as 1 Gyr, as required by the evolutionary model proposed by Krongold et al. (2002), where an interaction triggers first a circumnuclear starburst, and subsequently non-thermal nuclear activity. For the brightest end of nuclear activity a similar evolutionary trend is possible (from ULIRGs to luminous quasars). In this case a major merger would be required, affecting the overall properties of the host galaxy and moving it to the blue branch of the color-color diagram.

The evolutionary scheme can explain the lack of Sy 1 in both interacting and isolated galaxies. In the former there has not been enough time for the Sy 1 nucleus to appear. In the latter (where no interactions took place over the last 3 Gyr), either there has never been a Sy 1 phase, or if a strong interaction occurred in the past, the type 1 activity has already faded out.

We also note that the lack of high luminosity AGN in our samples points towards a dependence between environment/interactions and AGN luminosity. In this scenario, the extremely low fraction of type 1 AGN can also be understood if a BLR (broad line region) can be formed only at higher accretion rates/luminosities (Nicastro 2000; Elitzur & Ho 2009).

If AGN in isolated galaxies have low accretion rates, low efficiencies, low luminosities and almost a complete absence of broad lines in their spectra, it is probable that the BLR under these circumstances is not even able to formed. This is in accordance with the result by Tran (2003a,b) for the absence of broad components in polarized light for $\sim$50% of the galaxies in his sample. Several studies show evidence that the Sy2s with and without broad lines in polarized lines (in other words with and without a hidden BLR) are truly different in other respects as well (e.g. Gu et al. 2001a,b; Bianchi et al. 2012).

REFERENCES

Abazajian K. N. et al., 2009, ApJS, 182, 543

Alonso M. S., Coldwell G., Lambas D. G., 2013, Astronomy and Astrophysics, 549, A141

Baldwin J. A., Phillips M. M., Terlevich R., 1981, Publications of the ASP, 93, 5

Barton E. J., Geller M. J., Kenyon S. J., 2000, ApJ, 530, 660

Bertola F., Buson L. M., Zeilinger W. W., 1992, ApJL, 401, L79

Bianchi S. et al., 2012, MNRAS, 426, 3225

Binette L., Drissen L., Ubeda L., Raga A. C., Robert C., Krongold Y., 2009, Astronomy and Astrophysics, 500, 817

Caon N., Macchetto D., Pastoriza M., 2000, ApJS, 127, 39

Cid Fernandes R., Stasińska G., Mateus A., Vale Asari N., 2011, MNRAS, 413, 1687

Coziol R., Torres-Papaqui J. P., Plauchu-Frayn I., Islas-Islas J. M., Ortega-Minakata R. A., Neri-Larios D. M., Andernach H., 2011, Revista Mexicana de Astronomía y Astrofísica, 47, 361

Dahari O., 1985, ApJS, 57, 643

Dahari O. A., 1984, PhD thesis, California Univ., Santa Cruz.

de Mello D. F., Keel W. C., Sulentic J. W., Rampazzo R., 1995, in van der Kruit P. C., Gilmore G., eds, IAU Symposium Vol. 164, Stellar Populations. p. 434

de Mello D. F., Sulentic J. W., de Souza R. E., Reduzzi L., Rampazzo R., 1996, Astronomy and Astrophysics, 308, 387

Dultzin D. et al., 2008, ArXiv e-prints

Dultzin-Hacyan D., Krongold Y., Fuentes-Guridi I., Marziani P., 1999, ApJL, 513, L111

Elitzur M., Ho L. C., 2009, ApJL, 701, L91

Ellison S. L., Patton D. R., Mendel J. T., Scudder J. M., 2011, MNRAS, 418, 2043

Ellison S. L., Patton D. R., Simard L., McConnachie A. W., Baldry I. K., Mendel J. T., 2010, MNRAS, 407, 1514

Gu Q., Dultzin-Hacyan D., de Diego J. A., 2001, Revista Mexicana de Astronomía y Astrofísica, 37, 3

Gu Q., Maiolino R., Dultzin-Hacyan D., 2001, Astronomy and Astrophysics, 366, 765

Hao L. et al., 2005, Astronomical Journal, 129, 1783

Heckman T. M., 1980, Astronomy and Astrophysics, 87, 142

Hernandez X., Lee W. H., 2010, MNRAS, 404, L6

Hernández Toledo H. M., Dultzin-Hacyan D., Gonzalez J. J., Sulentic J. W., 1999, Astronomical Journal, 118, 108

Hernández-Toledo H. M., Vázquez-Mata J. A., Martínez-Vázquez L. A., Choi Y.-Y., Park C., 2010, Astronomical Journal, 139, 2525

Ho L. C., 2002, in Green R. F., Khachikian E. Y., Sanders D. B., eds, Astronomical Society of the Pacific Conference Series Vol. 284, IAU Colloq. 184: AGN Surveys. p. 13

Ho L. C., 2003, in Collin S., Combes F., Shlosman I., eds, Astronomical Society of the Pacific Conference Series Vol. 290, Active Galactic Nuclei: From Central Engine to Host Galaxy. p. 379

Ho L. C., 2009, ApJ, 699, 626

Ho L. C., Filippenko A. V., Sargent W. L. W., 1997a, ApJS, 112, 315

Ho L. C., Filippenko A. V., Sargent W. L. W., 1997b, ApJ, 487, 568

Ho L. C., Filippenko A. V., Sargent W. L. W., 1997c, ApJ, 487, 591

Karachentsev I. D., Makarov D. I., Karachentseva V. E., Melnyk O. V., 2011, Astrophysical Bulletin, 66, 1

Karachentseva V. E., 1973, Soobshcheniya Spetsial'noj Astrofizicheskoj Observatorii, 8, 3

Karachentseva V. E., Mitronova S. N., Melnyk O. V., Karachentsev I. D., 2010, in Verdes-Montenegro L., Del Olmo A., Sulentic J., eds, Astronomical Society of the Pacific Conference Series Vol. 421, Galaxies in Isolation: Exploring Nature Versus Nurture. p. 11

Kauffmann G. et al., 2003, MNRAS, 346, 1055

Keel W. C., 1983, ApJ, 269, 466

Keel W. C., 1993, Astronomical Journal, 106, 1771

Kennicutt Jr. R. C., Keel W. C., 1984, ApJL, 279, L5

Kennicutt Jr. R. C., Roettiger K. A., Keel W. C., van der Hulst J. M., Hummel E., 1987, Astronomical Journal, 93, 1011

Kewley L. J., Dopita M. A., Sutherland R. S., Heisler C. A., Trevena J., 2001, ApJ, 556, 121

Koulouridis E., Chavushyan V., Plionis M., Krongold Y., Dultzin-Hacyan D., 2006, ApJ, 651, 93

Koulouridis E., Plionis M., Chavushyan V., Dultzin-Hacyan D., Krongold Y., Goudis C., 2006, ApJ, 639, 37

Krongold Y., Dultzin-Hacyan D., Marziani P., 2001, Astronomical Journal, 121, 702

Krongold Y., Dultzin-Hacyan D., Marziani P., 2002, 572, 169

Krongold Y., Dultzin-Hacyan D., Marziani P., 2003, in Collin S., Combes F., Shlosman I., eds, Astronomical Society of the Pacific Conference Series Vol. 290, Active Galactic Nuclei: From Central Engine to Host Galaxy. p. 523

Krongold Y., Nicastro F., Elvis M., Brickhouse N., Binette L., Mathur S., Jiménez-Bailón E., 2007, ApJ, 659, 1022

Laurikainen E., Salo H., 1995, Astronomy and Astrophysics, 293, 683

Lee G.-H., Woo J.-H., Lee M. G., Hwang H. S., Lee J. C., Sohn J., Lee J. H., 2012, ApJ, 750, 141

Lin L. et al., 2007, ApJL, 660, L51

Lonsdale C. J., Persson S. E., Matthews K., 1984, ApJ, 287, 95

Márquez I., Masegosa J., 2008, in Revista Mexicana de Astronomia y Astrofisica Conference Series. pp 150–154

Martínez M. A., Del Olmo A., Coziol R., Perea J., 2010, Astronomical Journal, 139, 1199

Miller C. J., Nichol R. C., Gómez P. L., Hopkins A. M., Bernardi M., 2003, ApJ, 597, 142

Moles M., Marquez I., Perez E., 1995, ApJ, 438, 604

Narayan R., McClintock J. E., 2008, New Astronomy Reviews, 51, 733

Nicastro F., 2000, ApJL, 530, L65

Pérez-González P. G., Alonso-Herrero A., Donley J., Rieke G., Barro G., Gallego J., Zamorano J., 2010, in Diego J. M., Goicoechea L. J., González-Serrano J. I., Gorgas J., eds, Highlights of Spanish Astrophysics V. p. 337

Pimbblet K. A., Jensen P. C., 2012, MNRAS, 426, 1632

Pimbblet K. A., Shabala S. S., Haines C. P., Fraser-McKelvie A., Floyd D. J. E., 2013, MNRAS, 429, 1827

Rogers B., Ferreras I., Kaviraj S., Pasquali A., Sarzi M., 2009, MNRAS, 399, 2172

Ruderman J. T., Ebeling H., 2005, ApJL, 623, L81

Sabater J., Verdes-Montenegro L., Leon S., Best P., Sulentic J., 2012, Astronomy and Astrophysics, 545, A15

Sarzi M. et al., 2006, MNRAS, 366, 1151

Schmitt H. R., 2001, Astronomical Journal, 122, 2243

Shapovalova A. I. et al., 2012, ApJS, 202, 10

Shapovalova A. I., Popović L. Č., Collin e. a., 2008, Astronomy and Astrophysics, 486, 99

Sorrentino G., Radovich M., Rifatto A., 2006, Astronomy and Astrophysics, 451, 809

Stasińska G., Cid Fernandes R., Mateus A., Sodré L., Asari N. V., 2006, MNRAS, 371, 972

Stauffer J. R., 1982a, ApJ, 262, 66

Stauffer J. R., 1982b, ApJS, 50, 517

Storchi-Bergmann T., 2008, in Revista Mexicana de Astronomia y Astrofisica Conference Series. pp 139–146

Sulentic J. W. et al., 2006, Astronomy and Astrophysics, 449, 937

Tran H. D., 2003a, ApJ, 583, 632

Tran H. D., 2003b, in Collin S., Combes F., Shlosman I., eds, Astronomical Society of the Pacific Conference Series Vol. 290, Active Galactic Nuclei: From Central Engine to Host Galaxy. p. 31

Trouille L., Barger A. J., Tremonti C., 2011, ApJ, 742, 46

Varela J., Moles M., Márquez I., Galletta G., Masegosa J., Bettoni D., 2004, Astronomy and Astrophysics, 420, 873

Veilleux S., Osterbrock D. E., 1987, ApJS, 63, 295

Verdes-Montenegro L., Sulentic J., Lisenfeld U., Leon S., Espada D., Garcia E., Sabater J., Verley S., 2005, Astronomy and Astrophysics, 436, 443

Verley S. et al., 2007, Astronomy and Astrophysics, 472, 121

von der Linden A., Wild V., Kauffmann G., White S. D. M., Weinmann S., 2010, MNRAS, 404, 1231

Winkler H., 1992, MNRAS, 257, 677

Woods D. F., Geller M. J., 2007, Astronomical Journal,

12   *F. J. Hernández-Ibarra, D. Dultzin, Y. Krongold, A. Del Olmo, J. Perea, J. González*

134, 527

Table 6: Logarithm intensity ratios with their errors and AGN type for
the CIG sample. M.T.- Morphological Type. AGN classification denotes
those galaxies that are AGN according to the [N II] diagrams but not
to the [S II] and/or [O I]. † L-S classification means that galaxies fall
in the separation line for Seyfert and LINER according to [S II] and
[O I] diagrams. * Type with weak broad component in permitted lines.
Seyfert quantitative classification according to Winkler (1992).

Object	M.T. [a]	LOG([OIII]/Hβ)	LOG([N II]/Hα)	LOG([S II]/Hα)	LOG([O I]/Hα)	Type
Elliptical						
KIG378	E	0.2831 ± 0.1763	0.2970 ± 0.0806	0.0332 ± 0.1534	-0.7559± 0.3383	LINER
KIG393	E-SO	-0.0234 ± 0.0074	-0.4586 ± 0.0066	-0.6059 ± 0.0091	-1.9412±0.0287	HII
KIG437	E-SO	0.0909 ± 0.1939	0.0919 ± 0.0589	-0.1233 ± 0.1182	-0.8432± 0.2380	LINER
KIG462	E	-0.7172 ± 0.0384	-0.4667 ± 0.0098	-0.5874 ± 0.0155	-1.8481± 0.0740	HII
KIG555	E	0.2234 ± 0.0401	-0.8536 ± 0.0429	-0.3324 ± 0.0298	-1.2193± 0.0865	HII
KIG556	E	0.8151 ± 0.5101	0.5997 ± 0.2621	0.8841 ± 0.2651	-0.0295± 0.4288	LINER
KIG582	E	1.0277 ± 0.6437	0.4476 ± 0.1483	0.3357 ± 0.2130	-0.6587± 0.5464	LINER
KIG595	E	-0.0732 ± 0.2877	-0.0465 ± 0.2346	-0.0569 ± 0.3745	-	LINER
KIG602	E	0.2051 ± 0.1068	-0.0084 ± 0.0247	-0.1233 ± 0.0420	-0.7662± 0.0711	LINER
KIG685	E	-0.0750 ± 0.1945	0.2877 ± 0.2436	0.1754 ± 0.3742	-0.7523± 1.0180	LINER
KIG705	E	0.6353 ± 0.5484	0.4970 ± 0.0898	0.1829 ± 0.1587	-0.5566± 0.3031	LINER
KIG735	E-S0	0.6529 ± 0.3846	0.0049 ± 0.1637	-0.1656 ± 0.3282	-0.4449± 0.3062	L-S†
KIG768	E	-0.4878 ± 0.0242	-0.4003 ± 0.0090	-0.5381 ± 0.0142	-1.6419± 0.0481	HII
KIG1029	E	0.7769 ± 0.2027	0.0280 ± 0.0334	-0.1154 ± 0.0598	-0.8457± 0.1231	Sy2
Spheroidal						
KIG213	S0a	0.4819 ± 0.1403	0.2505 ± 0.0532	-0.0091 ± 0.1031	-0.6965 ± 0.1868	S-L†
KIG228	S0	-0.3462 ± 0.1376	-0.2004 ± 0.0294	-0.5771 ± 0.0894	-1.3772 ± 0.2291	AGN
KIG244	S0-a	-0.4046 ± 0.1778	-0.3080 ± 0.0441	-0.5467 ± 0.1134	-2.0040 ± 1.2503	HII
KIG272	S0-a	-0.6374 ± 0.0387	-0.4888 ± 0.0104	-0.5050 ± 0.0158	-1.6710 ± 0.0644	HII
KIG332	S0	0.7437 ± 0.0367	-0.0622 ± 0.0176	-0.2335 ± 0.0310	-0.9269 ± 0.0562	Sy2
KIG338	S0	0.6551 ± 0.2278	0.0325 ± 0.0833	0.0000 ± 0.1304	-0.6331 ± 0.2261	S-L†
KIG349	S0-a	0.3299 ± 0.0320	-0.1181 ± 0.0072	-0.2973 ± 0.0126	-1.1286 ± 0.0261	Sy1.9
KIG394	S0-a	0.1737 ± 0.0405	-0.2196 ± 0.0171	-0.3860 ± 0.0321	-1.4940 ± 0.1219	AGN
KIG413	S0-a	0.7853 ± 0.5114	0.2708 ± 0.0746	0.1349 ± 0.1219	-0.3785 ± 0.1575	S-L†
KIG441	S0-a	-0.1001 ± 0.0430	-0.5103 ± 0.0184	-0.3426 ± 0.0245	-1.2934 ± 0.0697	HII
KIG460	S0-a	-0.4401 ± 0.0373	-0.4800 ± 0.0120	-0.4691 ± 0.0181	-1.6159 ± 0.0721	HII
KIG480	S0-a	0.4907 ± 0.0396	0.0117 ± 0.0140	-0.0060 ± 0.0200	-0.8059 ± 0.0399	S-L†
KIG483	S0	0.3258 ± 0.2015	0.2305 ± 0.0747	0.1035 ± 0.1225	-0.8513 ± 0.3551	LINER
KIG485	S0	0.7681 ± 0.1890	0.3413 ± 0.1876	0.3951 ± 0.2365	-0.8834 ± 1.0911	S-L†
KIG501	S0-a	0.0201 ± 0.1278	-0.0320 ± 0.0430	-0.2650 ± 0.0960	-0.9375 ± 0.1773	LINER
KIG504	S0-a	-0.6740 ± 0.0316	-0.4325 ± 0.0086	-0.5243 ± 0.0135	-1.7358 ± 0.0537	HII
KIG571	S0	-0.6063 ± 0.3602	-0.2589 ± 0.0405	-0.3824 ± 0.0783	-1.4961 ± 0.4203	AGN
KIG577	S0	0.2411 ± 0.0122	-1.2983 ± 0.0253	-0.6328 ± 0.0151	-1.6963 ± 0.0596	HII
KIG586	S0	0.7678 ± 1.1443	0.2291 ± 0.0869	0.0838 ± 0.1498	-0.7745 ± 0.3665	S-L†
KIG591	S0-a	0.7111 ± 0.0342	-0.2711 ± 0.0097	-0.4634 ± 0.0129	-1.2657 ± 0.0211	S-L†
KIG592	S0	-0.4802 ± 0.0135	-0.2864 ± 0.0049	-0.5709 ± 0.0084	-1.7710 ± 0.0342	AGN
KIG614	S0	0.6198 ± 0.3960	0.2532 ± 0.0730	0.2217 ± 0.1040	-0.5475 ± 0.1990	LINER
KIG616	S0-a	0.0445 ± 0.1190	-0.0163 ± 0.0317	-0.2263 ± 0.0646	-1.1197 ± 0.1822	AGN
KIG665	S0-a	-0.3872 ± 0.2416	-0.2928 ± 0.0334	-0.3188 ± 0.0597	-	AGN
KIG678	S0-a	-0.3386 ± 0.0098	-0.3503 ± 0.0050	-0.6172 ± 0.0078	-1.9816 ± 0.0325	HII
KIG697	S0	0.6852 ± 0.1816	0.3973 ± 0.1063	0.1287 ± 0.1877	-1.0169 ± 0.8012	S-L†
KIG698	S0-a	0.8826 ± 0.3627	0.0618 ± 0.1145	0.1613 ± 0.1473	-0.5063 ± 0.2470	S-L†
KIG893	S0	1.4052 ± 0.0713	0.1830 ± 0.0197	-0.1051 ± 0.0382	-0.6296 ± 0.0517	Sy2

Object	M.T. [a]	LOG([OIII]/Hβ)	LOG([N II]/Hα)	LOG([S II]/Hα)	LOG([O I]/Hα)	Type
KIG903	S0	0.4668 ± 0.0943	-0.0474 ± 0.0432	0.0909 ± 0.0539	-0.6165 ± 0.0963	LINER
KIG1014	S0-a	-0.6140 ± 0.0522	-0.3787 ± 0.0114	-0.5127 ± 0.0204	-1.6142 ± 0.0813	HII
KIG1032	S0-a	0.1383 ± 0.0203	-0.8297 ± 0.0181	-0.3772 ± 0.0150	-1.3063 ± 0.0422	HII

Sa

KIG60	Sab	-0.3866 ± 0.0555	-0.4230 ± 0.0172	-0.3848 ± 0.0253	-1.6110 ± 0.1263	HII
KIG223	Sa	-0.6819 ± 0.1626	-0.4807 ± 0.0272	-0.7504 ± 0.0713	-1.5133 ± 0.1730	HII
KIG231	Sab	-0.5167 ± 0.0964	-0.2686 ± 0.0164	-0.4271 ± 0.0323	-1.4044 ± 0.0995	AGN
KIG236	SBa	-0.7215 ± 0.0548	-0.4210 ± 0.0119	-0.6344 ± 0.0232	-1.8161 ± 0.1170	HII
KIG258	SBab	-0.5920 ± 0.0248	-0.3249 ± 0.0085	-0.4913 ± 0.0129	-1.6713 ± 0.0451	HII
KIG285	SBab	1.0432 ± 0.4782	0.3912 ± 0.0760	0.2782 ± 0.1113	-0.8187 ± 0.3631	S-L†
KIG287	SABa	-0.6678 ± 0.0682	-0.3596 ± 0.0102	-0.5863 ± 0.0211	-1.8515 ± 0.1293	HII
KIG298	SBa	-0.0011 ± 0.1879	0.2557 ± 0.0732	-0.0676 ± 0.1584	-0.8098 ± 0.3546	LINER
KIG304	SBab	-0.1576 ± 0.1155	-0.2774 ± 0.0276	-0.3806 ± 0.0509	-1.4082 ± 0.2109	AGN
KIG327	Sab	1.1816 ± 1.2340	0.0599 ± 0.0641	-0.1092 ± 0.1248	-0.8344 ± 0.2536	Sy2
KIG334	Sab	0.4732 ± 0.2825	-0.2691 ± 0.0651	0.0610 ± 0.0682	-0.8230 ± 0.1900	S-L†
KIG351	Sab	0.1406 ± 0.2719	-0.0577 ± 0.0659	-0.1010 ± 0.1179	-0.9593 ± 0.3057	LINER
KIG374	Sab	-0.1091 ± 0.0600	-0.2005 ± 0.0174	-0.4553 ± 0.0437	-1.1498 ± 0.0908	AGN
KIG456	Sa	0.1581 ± 0.1621	0.0700 ± 0.0371	-0.1297 ± 0.0720	-1.0251 ± 0.2010	LINER
KIG475	Sab	0.6911 ± 0.5663	0.1942 ± 0.0818	-0.0247 ± 0.1525	-0.4609 ± 0.1821	S-L†
KIG491	SABa	-0.5626 ± 0.0523	-0.3131 ± 0.0105	-0.5756 ± 0.0218	-1.7119 ± 0.0938	HII
KIG500	Sab	0.5456 ± 0.2248	0.4682 ± 0.0888	0.4216 ± 0.1182	-0.4914 ± 0.2584	LINER
KIG505	Sab	-0.3583 ± 0.0419	-0.5140 ± 0.0156	-0.3898 ± 0.0199	-1.5789 ± 0.0897	HII
KIG539	Sab	0.8060 ± 0.3284	0.1381 ± 0.0699	0.0253 ± 0.1168	-0.9064 ± 0.3378	Sy2
KIG544	SBa	0.9565 ± 0.0199	0.0818 ± 0.0132	-0.1683 ± 0.0233	-0.9021 ± 0.0433	Sy2
KIG579	Sab	0.6906 ± 0.1883	0.1090 ± 0.0857	0.1058 ± 0.1273	-0.8792 ± 0.3909	S-L†
KIG587	Sab	-0.0494 ± 0.1044	-0.0844 ± 0.0513	0.0225 ± 0.0683	-1.1843 ± 0.3363	LINER
KIG596	Sab	0.5441 ± 0.2149	0.3872 ± 0.0477	0.2939 ± 0.0681	-0.6766 ± 0.1792	LINER
KIG605	SBab	0.3735 ± 0.0829	0.0719 ± 0.0317	0.0704 ± 0.0445	-0.6850 ± 0.0857	LINER*
KIG609	Sab	-0.4148 ± 0.0592	-0.4391 ± 0.0184	-0.3427 ± 0.0241	-1.6384 ± 0.1414	HII
KIG620	Sa	-0.7380 ± 0.0371	-0.3948 ± 0.0095	-0.6545 ± 0.0177	-1.8541 ± 0.0793	HII
KIG622	SBa	-0.4486 ± 0.0280	-0.2958 ± 0.0094	-0.4994 ± 0.0158	-1.7003 ± 0.0676	AGN
KIG633	Sa	-0.5798 ± 0.0375	-0.4364 ± 0.0117	-0.4775 ± 0.0179	-1.7460 ± 0.0978	HII
KIG641	SBa	-0.1560 ± 0.0356	-0.0700 ± 0.0117	-0.2408 ± 0.0209	-0.9847 ± 0.0409	LINER
KIG643	Sab	1.2605 ± 0.1875	0.3219 ± 0.0394	-0.0545 ± 0.0832	-0.6583 ± 0.1328	AGN
KIG669	Sa	-0.0118 ± 0.0445	-0.1884 ± 0.0128	-0.2522 ± 0.0163	-1.2563 ± 0.0363	AGN
KIG689	Sa	-0.0512 ± 0.0503	-0.5467 ± 0.0273	-0.2447 ± 0.0290	-1.2447 ± 0.0911	HII
KIG690	Sa	-0.3202 ± 0.2628	-0.2693 ± 0.0435	-0.5399 ± 0.1168	-1.3068 ± 0.2894	AGN
KIG694	Sa	0.3090 ± 0.1477	0.3362 ± 0.0473	0.2738 ± 0.0670	-0.9554 ± 0.2908	S-L†
KIG695	Sa	-0.8004 ± 0.2952	-0.2958 ± 0.0331	-0.5470 ± 0.0828	-	HII
KIG696	Sab	0.7896 ± 0.5096	0.1894 ± 0.0604	0.1316 ± 0.0927	-0.7796 ± 0.2419	S-L†
KIG726	SBa	0.0040 ± 0.0216	-0.2250 ± 0.0085	-0.5556 ± 0.0171	-1.6008 ± 0.0601	LINER
KIG751	Sa	-0.7696 ± 0.0622	-0.3224 ± 0.0103	-0.6736 ± 0.0229	-1.8492 ± 0.1155	HII

Sb

KIG56	Sb	-0.7559 ± 0.0348	-0.3010 ± 0.0085	-0.5817 ± 0.0149	-1.7328 ± 0.0589	HII
KIG187	SABb	1.6055 ± 0.4364	0.3196 ± 0.0426	-0.1455 ± 0.1105	-0.9294 ± 0.2553	Sy2
KIG204	Sbc	0.5674 ± 0.1174	0.1586 ± 0.0394	0.1695 ± 0.0532	-0.5080 ± 0.0865	LINER*
KIG208	Sb	-0.3569 ± 0.1560	-0.4187 ± 0.0289	-0.3145 ± 0.0393	-1.6075 ± 0.2612	HII
KIG211	Sb	0.5423 ± 0.2881	0.5772 ± 0.0972	0.3688 ± 0.1446	-1.0157 ± 0.8193	S-L†
KIG212	SABb	-0.0853 ± 0.0922	-0.4301 ± 0.0478	-0.2048 ± 0.0532	-1.0000 ± 0.1272	HII
KIG214	Sb	0.9009 ± 0.0800	-0.4887 ± 0.0567	-0.4235 ± 0.0581	-1.2426 ± 0.0934	Sy1.5
KIG220	Sb	0.4774 ± 0.5816	0.0746 ± 0.0781	-0.2010 ± 0.1732	-1.1532 ± 0.5865	Sy2

Object	M.T. [a]	LOG([OIII]/Hβ)	LOG([N II]/Hα)	LOG([S II]/Hα)	LOG([O I]/Hα)	Type
KIG222	SABb	-0.6667 ± 0.1988	-0.3135 ± 0.0219	-0.5975 ± 0.0542	-2.2160 ± 0.8544	HII
KIG226	Sbc	0.8337 ± 0.0774	-0.0526 ± 0.0339	-0.2098 ± 0.0659	-1.0294 ± 0.1616	Sy2
KIG238	Sb	-0.7053 ± 0.0381	-0.3338 ± 0.0089	-0.6206 ± 0.0162	-1.8174 ± 0.0707	HII
KIG242	Sb	0.1977 ± 0.0211	-0.7730 ± 0.0188	-0.4173 ± 0.0191	-1.4277 ± 0.0582	HII
KIG249	Sbc	-0.2851 ± 0.0659	-0.5030 ± 0.0262	-0.2970 ± 0.0348	-1.4178 ± 0.1369	HII
KIG250	SABb	0.2520 ± 0.0252	-0.5367 ± 0.0152	-0.3095 ± 0.0175	-1.0134 ± 0.0320	HII
KIG252	Sbc	-0.2762 ± 0.1683	-0.2896 ± 0.0270	-0.3764 ± 0.0502	-1.5128 ± 0.2730	AGN
KIG270	Sbc	-0.3287 ± 0.0215	-0.3372 ± 0.0068	-0.5713 ± 0.0123	-1.7360 ± 0.0485	HII
KIG274	Sbc	-0.3233 ± 0.0227	-0.1458 ± 0.0064	-0.5038 ± 0.0115	-1.5038 ± 0.0298	AGN
KIG275	Sbc	-0.2095 ± 0.2588	-0.1943 ± 0.0376	-0.5096 ± 0.1029	-1.4779 ± 0.4432	AGN
KIG278	SBb	0.4472 ± 0.0813	-0.1489 ± 0.0624	0.0039 ± 0.0784	-0.9399 ± 0.2305	S-L†
KIG284	Sb	-0.6951 ± 0.0469	-0.5003 ± 0.0133	-0.5432 ± 0.0194	-1.6981 ± 0.0839	HII
KIG288	Sbc	-0.7337 ± 0.1083	-0.4823 ± 0.0206	-0.5405 ± 0.0409	-1.5252 ± 0.1363	HII
KIG311	Sbc	-0.6742 ± 0.0351	-0.4130 ± 0.0093	-0.5772 ± 0.0162	-1.6907 ± 0.0579	HII
KIG318	Sbc	0.5347 ± 0.7083	-0.1096 ± 0.0622	-0.3835 ± 0.1517	-1.1860 ± 0.3973	Sy2
KIG329	SBbc	0.5302 ± 0.2424	0.2064 ± 0.0702	-0.0162 ± 0.1327	-0.9224 ± 0.3719	S-L†
KIG333	Sbc	0.1772 ± 0.3288	-0.1385 ± 0.0752	-0.4639 ± 0.2067	-1.2180 ± 0.5029	AGN
KIG336	Sbc	-0.3357 ± 0.0250	-0.3257 ± 0.0105	-0.6850 ± 0.0208	-1.6651 ± 0.0658	HII*
KIG339	SBb	-0.6792 ± 0.0285	-0.3253 ± 0.0070	-0.6463 ± 0.0123	-1.7276 ± 0.0545	HII
KIG340	Sb	-0.2186 ± 0.1314	-0.3560 ± 0.0248	-0.4696 ± 0.0476	-1.4898 ± 0.1825	HII
KIG344	SBbc	-0.4169 ± 0.1361	-0.3762 ± 0.0350	-0.3059 ± 0.0546	-1.4624 ± 0.3040	HII
KIG356	Sb	-0.2596 ± 0.0378	-0.5304 ± 0.0188	-0.3174 ± 0.0230	-1.5083 ± 0.0991	HII
KIG364	Sb	-0.5493 ± 0.0279	-0.3674 ± 0.0079	-0.5175 ± 0.0130	-1.7447 ± 0.0538	HII
KIG366	SBb	-0.5647 ± 0.0526	-0.3177 ± 0.0100	-0.6205 ± 0.0223	-1.8340 ± 0.1178	HII
KIG372	Sb	-0.5201 ± 0.1946	-0.3069 ± 0.0221	-0.5438 ± 0.0483	-1.7394 ± 0.2948	HII
KIG375	Sb	0.7428 ± 0.7061	0.0497 ± 0.0597	-0.0861 ± 0.1054	-1.0066 ± 0.3168	S-L†
KIG381	Sbc	0.6149 ± 0.2660	0.6296 ± 0.1128	0.3971 ± 0.1658	-0.3771 ± 0.2953	LINER
KIG392	Sbc	0.3348 ± 0.1306	0.3275 ± 0.0466	0.2675 ± 0.0660	-0.4700 ± 0.1158	LINER
KIG401	SBbc	0.3140 ± 0.0744	-0.1632 ± 0.0206	-0.4415 ± 0.0486	-1.3965 ± 0.1591	AGN
KIG409	Sbc	-0.4652 ± 0.0483	-0.4932 ± 0.0147	-0.4599 ± 0.0216	-1.6408 ± 0.0949	HII
KIG411	Sbc	-0.0965 ± 0.2583	-0.0994 ± 0.0566	-0.3848 ± 0.1436	-	AGN
KIG414	Sb	0.4089 ± 0.0815	-0.2854 ± 0.0323	-0.4811 ± 0.0687	-1.1393 ± 0.1334	Sy2
KIG416	Sbc	-0.0035 ± 0.0237	-0.6216 ± 0.0137	-0.4171 ± 0.0161	-1.5132 ± 0.0595	HII
KIG417	Sbc	-0.7014 ± 0.3008	-0.3908 ± 0.0365	-0.8276 ± 0.1388	-1.5380 ± 0.3208	HII
KIG418	Sb	-0.4979 ± 0.0525	-0.4424 ± 0.0141	-0.4539 ± 0.0230	-1.4771 ± 0.0745	HII
KIG419	Sb	-0.2301 ± 0.0718	-0.2639 ± 0.0207	-0.5163 ± 0.0468	-1.5582 ± 0.2150	AGN
KIG427	Sbc	-0.2588 ± 0.0969	-0.1719 ± 0.0221	-0.4055 ± 0.0489	-1.1845 ± 0.1088	AGN
KIG430	Sbc	-0.5050 ± 0.0699	-0.2389 ± 0.0148	-0.3164 ± 0.0232	-1.2753 ± 0.0690	AGN
KIG450	Sb	-0.5942 ± 0.0750	-0.4627 ± 0.0172	-0.4417 ± 0.0260	-1.5650 ± 0.1121	HII
KIG451	Sb	-0.5078 ± 0.3730	-0.3353 ± 0.0555	-0.3692 ± 0.0997	-1.0835 ± 0.2247	HII
KIG457	Sbc	-0.2455 ± 0.0855	-0.2619 ± 0.0187	-0.2974 ± 0.0299	-1.1537 ± 0.0723	AGN
KIG458	Sbc	-0.6233 ± 0.1419	-0.3485 ± 0.0320	-0.4470 ± 0.0553	-1.3634 ± 0.1758	HII
KIG459	Sb	-0.6314 ± 0.0646	-0.5119 ± 0.0160	-0.4322 ± 0.0231	-1.5847 ± 0.0999	HII
KIG478	SABb	0.9666 ± 0.0553	0.1210 ± 0.0209	-0.1885 ± 0.0411	-0.9420 ± 0.0846	Sy2
KIG482	SABb	-0.6511 ± 0.3409	-0.3357 ± 0.0404	-0.4804 ± 0.0872	-1.2983 ± 0.2823	HII
KIG492	Sbc	0.3795 ± 0.1389	0.0537 ± 0.0361	-0.0790 ± 0.0629	-0.9022 ± 0.1503	S-L†
KIG493	Sb	-0.4810 ± 0.1741	-0.3907 ± 0.0302	-0.6328 ± 0.0742	-1.2148 ± 0.1249	HII
KIG497	Sb	-0.1938 ± 0.2375	-0.2924 ± 0.0457	-0.3791 ± 0.0916	-1.1761 ± 0.2208	AGN
KIG499	SBb	1.3071 ± 0.0608	0.0680 ± 0.0245	0.3363 ± 0.0253	-0.8398 ± 0.0850	Sy2
KIG507	Sbc	-0.2549 ± 0.1119	-0.5063 ± 0.0321	-0.2508 ± 0.0385	-1.3137 ± 0.1492	HII
KIG508	SBbc	-0.2771 ± 0.0096	-0.4934 ± 0.0064	-0.6521 ± 0.0100	-1.9427 ± 0.0348	HII
KIG510	Sbc	-0.3310 ± 0.0878	-0.3774 ± 0.0244	-0.3850 ± 0.0427	-1.4373 ± 0.1662	HII
KIG515	Sb	-0.6491 ± 0.0964	-0.4443 ± 0.0170	-0.5844 ± 0.0342	-1.6011 ± 0.1212	HII
KIG516	Sb	-0.4099 ± 0.0935	-0.4174 ± 0.0238	-0.3979 ± 0.0386	-1.3665 ± 0.1224	HII
KIG522	Sb	-0.4912 ± 0.0194	-0.2656 ± 0.0070	-0.6237 ± 0.0126	-1.8270 ± 0.0513	AGN
KIG525	SBb	-0.3920 ± 0.0297	-0.2504 ± 0.0100	-0.4911 ± 0.0183	-1.5030 ± 0.0568	AGN
KIG532	SBb	-0.4238 ± 0.0209	-0.5065 ± 0.0092	-0.5153 ± 0.0128	-1.7892 ± 0.0529	HII
KIG537	Sb	-0.6258 ± 0.0272	-0.2873 ± 0.0070	-0.5099 ± 0.0118	-1.6709 ± 0.0473	HII
KIG541	SABb	-0.5613 ± 0.2814	-0.3372 ± 0.0313	-0.3167 ± 0.0555	-1.3202 ± 0.1954	HII

Object	M.T. [a]	LOG([OIII]/Hβ)	LOG([N II]/Hα)	LOG([S II]/Hα)	LOG([O I]/Hα)	Type
KIG542	Sb	-0.7254 ± 0.0482	-0.4622 ± 0.0106	-0.5439 ± 0.0165	-1.7508 ± 0.0812	HII
KIG550	SBbc	0.0492 ± 0.1287	0.2926 ± 0.0769	0.0666 ± 0.1361	-0.9538 ± 0.4619	S-L†
KIG552	Sb	-0.3372 ± 0.0988	-0.3234 ± 0.0158	-0.6095 ± 0.0381	-1.4857 ± 0.1138	HII
KIG553	SBb	-0.6341 ± 0.0470	-0.1210 ± 0.0103	-0.6719 ± 0.0257	-1.7644 ± 0.1089	AGN*
KIG554	Sb	-0.6433 ± 0.2744	-0.3176 ± 0.0274	-0.6375 ± 0.0755	-1.3360 ± 0.1605	HII
KIG558	Sbc	-0.0983 ± 0.0804	-0.3517 ± 0.0251	-0.5904 ± 0.0580	-1.4666 ± 0.1748	AGN
KIG561	SBbc	0.9821 ± 0.1325	0.0696 ± 0.0412	-0.1530 ± 0.0829	-0.6976 ± 0.1191	LINER
KIG567	SABb	-0.8176 ± 0.0883	-0.3979 ± 0.0156	-0.6844 ± 0.0368	-1.7377 ± 0.1414	HII
KIG575	SABb	0.3158 ± 0.0141	-0.2156 ± 0.0092	-0.5143 ± 0.0157	-1.1820 ± 0.0254	AGN
KIG576	Sb	0.3784 ± 0.1310	-0.0164 ± 0.0468	-0.2118 ± 0.0982	-1.3500 ± 0.4741	S-L†
KIG580	Sbc	-0.7180 ± 0.0711	-0.4235 ± 0.0132	-0.5683 ± 0.0268	-1.7593 ± 0.1270	HII
KIG589	Sb	-0.4432 ± 0.0644	-0.3243 ± 0.0151	-0.5893 ± 0.0352	-1.6566 ± 0.1669	HII
KIG593	Sbc	0.4926 ± 0.0960	0.0763 ± 0.0371	0.0106 ± 0.0583	-0.7684 ± 0.1207	S-L†
KIG601	Sb	0.8555 ± 1.9465	0.1053 ± 0.1438	0.0279 ± 0.2509	-1.2635 ± 1.5425	AGN
KIG606	SBbc	-0.2529 ± 0.1221	-0.3989 ± 0.0285	-0.8009 ± 0.0968	-1.5779 ± 0.2567	HII
KIG607	Sb	-0.1921 ± 0.5565	0.0147 ± 0.1427	0.0456 ± 0.2145	-0.7858 ± 0.5420	LINER
KIG608	Sbc	0.2680 ± 0.6143	0.1017 ± 0.0924	-0.3117 ± 0.2570	-0.7202 ± 0.3178	S-L†
KIG611	Sb	-0.7421 ± 0.1384	-0.4178 ± 0.0172	-0.7155 ± 0.0461	-1.7411 ± 0.1895	HII
KIG612	SBb	0.4939 ± 0.0292	0.2430 ± 0.0145	0.1860 ± 0.0197	-0.5487 ± 0.0329	LINER
KIG613	Sbc	-0.0437 ± 0.3242	-0.2024 ± 0.0552	-0.3327 ± 0.1131	-1.2601 ± 0.3653	AGN
KIG618	Sb	-0.4638 ± 0.0265	-0.2434 ± 0.0068	-0.4148 ± 0.0111	-1.3825 ± 0.0306	AGN
KIG619	Sbc	-0.2723 ± 0.0341	-0.5084 ± 0.0150	-0.3835 ± 0.0203	-1.4994 ± 0.0737	HII
KIG628	Sbc	-0.4301 ± 0.1310	-0.3787 ± 0.0274	-0.4404 ± 0.0490	-1.9469 ± 0.5660	HII
KIG630	Sb	-0.2663 ± 0.1469	-0.2334 ± 0.0291	-0.3971 ± 0.0605	-2.2022 ± 1.4310	AGN
KIG631	Sb	-0.5954 ± 0.0440	-0.4219 ± 0.0137	-0.5790 ± 0.0242	-1.7948 ± 0.1268	HII
KIG635	Sbc	-0.0605 ± 0.0426	-0.6351 ± 0.0247	-0.3359 ± 0.0265	-1.2262 ± 0.0670	HII
KIG640	Sbc	-0.7829 ± 0.0424	-0.4855 ± 0.0104	-0.6181 ± 0.0168	-1.7104 ± 0.0603	HII
KIG645	Sb	-1.0284 ± 0.0775	-0.5262 ± 0.0113	-0.6688 ± 0.0190	-1.9445 ± 0.1173	HII
KIG650	Sb	-0.4851 ± 0.1467	-0.3629 ± 0.0247	-0.6360 ± 0.0642	-1.5272 ± 0.1993	HII
KIG653	Sb	0.5015 ± 0.1314	0.1930 ± 0.0415	0.0018 ± 0.0741	-0.7381 ± 0.1466	S-L†
KIG667	Sb	1.2609 ± 1.3490	0.2107 ± 0.0908	-0.0127 ± 0.1776	-0.9536 ± 0.5456	Sy2
KIG675	SBb	0.1830 ± 0.0679	0.0000 ± 0.0267	-0.0510 ± 0.0412	-0.8440 ± 0.0877	LINER
KIG676	Sb	0.0938 ± 0.1327	-0.2581 ± 0.0388	-0.1549 ± 0.0559	-1.0458 ± 0.1425	LINER
KIG719	SBb	-0.4437 ± 0.0076	-0.6990 ± 0.0066	-1.1832 ± 0.0172	-1.8900 ± 0.0297	HII*
KIG723	SBb	-0.3979 ± 0.1915	-0.3445 ± 0.0376	-0.5461 ± 0.0883	-1.6775 ± 0.4815	HII
KIG725	Sb	-0.7979 ± 0.0363	-0.4168 ± 0.0091	-0.6624 ± 0.0154	-1.7119 ± 0.0506	HII
KIG731	Sb	-0.5917 ± 0.0991	-0.3672 ± 0.0162	-0.5294 ± 0.0313	-1.7035 ± 0.1618	HII
KIG739	Sbc	-0.5110 ± 0.0384	-0.4791 ± 0.0121	-0.5153 ± 0.0195	-1.6923 ± 0.0892	HII
KIG743	Sb	-0.4183 ± 0.0469	-0.2722 ± 0.0116	-0.3680 ± 0.0186	-1.4667 ± 0.0659	AGN
KIG749	Sbc	0.7515 ± 0.0216	-0.0310 ± 0.0124	-0.0610 ± 0.0169	-0.7634 ± 0.0281	Sy1.8
KIG752	Sb	-0.5832 ± 0.0921	-0.3512 ± 0.0171	-0.5556 ± 0.0323	-1.7687 ± 0.1733	HII
KIG757	Sb	0.6113 ± 0.0429	-0.1168 ± 0.0220	-0.4439 ± 0.0550	-1.3613 ± 0.1694	Sy2
KIG762	Sbc	0.8411 ± 0.3795	0.3430 ± 0.0535	0.2583 ± 0.0781	-0.6873 ± 0.1914	S-L†
KIG767	Sb	0.7086 ± 0.5268	0.2822 ± 0.0986	-0.3372 ± 0.3500	-0.5859 ± 0.3153	Sy2
KIG780	Sb	1.0785 ± 0.2355	0.1658 ± 0.0320	-0.3241 ± 0.0877	-1.2505 ± 0.2828	Sy2
KIG795	Sb	-0.0775 ± 0.0938	-0.1820 ± 0.0127	-0.3554 ± 0.0250	-1.3358 ± 0.0877	AGN
KIG807	Sbc	-0.7275 ± 0.1407	-0.2921 ± 0.0155	-0.5002 ± 0.0338	-1.3789 ± 0.0926	HII
KIG884	Sbc	-0.0912 ± 0.2233	-0.2999 ± 0.0316	-0.4766 ± 0.0711	-1.4094 ± 0.2327	AGN
KIG892	Sbc	-0.6198 ± 0.2338	-0.3832 ± 0.0255	-0.7560 ± 0.0794	-2.3737 ± 1.3022	HII
KIG907	Sbc	-0.1022 ± 0.0932	-0.5283 ± 0.0413	-0.2481 ± 0.0506	-1.1883 ± 0.1483	HII
KIG912	Sb	-0.7228 ± 0.0731	-0.4308 ± 0.0142	-0.5156 ± 0.0240	-1.6445 ± 0.1000	HII
KIG923	Sb	-0.3809 ± 0.0710	-0.3515 ± 0.0144	-0.4158 ± 0.0242	-1.8544 ± 0.1882	HII
KIG931	Sbc	-0.9289 ± 0.0778	-0.4692 ± 0.0102	-0.5506 ± 0.0178	-1.7904 ± 0.1032	HII
KIG943	Sb	-0.6898 ± 0.0272	-0.3556 ± 0.0073	-0.6048 ± 0.0130	-1.7271 ± 0.0505	HII
KIG1008	SBb	1.1463 ± 0.0465	0.1739 ± 0.0240	-0.0825 ± 0.0394	-0.6212 ± 0.0535	Sy1.5

Sc

Object	M.T. [a]	LOG([OIII]/Hβ)	LOG([N II]/Hα)	LOG([S II]/Hα)	LOG([O I]/Hα)	Type
KIG198	SABc	-0.3940 ± 0.1875	-0.4120 ± 0.0263	-0.7347 ± 0.0794	-1.6353 ± 0.2751	HII
KIG199	Sc	-0.6611 ± 0.0956	-0.4273 ± 0.0161	-0.5352 ± 0.0288	-1.8179 ± 0.1902	HII
KIG203	SABc	-0.8569 ± 0.4712	-0.3949 ± 0.0360	-0.4559 ± 0.0736	-1.1814 ± 0.1748	HII
KIG216	Sc	-0.4758 ± 0.2365	-0.3753 ± 0.0286	-0.5737 ± 0.0708	-1.5198 ± 0.2344	HII
KIG217	Sc	-0.9164 ± 0.0545	-0.4944 ± 0.0104	-0.6484 ± 0.0170	-1.8422 ± 0.0775	HII
KIG221	Sc	-0.3468 ± 0.0891	-0.2996 ± 0.0227	-0.5924 ± 0.0574	-1.7947 ± 0.3442	AGN
KIG225	Sc	-0.6280 ± 0.3485	-0.2305 ± 0.0479	-0.5263 ± 0.1293	-1.4466 ± 0.4868	AGN
KIG229	Sc	-0.4510 ± 0.1911	-0.3274 ± 0.0364	-0.3878 ± 0.0633	-1.1301 ± 0.1601	HII
KIG241	Sc	-0.3639 ± 0.0452	-0.4714 ± 0.0159	-0.4442 ± 0.0231	-1.7636 ± 0.1450	HII
KIG248	Sc	1.0423 ± 0.0081	-0.0423 ± 0.0050	-0.2417 ± 0.0074	-0.8813 ± 0.0103	Sy2
KIG254	Sc	-0.9208 ± 0.1033	-0.4021 ± 0.0145	-0.6721 ± 0.0301	-1.8473 ± 0.1582	HII
KIG260	Sc	-0.3859 ± 0.1531	-0.4424 ± 0.0362	-0.5610 ± 0.0756	-2.1611 ± 1.1609	HII
KIG263	Sc	0.7272 ± 0.5186	0.2105 ± 0.0822	0.1284 ± 0.1218	-0.8566 ± 0.3604	S-L†
KIG268	SABc	-0.3799 ± 0.2076	-0.4847 ± 0.0603	-0.3298 ± 0.0775	-1.7922 ± 0.7811	HII
KIG271	Sc	-0.5853 ± 0.2039	-0.3401 ± 0.0302	-0.5427 ± 0.0723	-1.6380 ± 0.3510	HII
KIG273	Sc	-0.9066 ± 0.0568	-0.2990 ± 0.0081	-0.6857 ± 0.0166	-1.8872 ± 0.0824	HII
KIG282	Sc	-0.2090 ± 0.1574	-0.2501 ± 0.0223	-0.4277 ± 0.0465	-1.3762 ± 0.1526	AGN
KIG289	Sc	0.2165 ± 0.1065	-0.1635 ± 0.0310	-0.4142 ± 0.0706	-1.6038 ± 0.4342	AGN
KIG291	Scd	-0.3190 ± 0.0405	-0.5553 ± 0.0163	-0.3600 ± 0.0188	-1.5727 ± 0.1107	HII
KIG294	Sc	-0.0073 ± 0.1698	-0.4654 ± 0.0435	-0.3224 ± 0.0611	-1.2101 ± 0.1705	HII
KIG296	Sc	-0.7204 ± 0.1316	-0.3901 ± 0.0229	-0.4451 ± 0.0405	-1.6912 ± 0.2496	HII
KIG300	Sc	0.3790 ± 0.0177	-1.0948 ± 0.0249	-0.4973 ± 0.0179	-1.4475 ± 0.0537	HII
KIG306	Sc	-0.3548 ± 0.0927	-0.4394 ± 0.0216	-0.3509 ± 0.0322	-1.8250 ± 0.3316	HII
KIG307	Sc	0.2462 ± 0.2639	-0.0352 ± 0.0545	-0.1816 ± 0.1061	-1.3388 ± 0.5529	S-L†
KIG308	Sc	-0.0462 ± 0.3078	-0.1372 ± 0.0655	-0.3954 ± 0.1609	-1.6338 ± 1.0450	AGN
KIG314	SABc	-0.2541 ± 0.0447	-0.3206 ± 0.0214	-0.6235 ± 0.0496	-2.2972 ± 0.8334	AGN
KIG321	Sc	-0.2127 ± 0.0666	-0.5433 ± 0.0232	-0.3566 ± 0.0318	-1.2098 ± 0.0829	HII
KIG322	Sc	-0.4786 ± 0.0661	-0.3720 ± 0.0187	-0.4091 ± 0.0296	-1.7492 ± 0.2186	HII
KIG323	Sc	-0.3838 ± 0.1108	-0.3308 ± 0.0206	-0.5184 ± 0.0445	-1.4326 ± 0.1359	HII
KIG326	SBc	-0.0369 ± 0.1847	-0.3616 ± 0.0622	-0.0756 ± 0.0633	-1.0533 ± 0.2470	LINER
KIG328	SABc	-0.3110 ± 0.0915	-0.2665 ± 0.0270	-0.4153 ± 0.0560	-1.4968 ± 0.2389	AGN
KIG330	Sc	-0.4832 ± 0.1200	-0.37037± 0.0271	-0.4190 ± 0.0487	-1.6139 ± 0.2766	AGN
KIG337	Sc	0.7518 ± 0.2335	0.0899 ± 0.0408	-0.2396 ± 0.0924	-1.1599 ± 0.2894	Sy2
KIG343	SBc	-0.8360 ± 0.0828	-0.4859 ± 0.0131	-0.5192 ± 0.0228	-1.8243 ± 0.1539	HII
KIG348	Sc	0.1154 ± 0.0140	-0.6746 ± 0.0117	-0.4785 ± 0.0137	-1.4493 ± 0.0346	HII
KIG353	Sc	-0.6722 ± 0.0411	-0.5039 ± 0.0108	-0.5129 ± 0.0168	-1.6810 ± 0.0809	HII
KIG360	Sc	-0.3699 ± 0.0424	-0.4564 ± 0.0152	-0.4383 ± 0.0219	-1.4498 ± 0.0754	HII
KIG362	Sc	0.2775 ± 0.0680	0.1049 ± 0.0231	0.0840 ± 0.0345	-0.7344 ± 0.0732	LINER
KIG365	Sc	-0.5798 ± 0.0236	-0.4098 ± 0.0086	-0.5431 ± 0.0131	-1.9773 ± 0.0759	HII
KIG367	SABc	-0.5025 ± 0.1428	-0.4254 ± 0.0280	-0.3999 ± 0.0475	-1.7043 ± 0.3366	HII
KIG368	Sc	-0.9190 ± 0.1051	-0.3950 ± 0.0134	-0.6971 ± 0.0313	-1.6126 ± 0.0915	HII
KIG370	Sc	-0.8182 ± 0.0797	-0.4485 ± 0.0113	-0.7419 ± 0.0255	-2.1264 ± 0.2139	HII
KIG373	Sc	-0.8433 ± 0.1244	-0.3724 ± 0.0155	-0.5514 ± 0.0334	-1.6996 ± 0.1577	HII
KIG384	Sc	-0.3252 ± 0.1262	-0.4385 ± 0.0326	-0.5818 ± 0.0607	-1.8999 ± 0.5140	HII
KIG386	Sc	-0.4308 ± 0.0822	-0.2396 ± 0.0165	-0.3974 ± 0.0310	-1.6777 ± 0.1898	AGN
KIG391	Sc	0.2374 ± 0.0526	-0.6375 ± 0.0399	-0.2390 ± 0.0373	-1.2277 ± 0.1169	HII
KIG395	Sc	0.4926 ± 0.0955	0.4213 ± 0.0544	0.1874 ± 0.0895	-0.4904 ± 0.1469	LINER
KIG398	Sc	-0.4113 ± 0.1728	-0.3639 ± 0.0338	-0.5659 ± 0.0761	-2.2222 ± 1.2918	HII
KIG399	SBc	-0.4976 ± 0.0659	-0.4616 ± 0.0154	-0.7162 ± 0.0349	-1.6450 ± 0.1091	HII
KIG403	Sc	0.0416 ± 0.3936	-0.1835 ± 0.0611	-0.3110 ± 0.1202	-1.0981 ± 0.3055	LINER
KIG405	SABc	-0.7206 ± 0.0882	-0.4599 ± 0.0160	-0.4800 ± 0.0264	-1.6434 ± 0.1172	HII
KIG406	Sc	-0.6869 ± 0.0745	-0.4215 ± 0.0140	-0.5105 ± 0.0239	-1.7292 ± 0.1210	HII
KIG407	Sc	0.5809 ± 0.0136	-1.2032 ± 0.0243	-0.6533 ± 0.0175	-1.6662 ± 0.0608	HII
KIG408	Sc	-0.5202 ± 0.0842	-0.4492 ± 0.0215	-0.3755 ± 0.0336	-1.4595 ± 0.1372	HII
KIG410	Sc	-0.1348 ± 0.0090	-0.4794 ± 0.0057	-0.5713 ± 0.0081	-1.7658 ± 0.0233	HII
KIG428	SBc	0.6087 ± 0.5510	-0.3683 ± 0.0997	-0.0313 ± 0.0959	-0.8327 ± 0.2308	S-L†
KIG429	Sc	0.1542 ± 0.4310	-0.1788 ± 0.0547	-0.4304 ± 0.1336	-	AGN
KIG432	Scd	0.0021 ± 0.1392	0.1091 ± 0.1830	0.0797 ± 0.2714	-1.1747 ± 1.5783	LINER

Object	M.T.[a]	LOG([OIII]/Hβ)	LOG([N II]/Hα)	LOG([S II]/Hα)	LOG([O I]/Hα)	Type
KIG436	SBc	-0.6726 ± 0.0526	-0.4329 ± 0.0128	-0.4914 ± 0.0218	-1.6115 ± 0.0901	HII
KIG440	Sc	1.1854 ± 1.3201	0.1239 ± 0.0561	-0.5199 ± 0.2369	-0.7619 ± 0.1950	Sy2
KIG442	SBc	-0.0942 ± 0.0620	-0.4464 ± 0.0278	-0.1781 ± 0.0291	-1.3940 ± 0.1487	HII
KIG445	Sc	-0.8403 ± 0.2002	-0.4075 ± 0.0226	-0.6364 ± 0.0525	-1.4098 ± 0.1257	HII
KIG446	SBc	-0.7051 ± 0.1581	-0.4457 ± 0.0236	-0.8129 ± 0.0745	-2.0652 ± 0.5377	HII
KIG448	SABc	-0.9581 ± 0.0194	-0.4005 ± 0.0050	-0.7380 ± 0.0086	-2.1090 ± 0.0423	HII
KIG453	Sc	-0.1938 ± 0.1556	-0.2848 ± 0.0285	-0.5543 ± 0.0751	-1.5441 ± 0.2815	AGN
KIG454	Sc	-0.6045 ± 0.1290	-0.3909 ± 0.0235	-0.5985 ± 0.0580	-1.4907 ± 0.1867	HII
KIG473	SABc	-0.2148 ± 0.1502	-0.3366 ± 0.0414	-0.2623 ± 0.0717	-1.0582 ± 0.1504	AGN
KIG474	Sc	-0.0374 ± 0.0356	-0.6191 ± 0.0199	-0.3771 ± 0.0249	-1.4477 ± 0.0902	HII
KIG476	Scd	0.0824 ± 0.0315	-0.7432 ± 0.0227	-0.4151 ± 0.0232	-1.5135 ± 0.0979	HII
KIG477	Sc	0.4178 ± 0.0238	-0.1635 ± 0.0131	-0.4579 ± 0.0262	-1.3465 ± 0.0689	Sy2
KIG486	Sc	0.3076 ± 0.0550	-1.0042 ± 0.0781	-0.4722 ± 0.0546	-1.5040 ± 0.2361	HII
KIG487	SBcd	0.3345 ± 0.0096	-0.8796 ± 0.0098	-0.5919 ± 0.0110	-1.6670 ± 0.0368	HII
KIG498	Sc	-0.5868 ± 0.0204	-0.3058 ± 0.0058	-0.4559 ± 0.0089	-1.6054 ± 0.0298	HII
KIG502	SABc	0.2796 ± 0.0177	-0.8653 ± 0.0181	-0.5028 ± 0.0173	-1.5729 ± 0.0772	HII
KIG509	SABc	-0.2996 ± 0.0674	-0.4489 ± 0.0231	-0.3198 ± 0.0286	-1.5614 ± 0.1650	HII
KIG512	Sc	-0.5086 ± 0.0938	-0.4669 ± 0.0221	-0.4237 ± 0.0326	-2.0899 ± 0.5159	HII
KIG518	SABc	-0.8838 ± 0.5779	-0.3348 ± 0.0326	-0.4637 ± 0.0621	-1.7497 ± 0.4449	HII
KIG524	Scd	-0.0691 ± 0.0266	-0.7193 ± 0.0177	-0.3002 ± 0.0165	-1.2848 ± 0.0581	HII
KIG526	Sc	-0.3985 ± 0.0720	-0.3299 ± 0.0145	-0.4979 ± 0.0283	-1.4314 ± 0.1058	HII
KIG546	Sc	-0.6198 ± 0.2869	-0.3236 ± 0.0362	-0.5079 ± 0.0826	-1.6534 ± 0.4771	HII
KIG547	SABc	-0.5136 ± 0.1139	-0.5091 ± 0.0360	-0.2687 ± 0.0392	-1.6509 ± 0.3420	HII
KIG551	SABc	0.4260 ± 0.1333	-0.5306 ± 0.0721	-0.1670 ± 0.0669	-0.8214 ± 0.1310	AGN
KIG560	Sc	0.0687 ± 0.0174	-0.6555 ± 0.0133	-0.3778 ± 0.0153	-1.3371 ± 0.0391	HII
KIG563	Sc	-0.4012 ± 0.0388	-0.4000 ± 0.0138	-0.4471 ± 0.0213	-1.6111 ± 0.1091	HII
KIG565	Sc	-0.2981 ± 0.1312	-0.3181 ± 0.0291	-0.4666 ± 0.0599	-1.4309 ± 0.2196	AGN
KIG566	Sc	0.3478 ± 0.0204	-1.0096 ± 0.0252	-0.5568 ± 0.0215	-1.6160 ± 0.0985	HII
KIG568	Sc	0.1594 ± 0.7950	0.2174 ± 0.1064	-0.0430 ± 0.2185	-0.7412 ± 0.4141	LINER
KIG583	Sc	-0.5283 ± 0.1807	-0.3930 ± 0.0289	-0.5853 ± 0.0690	-1.4791 ± 0.2142	HII
KIG590	Sc	-0.2762 ± 0.0154	-0.6464 ± 0.0109	-0.4731 ± 0.0126	-1.7940 ± 0.0546	HII
KIG594	Sc	-0.4446 ± 0.0383	-0.4484 ± 0.0131	-0.5147 ± 0.0204	-1.6548 ± 0.0858	HII
KIG598	Sc	-0.3378 ± 0.0838	-0.3797 ± 0.0299	-0.6079 ± 0.0777	-1.7806 ± 0.4383	HII
KIG600	Scd	-0.1721 ± 0.1535	-0.4560 ± 0.0451	-0.2436 ± 0.0567	-1.3257 ± 0.2327	HII
KIG603	Sc	0.1781 ± 0.1156	0.0483 ± 0.0230	0.1587 ± 0.0296	-0.4901 ± 0.0441	LINER*
KIG610	SABc	-0.5699 ± 0.0431	-0.3919 ± 0.0123	-0.5891 ± 0.0219	-1.6704 ± 0.0834	HII
KIG625	Sc	-0.5398 ± 0.0882	-0.3936 ± 0.0160	-0.4439 ± 0.0266	-1.5243 ± 0.1095	HII
KIG626	SABc	-0.4974 ± 0.0399	-0.4910 ± 0.0120	-0.5275 ± 0.0179	-1.7206 ± 0.0883	HII
KIG639	Sc	-0.4978 ± 0.1549	-0.3795 ± 0.0260	-0.4834 ± 0.0523	-1.9841 ± 0.5599	HII
KIG648	Sc	-0.5528 ± 0.1171	-0.4117 ± 0.0227	-0.6253 ± 0.0535	-1.7270 ± 0.2531	HII
KIG651	SBc	0.2553 ± 0.0128	-0.7991 ± 0.0125	-0.4875 ± 0.0131	-1.5145 ± 0.0377	HII
KIG652	Sc	-0.5891 ± 0.0536	-0.4092 ± 0.0123	-0.4716 ± 0.0189	-1.5628 ± 0.0685	HII
KIG655	Sc	-0.4754 ± 0.7579	-0.0501 ± 0.0851	-0.2672 ± 0.1892	-0.9730 ± 0.4011	AGN
KIG659	Sc	-0.5086 ± 0.1769	-0.4156 ± 0.0355	-0.4631 ± 0.0664	-1.2537 ± 0.1656	HII
KIG668	Sc	-0.3766 ± 0.1273	-0.4480 ± 0.0238	-0.4281 ± 0.0385	-1.4956 ± 0.1523	HII
KIG672	Sc	0.0713 ± 0.1848	-0.2318 ± 0.0400	-0.3023 ± 0.0777	-1.4365 ± 0.3575	AGN
KIG680	Sc	-0.1041 ± 0.2175	-0.2030 ± 0.0427	-0.6550 ± 0.1577	-1.0325 ± 0.1763	AGN
KIG681	Scd	-0.1487 ± 0.1917	-0.3696 ± 0.0461	-0.4068 ± 0.0716	-1.2545 ± 0.2159	AGN
KIG683	Sc	-0.5643 ± 0.1252	-0.4190 ± 0.0167	-0.6486 ± 0.0370	-2.3988 ± 0.7433	HII
KIG688	Sc	-0.5421 ± 0.1242	-0.3741 ± 0.0209	-0.5427 ± 0.0473	-1.5691 ± 0.1894	HII
KIG691	SBcd	-0.3228 ± 0.0792	-0.4572 ± 0.0199	-0.3316 ± 0.0245	-1.7552 ± 0.2404	HII
KIG693	Sc	-0.7150 ± 0.1728	-0.4271 ± 0.0252	-0.6320 ± 0.0624	-1.7152 ± 0.3057	HII
KIG700	Scd	-0.1759 ± 0.1425	-0.3546 ± 0.0480	-0.2215 ± 0.0650	-1.3888 ± 0.3886	AGN
KIG709	Sc	0.4863 ± 1.4057	-0.1015 ± 0.0432	-0.4466 ± 0.1154	-1.2837 ± 0.3242	Sy2
KIG716	Sc	0.2789 ± 0.1337	0.2548 ± 0.0703	0.1630 ± 0.1071	-0.5213 ± 0.1833	LINER
KIG717	Sc	-0.5746 ± 0.1918	-0.4114 ± 0.0233	-0.5526 ± 0.0504	-2.2380 ± 0.7953	HII
KIG721	Sc	-0.6518 ± 0.0890	-0.4415 ± 0.0192	-0.6844 ± 0.0434	-1.8561 ± 0.2447	HII
KIG744	Sc	0.0489 ± 0.1837	-0.3825 ± 0.0435	-0.1585 ± 0.0501	-0.9633 ± 0.1311	LINER
KIG747	Sc	0.3158 ± 0.0220	-0.1517 ± 0.0113	-0.5229 ± 0.0218	-1.2944 ± 0.0449	Sy1.5

Object	M.T. [a]	LOG([OIII]/Hβ)	LOG([N II]/Hα)	LOG([S II]/Hα)	LOG([O I]/Hα)	Type
KIG748	SBc	0.3615 ± 0.0513	-0.7205 ± 0.0475	-0.3451 ± 0.0416	-1.4186 ± 0.1837	HII
KIG754	Scd	-0.5846 ± 0.0988	-0.4161 ± 0.0227	-0.4729 ± 0.0429	-1.4281 ± 0.1281	HII
KIG902	Sc	-0.8253 ± 0.1299	-0.4449 ± 0.0157	-0.6600 ± 0.0335	-1.8632 ± 0.1846	HII
KIG928	Sc	-0.5977 ± 0.0492	-0.4458 ± 0.0132	-0.5908 ± 0.0241	-1.7567 ± 0.1068	HII
KIG980	Sc	-0.1461 ± 0.0250	-0.5747 ± 0.0126	-0.4733 ± 0.0173	-1.5829 ± 0.0594	HII
KIG1030	SBc	-0.1305 ± 0.0487	-0.6196 ± 0.0234	-0.3989 ± 0.0275	-1.6204 ± 0.1619	HII
KIG1041	Sc	-0.1243 ± 0.1771	-0.3244 ± 0.0445	-0.1947 ± 0.0624	-1.4422 ± 0.4265	AGN

Sm						

Object	M.T.	LOG([OIII]/Hβ)	LOG([N II]/Hα)	LOG([S II]/Hα)	LOG([O I]/Hα)	Type
KIG280	Sm	-0.1951 ± 0.2746	-0.3680 ± 0.0673	-0.1298 ± 0.0855	-1.7026 ± 1.0415	HII
KIG283	Irr	0.0976 ± 0.0322	-0.7516 ± 0.0221	-0.3673 ± 0.0212	-1.5913 ± 0.1111	HII
KIG290	SABd	0.0000 ± 0.0889	-0.7892 ± 0.0750	-0.2253 ± 0.0491	-1.4944 ± 0.3311	HII
KIG299	SBm	0.2350 ± 0.0485	-0.8851 ± 0.0514	-0.4300 ± 0.0388	-1.1289 ± 0.0936	HII
KIG313	Sd	0.0000 ± 0.1697	-0.2189 ± 0.0413	-0.6978 ± 0.1489	-1.8633 ± 0.8821	AGN
KIG354	Sm	0.0804 ± 0.1385	-0.5136 ± 0.0403	-0.2366 ± 0.0435	-1.3186 ± 0.2033	HII
KIG355	Irr	-0.5558 ± 0.0238	-0.4612 ± 0.0083	-0.4600 ± 0.0115	-1.6367 ± 0.0398	HII
KIG439	Sdm	-0.1691 ± 0.0500	-0.5207 ± 0.0190	-0.4420 ± 0.0304	-1.5046 ± 0.1151	HII
KIG447	Irr	0.2305 ± 0.0094	-0.9002 ± 0.0092	-0.6691 ± 0.0103	-1.8389 ± 0.0306	HII
KIG470	Irr	0.2109 ± 0.0266	-0.9434 ± 0.0333	-0.4939 ± 0.0258	-1.4647 ± 0.0958	HII
KIG536	Sd	0.4303 ± 0.0316	-1.0425 ± 0.0533	-0.5223 ± 0.0359	-1.4192 ± 0.1088	HII
KIG569	Sd	0.3600 ± 0.0102	-1.0040 ± 0.0117	-0.6116 ± 0.0112	-1.6435 ± 0.0368	HII
KIG584	Irr	0.0670 ± 0.2626	-0.7595 ± 0.2265	-0.1912 ± 0.1350	-0.9828 ± 0.3666	HII
KIG585	Sd	-0.3652 ± 0.0654	-0.5155 ± 0.0180	-0.4048 ± 0.0260	-1.4033 ± 0.0786	HII
KIG642	SABd	0.0637 ± 0.0291	-0.7332 ± 0.0219	-0.4192 ± 0.0225	-1.2843 ± 0.0633	HII
KIG662	SBd	0.6521 ± 0.0102	-1.3676 ± 0.0185	-0.8652 ± 0.0144	-1.9460 ± 0.0502	HII
KIG674	Sm	0.6314 ± 0.3125	-0.1586 ± 0.0617	-0.4863 ± 0.2035	-1.0995 ± 0.3442	Sy2
KIG909	Sdm	-0.7043 ± 0.2292	-0.4137 ± 0.0259	-0.6653 ± 0.0651	-1.7201 ± 0.2953	HII
KIG937	SBd	-0.2003 ± 0.2570	-0.3921 ± 0.1261	0.0288 ± 0.1193	-1.0904 ± 0.5402	HII
KIG990	IAB	0.6726 ± 0.0081	-1.3646 ± 0.0135	-0.9131 ± 0.0124	-1.9868 ± 0.0420	HII

Table 7: Logarithm intensity ratios with their errors and AGN type
for the Varela's sample. M.T.- Morphological Type. AGN classification
denotes those galaxies that are AGN according to the [N II] diagrams
but not to the [S II] and/or [O I]. † L-S classification means that galaxies
fall in the separation line for Seyfert and LINER according to [S II] and
[O I] diagrams. * Type with weak broad component in permitted lines.
Seyfert quantitative classification according to Winkler (1992).

Object	M.T. [a]	LOG([OIII]/Hβ)	LOG([N II]/Hα)	LOG([S II]/Hα)	LOG([O I]/Hα)	Type
Elliptical						
PGC29177	E-SO	-0.0385 ± 0.0075	-0.4953 ± 0.0064	-0.6389 ± 0.0090	-1.9657 ± 0.0284	HII
PGC36037	E-SO	0.6757 ± 0.2136	-0.0778 ± 0.0767	-0.0145 ± 0.1076	-0.8049 ± 0.2415	S-L†
PGC36211	E	0.1761 ± 0.0310	-0.5803 ± 0.0225	-0.2478 ± 0.0225	-1.3349 ± 0.0808	HII
PGC43121	E-SO	0.4754 ± 0.0048	-0.9475 ± 0.0054	-0.8785 ± 0.0066	-1.9157 ± 0.0141	HII
Spheroidal						
PGC25467	S0-a	-0.4046 ± 0.0283	-0.3493 ± 0.0119	-0.4011 ± 0.0177	-1.5501 ± 0.0721	HII
PGC28259	S0	0.5808 ± 0.0168	-0.4437 ± 0.0169	-0.2733 ± 0.0206	-0.8945 ± 0.0330	Sy2
PGC28758	S0-a	0.7331 ± 0.0062	-1.2866 ± 0.0097	-1.0391 ± 0.0110	-2.0580 ± 0.0283	HII
PGC31601	S0	0.2531 ± 0.0109	-0.5715 ± 0.0092	-0.6821 ± 0.0158	-1.4981 ± 0.0367	HII
PGC31945	S0	0.3114 ± 0.0078	-0.7400 ± 0.0077	-0.6240 ± 0.0094	-1.7853 ± 0.0261	HII
PGC37574	S0	0.5721 ± 0.1763	0.1109 ± 0.0813	0.3262 ± 0.0894	-0.7749 ± 0.2968	S-L†
PGC37795	S0	0.2274 ± 0.0869	-0.1798 ± 0.0652	-0.0085 ± 0.0795	-0.6710 ± 0.1398	LINER
PGC38527	S0-a	-0.5243 ± 0.1138	-0.3784 ± 0.0264	-0.6363 ± 0.0662	-1.8257 ± 0.4031	HII
PGC39681	S0-a	-0.4022 ± 0.0433	-0.5761 ± 0.0196	-0.5402 ± 0.0273	-1.9586 ± 0.2593	HII
PGC42497	S0	-0.6131 ± 0.0237	-0.5466 ± 0.0088	-0.6258 ± 0.0124	-2.0000 ± 0.0691	HII
PGC49927	S0-a	-0.0588 ± 0.0085	-0.5192 ± 0.0064	-0.6233 ± 0.0088	-2.0442 ± 0.0365	HII
PGC49956	S0-a	0.8751 ± 0.2953	0.3010 ± 0.0670	0.1846 ± 0.1030	-0.8093 ± 0.3120	S-L†
PGC58183	S0	0.8329 ± 0.2360	0.3401 ± 0.0796	0.2683 ± 0.1140	-0.4705 ± 0.2014	LINER
PGC48521	S0	1.0883 ± 0.0117	0.0723 ± 0.0076	-0.3273 ± 0.0143	-0.8754 ± 0.0190	Sy1.8
Sa						
PGC25985	SBa	0.0186 ± 0.0498	-0.6120 ± 0.0328	-0.1932 ± 0.0294	-1.1732 ± 0.0948	HII
PGC26218	Sa	-0.0440 ± 0.0097	-0.6207 ± 0.0068	-0.6754 ± 0.0092	-2.0514 ± 0.0384	HII
PGC27437	Sa	0.4566 ± 0.1065	0.2900 ± 0.0494	0.0912 ± 0.0839	-0.5104 ± 0.1302	LINER
PGC28145	Sa	-0.6816 ± 0.0373	-0.2678 ± 0.0078	-0.5870 ± 0.0139	-1.7602 ± 0.0546	HII
PGC38582	Sab	-0.8523 ± 0.0308	-0.5166 ± 0.0088	-0.5855 ± 0.0121	-2.0038 ± 0.0636	HII
PGC40475	Sa	-0.1320 ± 0.0143	-0.4863 ± 0.0092	-0.5244 ± 0.0128	-1.6922 ± 0.0437	HII
PGC42174	SABa	-0.1253 ± 0.0601	0.0771 ± 0.0187	-0.1549 ± 0.0330	-0.8434 ± 0.0603	LINER
PGC50198	Sa	-0.5946 ± 0.0278	-0.4892 ± 0.0093	-0.5302 ± 0.0128	-1.7903 ± 0.0528	HII
PGC50745	SBa	-0.7138 ± 0.0273	-0.2834 ± 0.0088	-0.5423 ± 0.0131	-1.7481 ± 0.0518	HII
PGC51091	SBa	-0.4356 ± 0.0259	-0.2945 ± 0.0094	-0.4890 ± 0.0156	-1.6721 ± 0.0641	AGN
PGC51951	Sa	-0.5768 ± 0.0359	-0.4364 ± 0.0117	-0.4763 ± 0.0179	-1.5721 ± 0.0673	HII
Sb						
PGC26690	SBbc	0.5302 ± 0.2424	0.2064 ± 0.0702	0.0142 ± 0.1266	-0.9224 ± 0.3719	S-L†
PGC27311	Sbc	0.4115 ± 0.0075	-1.0317 ± 0.0092	-0.6730 ± 0.0092	-1.8906 ± 0.0278	HII
PGC27518	Sbc	-0.7164 ± 0.0532	-0.4294 ± 0.0120	-0.6720 ± 0.0250	-1.9476 ± 0.1586	HII

Object	M.T. [a]	LOG([OIII]/Hβ)	LOG([N II]/Hα)	LOG([S II]/Hα)	LOG([O I]/Hα)	Type
PGC27796	SBb	-0.2766 ± 0.1091	-0.1786 ± 0.0197	-0.3907 ± 0.0388	-1.3352 ± 0.1223	AGN
PGC29347	SBb	0.3436 ± 0.0074	-0.8179 ± 0.0075	-0.6724 ± 0.0089	-2.0031 ± 0.0291	HII
PGC29715	SBb	-0.3502 ± 0.0624	-0.3763 ± 0.0169	-0.5435 ± 0.0324	-1.4794 ± 0.0993	HII
PGC30010	Sb	-0.4184 ± 0.0298	-0.1828 ± 0.0091	-0.5548 ± 0.0181	-1.5933 ± 0.0621	AGN
PGC35314	Sb	0.4141 ± 0.0818	0.0241 ± 0.0312	0.0514 ± 0.0424	-0.9643 ± 0.1298	S-L†
PGC37928	Sb	-0.3429 ± 0.0163	-0.4129 ± 0.0083	-0.4976 ± 0.0116	-1.8935 ± 0.0562	HII
PGC38802	Sb	0.3390 ± 0.0651	0.1107 ± 0.0394	0.0181 ± 0.0619	-1.0505 ± 0.2307	S-L†
PGC39393	SABb	-0.2865 ± 0.1896	-0.2614 ± 0.0361	-0.5564 ± 0.0931	-1.7686 ± 0.5994	AGN
PGC43113	Sb	0.7704 ± 0.2383	-0.0286 ± 0.0427	0.0749 ± 0.0548	-0.9961 ± 0.1968	S-L†
PGC45836	SABb	0.3158 ± 0.0141	-0.2156 ± 0.0092	-0.5143 ± 0.0157	-1.1820 ± 0.0254	Sy2
PGC47482	SBb	-0.6782 ± 0.0462	-0.4185 ± 0.0123	-0.6252 ± 0.0229	-1.6744 ± 0.0842	HII
PGC47985	Sb	-0.2839 ± 0.0417	-0.4473 ± 0.0161	-0.3025 ± 0.0196	-1.3910 ± 0.0678	HII
PGC50889	Sb	-0.2788 ± 0.0389	-0.1876 ± 0.0116	-0.3563 ± 0.0194	-1.3643 ± 0.0603	AGN
PGC52488	SBb	-0.1362 ± 0.0362	-0.4720 ± 0.0174	-0.3628 ± 0.0235	-1.4771 ± 0.0946	HII
PGC52887	Sb	0.6649 ± 0.0417	-0.0303 ± 0.0303	-0.2710 ± 0.0628	-0.7351 ± 0.0789	Sy2
PGC55419	Sbc	-0.5714 ± 0.0265	-0.4478 ± 0.0108	-0.5763 ± 0.0168	-2.0686 ± 0.1290	HII
PGC71699	Sbc	-0.5825 ± 0.0773	-0.3239 ± 0.0153	-0.4023 ± 0.0263	-1.5000 ± 0.1227	HII
PGC8165	Sb	-0.4385 ± 0.0686	-0.3378 ± 0.0161	-0.5935 ± 0.0388	-1.7169 ± 0.1955	HII

Sc

Object	M.T. [a]	LOG([OIII]/Hβ)	LOG([N II]/Hα)	LOG([S II]/Hα)	LOG([O I]/Hα)	Type
PGC2600	SABc	-0.5967 ± 0.0427	-0.3670 ± 0.0105	-0.7098 ± 0.0245	-1.8781 ± 0.1226	HII
PGC27968	SABc	0.2112 ± 0.0363	-0.7672 ± 0.0285	-0.4197 ± 0.0284	-1.3424 ± 0.0962	HII
PGC28485	SABc	-0.3216 ± 0.2285	-0.2406 ± 0.0381	-0.4330 ± 0.0828	-2.3499 ± 2.6570	AGN
PGC30197	Sc	-0.6006 ± 0.0406	-0.3603 ± 0.0091	-0.4818 ± 0.0141	-1.8556 ± 0.0831	HII
PGC30569	Sc	-0.5203 ± 0.0579	-0.4690 ± 0.0151	-0.3830 ± 0.0206	-1.5418 ± 0.0964	HII
PGC30858	Sc	0.0000 ± 0.0367	-0.6320 ± 0.0272	-0.3158 ± 0.0273	-1.1761 ± 0.0759	HII
PGC31883	Sc	0.2561 ± 0.1406	0.0722 ± 0.0617	-0.1450 ± 0.1211	-0.9006 ± 0.2643	S-L†
PGC32183	SBc	-0.1205 ± 0.0604	-0.4301 ± 0.0281	-0.1619 ± 0.0295	-1.3777 ± 0.1490	HII
PGC34935	Sc	0.4217 ± 0.0241	-0.1635 ± 0.0131	-0.4579 ± 0.0262	-1.3465 ± 0.0689	Sy2
PGC36930	Sc	0.1207 ± 0.0143	-0.8679 ± 0.0129	-0.5590 ± 0.0128	-1.7928 ± 0.0527	HII
PGC37352	SABc	-0.2688 ± 0.0615	-0.4489 ± 0.0231	-0.3198 ± 0.0286	-1.4523 ± 0.1300	HII
PGC37444	Sc	-0.5434 ± 0.0918	-0.4669 ± 0.0221	-0.3840 ± 0.0304	-2.0899 ± 0.5159	HII
PGC37584	Scd	-0.3540 ± 0.0505	-0.5241 ± 0.0154	-0.4119 ± 0.0195	-1.6200 ± 0.1108	HII
PGC37838	Sc	0.4091 ± 0.0562	-0.8096 ± 0.0575	-0.3734 ± 0.0452	-1.0314 ± 0.0854	HII
PGC38150	SABc	-0.9508 ± 0.5681	-0.3415 ± 0.0329	-0.4637 ± 0.0621	-1.7497 ± 0.4449	HII
PGC38277	S?	0.3059 ± 0.0169	-0.9774 ± 0.0166	-0.5873 ± 0.0155	-1.8220 ± 0.0733	HII
PGC38286	Sc	0.3501 ± 0.0958	-0.8921 ± 0.0703	-0.3268 ± 0.0437	-1.1139 ± 0.1129	HII
PGC44370	Sc	0.1347 ± 0.0296	-0.6326 ± 0.0244	-0.3648 ± 0.0275	-1.5586 ± 0.1378	HII
PGC44797	SBc	-0.9261 ± 0.0190	-0.4801 ± 0.0060	-0.6909 ± 0.0090	-2.3028 ± 0.0668	HII
PGC47577	Sc	-0.2762 ± 0.0154	-0.6306 ± 0.0110	-0.4573 ± 0.0127	-1.7782 ± 0.0547	HII
PGC48959	SABc	-0.5680 ± 0.0566	-0.3579 ± 0.0124	-0.3907 ± 0.0183	-1.4153 ± 0.0603	HII
PGC49112	SABc	0.0130 ± 0.1143	-0.1027 ± 0.0333	-0.2990 ± 0.0666	-1.1916 ± 0.2003	S-L†
PGC52607	Sc	-0.9324 ± 0.0811	-0.4480 ± 0.0138	-0.5572 ± 0.0227	-1.9501 ± 0.1731	HII
PGC58115	Sc	-0.7097 ± 0.0779	-0.4992 ± 0.0163	-0.5993 ± 0.0282	-2.1493 ± 0.3284	HII
PGC58336	Sc	-0.1787 ± 0.2136	-0.2606 ± 0.0475	-0.2704 ± 0.0774	-1.0571 ± 0.2865	LINER
PGC32543	Scd	0.3692 ± 0.0128	-0.9844 ± 0.0184	-0.5072 ± 0.0153	-1.6016 ± 0.0541	HII
PGC32364	Scd	0.2784 ± 0.0155	-0.9480 ± 0.0204	-0.4698 ± 0.0167	-1.5613 ± 0.0571	HII

Sm

Object	M.T. [a]	LOG([OIII]/Hβ)	LOG([N II]/Hα)	LOG([S II]/Hα)	LOG([O I]/Hα)	Type
PGC27792	Sd	-0.1027 ± 0.0880	-0.4600 ± 0.0357	-0.3258 ± 0.0469	-1.4637 ± 0.2458	HII
PGC34967	Sd	0.1557 ± 0.0141	-0.6801 ± 0.0101	-0.4639 ± 0.0117	-1.5552 ± 0.0356	HII
PGC47938	Irr	0.5449 ± 0.0121	-1.4242 ± 0.0354	-0.7214 ± 0.0193	-1.8103 ± 0.0771	HII
PGC27157	Irr	0.5783 ± 0.0074	-1.2818 ± 0.0137	-0.7089 ± 0.0107	-1.7392 ± 0.0311	HII

Object	M.T. [a]	LOG([OIII]/Hβ)	LOG([N II]/Hα)	LOG([S II]/Hα)	LOG([O I]/Hα)	Type

Capítulo 4

Induced Nuclear Activity In Galaxy Pairs with Different Morphologies (E+E), (E+S) AND (S+S)

En este capítulo estudiamos la incidencia de la actividad nuclear de galaxias en pares aislados. Para ello seleccionamos el catálogo de pares aislados de galaxias de Karachentsev (CPG). Este catálogo considera solo objetos por arriba de $\delta \geq$ -3^0 y $b \geq 20^0$ (para evitar extinción galáctica) y la separación entre pares es $\leq$ 100 Kpc. Analizamos 385 espectros obtenidos del SDSS (DR7) que se encuentran en diferentes tipos de pares (E+E), (E+S) y (S+S). El método para extraer la componente estelar y medir líneas ha sido el mismo que en el artículo anterior para tener consistencia y homogeneidad al comparar resultados. La incidencia en la actividad nuclear entre las galaxias pares es de 49 % $\pm$ 6 % para galaxias con líneas de emisión y del 41 % $\pm$ 6 % para la muestra total (comparada con un 43 % $\pm$ 5 % y 41 % $\pm$ 5 % que posee una muestra de galaxias aisladas respectivamente). No parece haber una diferencia significativa entre las incidencias de galaxias en pares y aisladas excepto para un solo caso: el de galaxias Sb en pares mixtos (E+S) comparadas con Sb en aisladas. La diferencia es de un 17 % que tiene un nivel de significancia de 2.26 σ.

Mostramos como se aplana la distribución de la incidencia AGN cuando se incluyen en la muestra total de galaxias aquellas que no tienen líneas en emisión.

Este trabajo muestra la relación entre la morfología y la actividad AGN que en la mayoría de los casos (salvo las Sb) domina sobre los efectos de marea.

Si consideramos que una evolución secular puede mantener una actividad nuclear o AGN para galaxias de baja luminosidad y al mismo tiempo que la diferencia en las incidencias de AGN entre galaxias pares y aisladas no es del todo significativa, entonces tal vez las fuerzas de marea gravitacionales entre galaxias no son lo suficientemente importantes comparadas

con la evolución secular y solo se tornan significativas para detonar un AGN más energético cuando existe un encuentro violento o de tipo merger.

Artículo por enviar a la revista Monthly Notices of the Royal Astronomical Society.

Induced Nuclear Activity in Galaxy Pairs With Differents Morphologies (E+E), (E+S) and (S+S).

Francisco J. Hernández-Ibarra[1]*, Deborah Dultzin[1], Yair Krongold[1],
Ascensión del Olmo[2], Jaime Perea[2] and Jesús González[1]

[1]*Instituto de Astronomía, Universidad Nacional Autónoma de México, Apartado Postal 70-264, 04510 México DF, México.*
[2]*Instituto de Astrofísica de Andalucía (C.S.I.C.) Apartado 3004, 18080 Granada, Spain.*

ABSTRACT

We analyzed 385 galactic spectra from the SDSS (DR7) that belong to the catalog of isolated pairs of galaxies by Karachentsev. They are all physical pairs as defined by V $\leqslant$ 1200 Km/s and their separation is $\leqslant$ 100 Kpc. We search for the incidence of nuclear activity both thermal (Starburst) and non-thermal (AGN). After a careful extraction of the nuclear spectra, we plot our measurements in diagnostic diagrams, and find that: (1) the incidence of AGN activity is 49 % in the paired galaxies with emission lines and 41% for the total sample (as compared to $\sim$ 43 % and 41% respectively in a sample of isolated galaxies). When a subsample of Ellipticals and Spheroidal galaxies are considered in pairs containing those morphologies: (E+E) and (E+S), the incidence of AGN activity is $\sim$ 75 %. (2) Type 1 galaxies are almost absent from the AGN sample. This last result is in conflict with the simplest version of the so called Unified Model, but can be naturaly explained in the context of the evolutionary model (which may include an obscuration/orientation phase). The role of a bulge is essential for the tidal triggering of nuclear activity.

Key words: galaxies: active - galaxies: evolution - galaxies: interactions

1 INTRODUCTION

One of the outstanding problems in the understanding of the Active Galactic Nuclei (AGN) phenomenon is the feeding processes of the central Supermassive Black Hole. The gas fueling may be driven from extragalactic to galactic, and further to nuclear scales. The main proposed mechanism to induce gas inflow to the center of galaxies, on the extragalactic scales, consists primarily of interactions with other galaxies (Barnes & Hernquist 1992). In this paper we address very direct and specific observational evidence of the role of gravitational interactions in inducing nuclear activity. In an attempt to elucidate this question from an observational point of view in the past 20 years several efforts have focused in the study of the environment of AGN. Most of the investigations have dealt with samples of Seyfert galaxies, because these are the closest clearly non-thermal dominated active nuclei. LINERs are easy to observe, however, the nature of the dominating emission mechanism is not yet well established (Krongold et al. 2003; González-Martín et al. 2007). Starburst phenomena (particularly circumnuclear) have also been included as a type (and/or part) of activity. The first authors to propose a Starburst-AGN connection were Perry

& Dyson (1985). An excellent recent review on this topic can be found in Storchi-Bergmann (2008).

The first studies of the extragalactic influence on AGN, were devoted to investigate the difference in the environment between active and non-active galaxies, without distinguishing activity type, (Dahari 1984, 1985). But soon it became clear that it was necessary to distinguish between type 1 and type 2 AGN (and even Starburst or enhanced Star Forming activity). More recently, the importance of making a difference between close and large scale environment, has become clear. The first studies were affected by the lack of clear definitions, statistical biases and also biases introduced by sample selection effects. All these methodological problems have yielded contradictory results that can be found in the literature for over more than 20 years from Stauffer (1982b,a) to Koulouridis et al. (2006a,b). One of the first discussions of these effects is given in Dultzin-Hacyan et al. (1999) hereafter DH99, and a detailed account of these different results is reviewed and analyzed recently by Sorrentino et al. (2006).

As more refined studies have been performed, it has become clear that Seyfert 2 galaxies are in interaction with the same frequency than Star-Forming Galaxies (SFG) (Storchi-Bergmann 2008; Krongold et al. 2001), while Seyfert 1 galaxies are in interaction less frequently. Seyfert 1s are found with close companions comparably as often as non-active

* E-mail:hibarra@astro.unam.mx

2   *F. J. Hernández-Ibarra, D. Dultzin, Y. Krongold, A. Del Olmo, J. Perea, J. González*

Table 1. General statistics on every single galaxy subsample pair.

Sample	Total	No Emission	Excluded	Fitted	AGN+Comp	H II	AGN Type 1
(E+E)	58	31(53%)	3(5%)	25(43%)	19(33%)	6(10%)	2(3%)
(E+S)	103	23(22%)	2(2%)	78(76%)	48(47%)	30(29%)	1(1%)
(S+S)	224	9(4%)	9(4%)	203(91%)	83(37%)	120(54%)	1(0.4%)
TOTAL	385	63(16%)	14(4%)	306(79%)	150(39%)	156(41%)	4(1%)
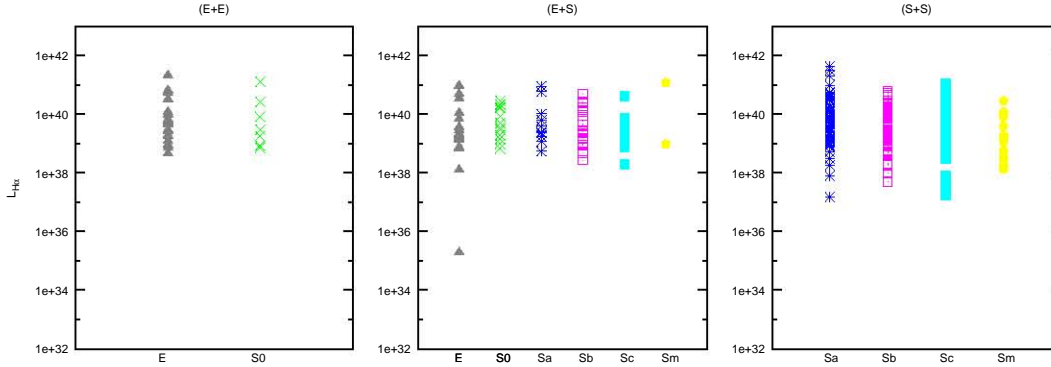
Figure 1. Morphological distribution of Hα luminosity for: left; (E+E) sample, middle; (E+S) sample and right; (S+S) sample. Mean values of AGN Hα luminosity for the three samples are $L_{H\alpha} = 2.28 \times 10^{40}\ erg\ s^{-1}$, $L_{H\alpha} = 2.92 \times 10^{40}\ erg\ s^{-1}$ and $L_{H\alpha} = 1.44 \times 10^{40}\ erg\ s^{-1}$ respectively.

galaxies (Krongold et al. 2002, DH99). The most recent studies confirm these findings considering only physical companions, i.e. not only from statistical considerations but from actual measurements of radial velocities for the neighboring galaxies (Koulouridis et al. 2006a,b). From the statistical point of view, Sorrentino et al. (2006) have made the comparison of the environment of AGN, SFG and normal galaxies, for a complete sample of 1829 Seyfert Galaxies (725 Sy1 and 1104 Sy2) and 6061 SFG from the Fourth Data Release (DR4) of the SDSS. This study fully confirms the results found by DH99 and by Koulouridis et al. (2006a,b). The authors state that for close systems ($\leqslant$ 100 kpc) they find a a higher fraction of Sy2 compared to Sy1 in agreement with DH99", moreover, the frequency of Sy2 is similar to that of SFGs. At large scales however, there is no strong evidence of a denser environment for AGN compared to "normal" galaxies in agreement with Schmitt (2001) and Koulouridis et al. (2006a). Any difference in the large-scale environment of Sy2 and Sy1 is more related to the morphological type of the host rather than to activity (see also Márquez & Masegosa 2008).

In all of the above analysis the environment of well defined samples of active vs. non-active galaxies were compared. In the present paper we adopt a complementary approach. We study the incidence of nuclear activity in a well defined sample of interacting galaxies. We focus on the sample of the Catalogue of Isolated Pairs in the Northern Hemisphere (Karachentsev 1972). We separate in three morphological pairs; 1) Elliptical plus Elliptical pair (E+E) considering galaxies with spheroidal morphology S0, 2) Elliptical plus Spiral pair (E+S) and 3) Spiral plus Spiral pair (S+S) in order to quantify the incidence of nuclear activity in every single pair sample.

Recently, galaxies in elliptical pairs (E+E) have shown

a raised on the level of recent star formation relative to a control sample of early-type galaxies (Rogers et al. 2009). The scenario after a first stage of the encounter that triggers residual star formation seems to be a more efficient inflow towards the center switching to an AGN phase. The possibility that external perturbations may enhance the frequency of nuclear activity among galaxies, as has been suggested by previous studies (Dultzin-Hacyan et al. 1999; Krongold et al. 2002, 2003; Rogers et al. 2009; Ellison et al. 2011).

Mixed galaxy pairs (E+S) are a unique laboratory to study the effect of tidal forces in triggering nuclear activity because they are relatively simple systems where a gas rich galaxy interacts with a gas poor one. In such systems a clean interpretation of the origin and evolution of the gaseous component is possible. Mixed pairs minimize the role of the relative orientation and pair component spin vectors, in driving interaction-induced effects (Keel 1993). Since the late-type spiral component is the primary source of gas in a mixed pair, it is therefore expected to be the site of all or most star formation and nuclear activity, although recent results have shown evidence of star formation and AGN activity in a non-negligible fraction of the early type components of the pairs (de Mello et al. 1995, 1996; Domingue et al. 2005, based on IRAS data). The presence of AGN activity on the early type components can be directly confirmed by means of spectroscopic data (Dultzin et al. 2008; Coziol et al. 2011; Sabater et al. 2012).

Previous studies, based on spiral-spiral pairs (S+S), have shown that starburst and possibly AGN activity in galaxies may be triggered by interactions. Kennicutt & Keel (1984) studied a sample of 56 nearby spirals in pairs vs. a control sample of 86 non-interacting galaxies, and found that interactions induce an enhancement of the level of nuclear

activity. Furthermore, they also found a significant fraction of Seyfert or Seyfert-like type nuclei. However, these studies have searched for activity without distinguishing between thermal (starburst, hereafter SB) and non-thermal (properly an AGN) activity. Thus these studies have not addressed the incidence of type 1 vs. type 2 AGN in pairs of galaxies.

In this work, we study the incidence of nuclear activity in a well isolated sample of galaxy pairs. Host spectra galaxy extraction and line emission measurements has been done with peculiar process in order to make a good quantification of data. We can define the activity type of AGN and separates between Seyfert and LINERs galaxies.

In the sections below, we present the sample and data analysis (Section 2), where we make a optical classification by diagnostic diagrams and present some peculiar features of morphology on some galaxies. On section 3 we present result of nuclear activity and find the almost absent of AGN type 1 for the entire sample. Discussion take place on section 4 and according with the results, the possible enhanced of nuclear activity by environment or morphology on this pairs is important to elucidate what model of AGN (Unified or Evolutionary) can be more according to the results. On section 5 we present the final conclusions of this work.

2 SAMPLE AND DATA ANALYSIS

Our study uses the Catalog of Isolated Pairs of galaxies (Karachentsev 1972, CPG) that contains around 600 galaxy pairs. This catalogue was based on a visual search of the Palomar Sky Survey with $\delta \geqslant -3^\circ$. The majority of objects have high galactic latitude $b \geqslant 20^\circ$ (in order to avoid galactic extinction) and magnitude limit $m_{Zw} \leqslant 15.7$. Karachentsev (1972) used a strong pair-isolation criterion in terms of the apparent angular separation between pairs ($\leqslant 100$ Kpc). The criteria used to build the CPG can be resumed by the following relations:

$$\frac{x_{ij}}{x_{12}} \geqslant \frac{5a_i}{a_j}; \qquad 0.5a_j \leqslant a_i \leqslant 4a_j \qquad (1)$$

where $j = 1, 2$ correspond to the pair components and i is the nearest neighbor, a represents the major-axis diameter and x the apparent separation. The overall completeness of this catalogue has been estimated in ~ 90 % (Hernández Toledo et al. 1999).

We obtain all available spectra from Sloan Digital Sky Survey Data Release 7 (SDSS-DR7) for this sample (Abazajian et al. 2009), spectra have a wavelength coverage from 3800-9200Å and a resolution of 1800-2200 with a signal-noise >4 per pixel at g=20.2. According to the SDSS spectroscopic limit (r = 17.77) 99% of our objects have a r-magnitud brigther than this and thus our sample is practically complete.

The SDSS spectra were taken through a fiber aperture of 3 arcsec in diameter (corresponding to 1.247 kpc at a redshift of 0.02), this way nuclei of galaxies was observed. Our sample consist of 385 galaxy spectrum from which 63 present no emission lines, 9 do not have above of 3 σ detection in all their lines, 4 have problems with the host galaxy spectra and 1 does not have the optic fiber in the galaxy center (not included in this work). A visual inspection was
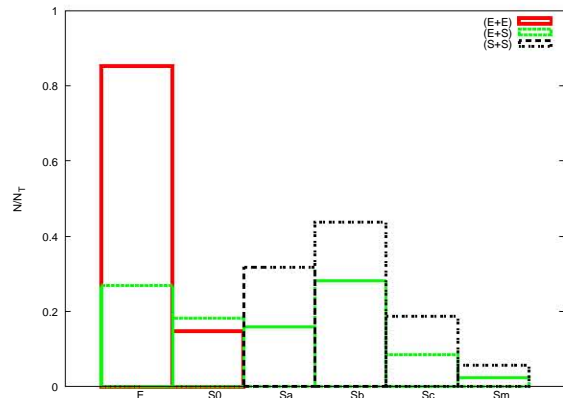
Figure 2. Morphological distribution of galaxies in elliptical, mixed and spiral pairs. Continuous red line correspond to (E+E) pair sample, green dashed line to (E+S) and black dotted line to (S+S) pair samples.
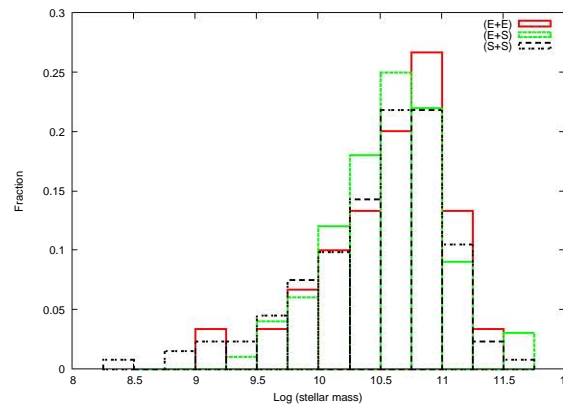
Figure 3. Mass distribution for the three subsample galaxy pairs. Labels like in Figure 2.

performed for all galaxies to confirm the morphological classification according to NED, SIMBAB and HYPERLEDA. In those few cases where an obvious misclassification was present, the morphology was corrected by us.

We were careful to distinguish between intrinsic no emission and a problem of detectability related to low S/N. For this purpose we set a threshold of 10^{38} erg s^{-1} in Hα luminosity. The galaxies below this threshold are the true no-emission objects with a probability of being an AGN of less than 2%. The distribution of morphology and Hα luminosity of our samples are presented in Figure 1.

We focus in measuring intensity of strong emission lines Hβ, [O III] $\lambda5007$, [O I] $\lambda6300$, Hα, [N II] $\lambda6584$ and [S II] $\lambda\lambda6717,31$ with a signal to noise ration (S/N)$\geqslant$ 3. There are 7 spectra which present less than 3 σ detection in their lines. KPG 303B in Hβ and [O I] $\lambda6300$ lines has > 1 σ, KPG 317A with [O I] $\lambda6300 > 2$ σ, KPG 339B has Hβ with > 2 σ detection and [O I] $\lambda6300 > 1$ σ, KPG 392A with Hβ < 1 σ and [O I] $\lambda6300 > 1$ σ, KPG 408A has > 2 σ and [O I] $\lambda6300 > 1$ σ, KPG 412B with Hβ > 1 σ, [O I] $\lambda6300 > 2$ σ and [O III] $\lambda5007 > 2$ σ and KPG 432A with Hβ > 2 σ, [O I] $\lambda6300 < 1$. KPG 058B does not have a good host galaxy
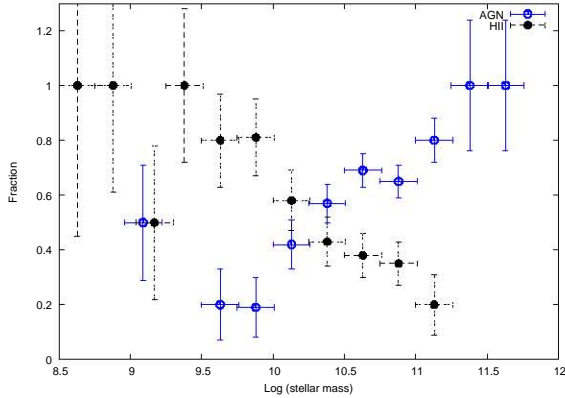
Figure 4. AGN and H II fraction of galaxies as a function of stellar mass. AGN are show as blue empty circles and H II objects by black filled circles. Errors in y-direction are the standard deviation per bin and the "error bars" in x-direction denote the range of mass in each bin.

extraction, so, we did not include in the sample. KPG 445A has only [N II] $\lambda6584$ and Hα lines above $3\,\sigma$ detection but, it can be possible make a preliminary classification with only this two lines as it shows on Figure 6(a).

The collected integrated spectroscopic area of the SDSS is 3 arcsecs, and this area might include stellar light contamination. This contamination turns out to be more significant at the central parts of the galaxies as the spheroidal/bulge component becomes more relevant. Therefore, in order to obtain a reliable nuclear classification based on the emission lines it is mandatory to subtract the stellar contribution. We applied the principal component analysis (PCA) method following Hao et al. (2005) to subtract this contribution. We used their first 8 eigenspectra from their low redshift range. These eigenspectra are the resulting eigenvectors of a PCA analysis applied to a sample of high S/N spectra of non-emission galaxies. In addition, as they pointed out, we included two more components, an A star spectrum accounting for the possible presence of poststarburst features and a power-law to take into account of the possible existence of a non-thermal component. The analysis is performed for all the spectra of our sample and it consists on a multiple regression of each spectrum to a linear combination of the 8 eigenspectra plus the two additional components. Previously to the fit each galaxy spectrum was moved to zero redshift which is the one of the template library. We also masked all those regions where emission lines may appear since the quality of the fit lies on the matching of the continua. Once the regression is performed, the direct subtraction of the resulting fit to the original (z=0) spectrum provides us with a pure emission line spectrum where all the underlying absorption components and eventually a non thermal component of the continuum are removed.

Fluxes were calculated with Sherpa software (http://cxc.cfa.harvard.edu/sherpa/) which comes in the CIAO distribution, http://cxc.harvard.edu/ciao/. This program fits emission lines with Gaussians, constraining width and velocity of the Balmer and forbidden lines to unique value in our fits. This way we can measured the intensity of each emission line.

We have evaluated two methods to fit the lines: see description in Hernández-Ibarra et al. (2013) hereafter (H-I13). We fitted the emission lines with the method which has less free parameters. For those objects where a broad component was required in addition to the narrow one, an individual broad Gaussian was fitted with fully independent free parameters.

Figures 2 and 3 show the morphological type and mass distributions respectively for the galaxies in the three subsamples of galaxy pairs. In Figure 4 we show the AGN and HII activity fraction versus the logarithm of stellar mass per bin. From this Figure we can see a tendency for higher mass galaxies to host an AGN, while lower mass emission line galaxies tend to be H II galaxies.

2.1   Optical classification

We based our optical classification on diagnostic diagrams (Baldwin et al. 1981; Veilleux & Osterbrock 1987). With the 7 emission lines that we have measured, we can build diagnostic diagrams with the four optical line ratios [O III]/Hβ, [N II]/Hα, [S II]/Hα and [O I]/Hα. We use two lines to separate galaxies into AGN, composite galaxies (whose spectra contain contributions of both AGN and Starburst features) and H II galaxies (without separated starburst from star formation galaxies). The first line is a "maximum starburst line" (Kewley et al. 2001) hereafter Ke01 line to separate galaxies with a AGN from starburst, beside this, one empirical line dividing pure star forming galaxies from AGN-starbursts composite objects (Kauffmann et al. 2003) hereafter Ka03.

In Figure 5 we present three diagnostic diagram for the (E+E) pair sample. (a) The LOG ([N II]/Hα) versus LOG ([O III]/Hβ) (hereafter [N II] diagram) diagnostic diagram. This diagram separates between tree different kind of activity in galaxies like AGN, Composite and H II like region galaxies. The green dashed line (Ke01) separates galaxies with a AGN from starburst. Continuous red line (Ka03) divides pure star forming galaxies from AGN-starbursts composite objects. If galaxies are between the two classification lines, they qualify like composites, meaning that they contain metal-rich stellar population and AGN features in their spectra. Composite galaxies consist of a circumnuclear Starburst surrounding a Seyfert or LINER nucleus.

(b) The LOG ([S II]/Hα) versus LOG ([O III]/Hβ) (hereafter [S II] diagram) diagnostic diagram separates between H II like region galaxies, Seyfert galaxies and LINERs. The green line is Ke01 and the dashed blue line (Ke06 line, see details in Kewley et al. (2006)) separates AGN activity between Seyfert and LINER . Objects below Ke01 line are classed like HII like regions and above the line like AGN. On this diagram objects above Ke01 line can be Seyfert objects (above Ke06 line) or LINERs objects (below Ke06 line). (c) The LOG ([O I]/Hα) versus LOG ([O III]/Hβ) (hereafter [O I] diagram) diagnostic diagram separates between H II like region galaxies, Seyfert galaxies and LINERs with O I/Hα ratio in the same way that (b) diagram.

Figure 6, shows the [N II], [S II] and [O I] diagrams for the (E+S) pair sample. Similarly Figures 7, 8 and 9 show [N II], [S II] and [O I] diagnostic diagrams for the (S+S) pair sample. We separated by morphological classification
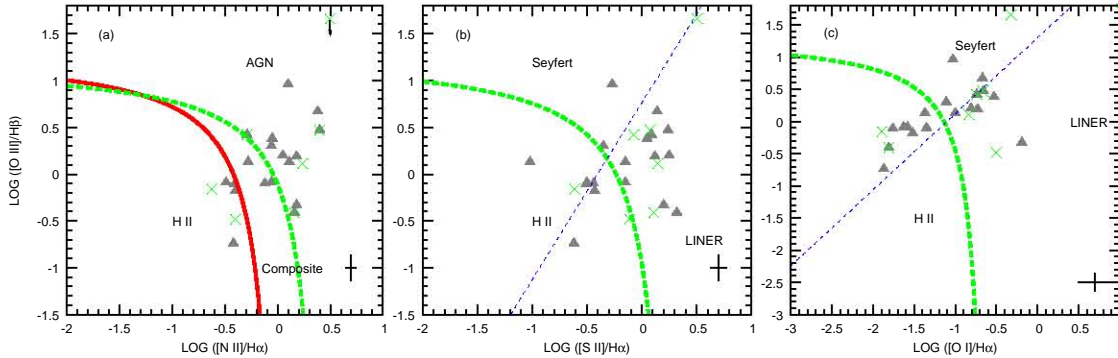
Figure 5. Diagnostic diagrams of galaxies in (E+E) pairs. (a) The [N II] diagnostic diagram. (b) The [S II] diagnostic diagram. (c) The [O I] diagnostic diagram. Blue dashed line represents Seyfert/LINER line. Elliptical galaxies can be seen on filled grey triangles, lenticular on green crosses and the black crosses down on the right represents the mean error data.
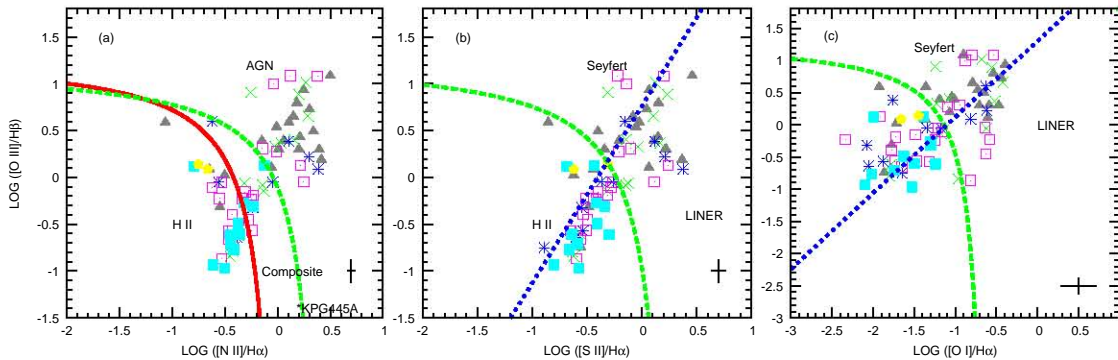
Figure 6. The [N II] diagnostic diagram for (E+S) pair sample. Morphological classification is show to every object, elliptical galaxies can be seen on filled grey triangles, lenticular on green crosses, Sa on blue asterisks, Sb red squares with point, Sc filled cyan squares and Sm yellow pentagons. Mean error data are represented by the black cross down at right.

the galaxies on Figures 5,6,7,8 and 9 to see distribution of every kind of galaxy type. Elliptical, Lenticular, Sa with all minor features like bars, rings and so on and the same for Sb, Sc and Sm galaxies.

Ambiguous galaxies can be present in borders of lines separation. Galaxies that can be classified as one type of activity in one diagram can be other type in another one. So, ambiguous galaxies can be those that lie in different regions for diagrams on Figures 5(b)(c), 6(b)(c), 8 and 9 or composite objects that can be classified as H II or AGN activity.

In this work, we consider composite galaxies as AGN, because they could be obscured or low accretion rates AGN galaxies. This is supported by the fact that composite galaxies present a X-ray hard emission, and are considered AGN in other types of diagnostic diagrams such as the TBT diagram (see Trouille et al. 2011).

2.2 Morphological classification

KPG 466B is clearly spiral in SLOAN image and could be part of the S+S pairs. According to NED KPG 167A is elliptical type, but it is evident from the SLOAN image that it is a spiral. KPG 167B is Sb type according NED again, but we can see clearly an elliptical. It is possible that morphology has been changed in this pair. KPG 466A presents in its lines a double component in both the permitted and forbidden lines. This might be due to a circumgalactic ring that can be see distinguished in the SLOAN image. We examined the morphological classification of KPG 419A from a surface photometry study by Franco-Balderas et al. (2004) in order to avoid ambiguity between NED, SIMBAD and HYPERLEDA data.

3 RESULTS

AGN activity is present more frequently in early morphological types (E,S0) as can be seen in Figure 5 and 6 and
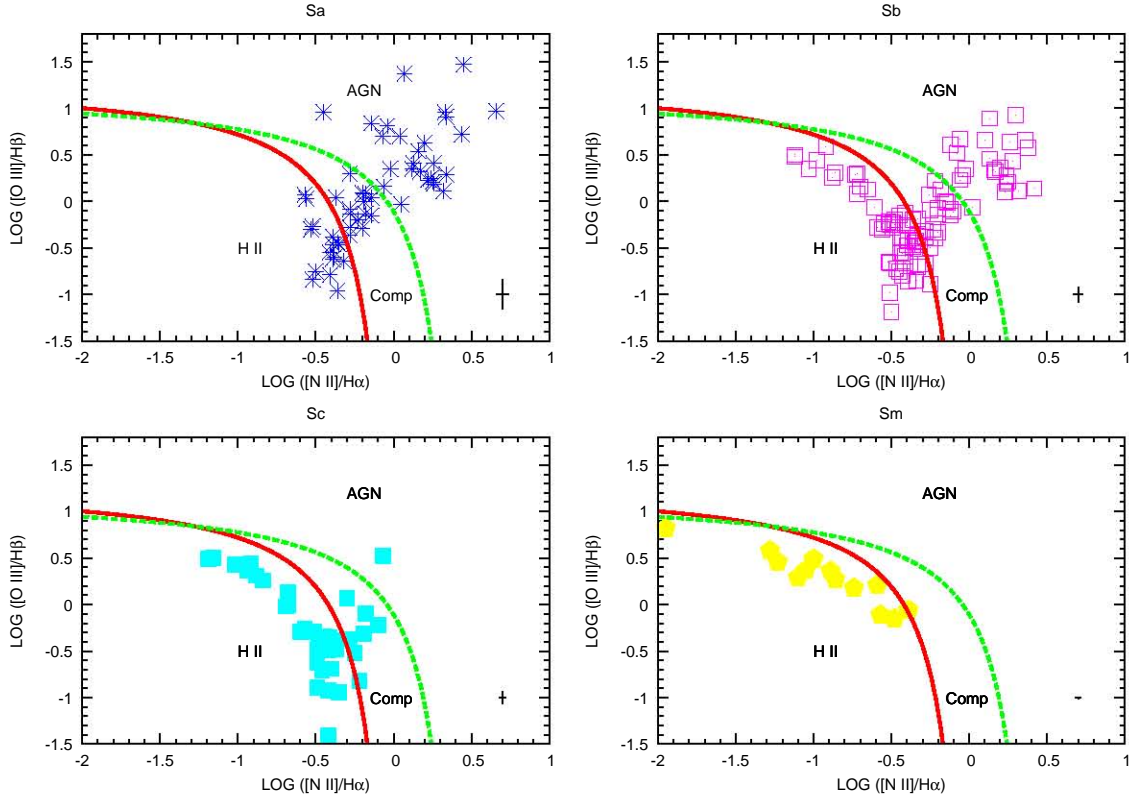
Figure 7. Diagnostic diagram [N II] for galaxies in (S+S) pairs.

Table 2. Morphology distribution and incidence of nuclear activity in (E+E) pair sub-sample derived from [N II] BPT diagnostic diagram.

M.T.	Galaxies with Emission lines				Total sample			
	Total	H II	Comp	AGN+Comp	Total	H II	Comp	AGN+Comp
E	18	5(28%)	3(17%)	13(72%)	41	5(12%)	3(7%)	13(32%)
S0	7	2(29%)	1(14%)	5(71%)	14	2(14%)	1(7%)	5(36%)
Total	25	7(28%)	4(16%)	18(72%)	55	7(13%)	4(7%)	18(33%)

Table 3. Morphology distribution and incidence of nuclear activity in (E+S) pair sub-sample derived from [N II] BPT diagnostic diagram.

M.T.	Galaxies with Emission lines				Total sample			
	Total	H II	Comp	AGN+Comp	Total	H II	Comp	AGN+Comp
E	21	5(24%)	0(0%)	16(76%)	33	5(15%)	0(%)	16(48%)
S0	13	3(23%)	3(23%)	10(77%)	19	3(16%)	3(16%)	10(53%)
Sa	10	4(40%)	3(30%)	6(60%)	13	4(31%)	3(23%)	6(46%)
Sb	21	8(38%)	6(29%)	13(62%)	21	8(38%)	6(29%)	13(62%)
Sc	11	8(73%)	3(27%)	3(27%)	11	8(73%)	3(27%)	3(27%)
Sm	2	2(100%)	0(0%)	0(0%)	2	2(100%)	0(0%)	0(0%)
Total	78	30(38%)	15(19%)	48(62%)	99	30(30%)	15(15%)	48(48%)

Induced Nuclear Activity in Galaxy Pairs With Differents Morphologies (E+E), (E+S) and (S+S).   7
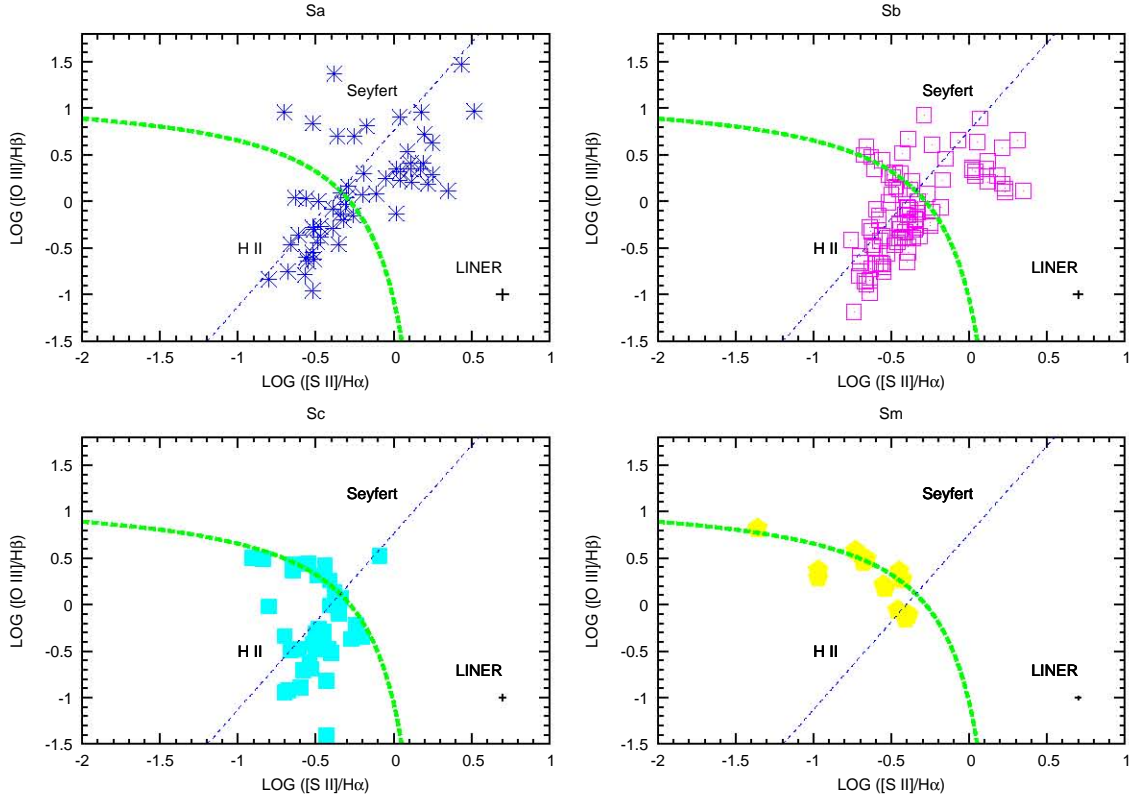
Figure 8. Diagnostic diagram [S II] for galaxies in (S+S) pairs.

Table 4. Morphology distribution and incidence of nuclear activity in (S+S) pair sub-sample derived from [N II] BPT diagnostic diagram.

M.T.	Galaxies with Emission lines				Total sample			
	Total	H II	Comp	AGN+Comp	Total	H II	Comp	AGN+Comp
Sa	60	22(37%)	12(20%)	36(60%)	65	22(34%)	12(18%)	38(58%)
Sb	92	54(59%)	16(17%)	38(41%)	97	54(56%)	16(16%)	38(39%)
Sc	39	33(85%)	6(15%)	6(15%)	40	33(83%)	6(15%)	6(15%)
Sm	12	11(92%)	1(8%)	1(8%)	12	11(92%)	1(8%)	1(8%)
Total	203	120(59%)	35(17%)	83(40%)	214	120(56%)	35(16%)	83(39%)

Tables 2 and 3. This tendency diminishes when we consider the complete sample including non-emission lines galaxies.

In general our sample of galaxy pairs present a 49 % of nuclear activity for galaxies with emission lines and for the total sample a 41%. We can compare this incidence with a sample of isolated galaxies that present nuclear activity of ∼ 43 % in emission lines galaxies and ∼40% for the total sample (H-I13). At first glance, this difference seems statistically insufficient to indicate any effect of tidal triggering of nuclear activity. This will be analyzed in more detail below.

In diagrams [S II] and [O I] of Figure 6 and Table 6, show that none of Sc or Sm galaxy has nuclear activity and that AGN types can be divided by blue dashed line (Ke06). The Ke01 line provide an upper limit to the galaxies which spectra present features of H II like region. Galaxies classified like AGN in Figure 6(a) are mostly in the LINER zone for diagrams on Figures 6(b) and 6(c) for galaxies with el-

liptical and spheroidal morphology, while galaxies classified as H II like region in Figure 6(a) are predominantly present in the same region in this diagram and the others.

In Figures 6 to 9 and Tables 6 and 7, we can see that a similar previous trend in Sa y Sb galaxies for (E+S) and (S+S) subsamples. Although, [OI] diagram differs only slightly from [NII] and [SII] in AGN numbers maybe because we do not consider composite nuclei objects in [SII] and [OI] diagrams. A difference in relative proportion of Seyfert and LINERs galaxies is present between [SII] and [OI] diagnostic diagrams. We point out that the [OI] line is weaker than the [SII] and the mean error is larger.

Sc and Sm galaxies show practically only H II like regions. As we can see in Tables 5, 6 and 7 for every galaxy, the morphological classification according to each BPT diagram taking in account the errors in data. COMP-H II means that galaxy is classified like AGN but can be H II
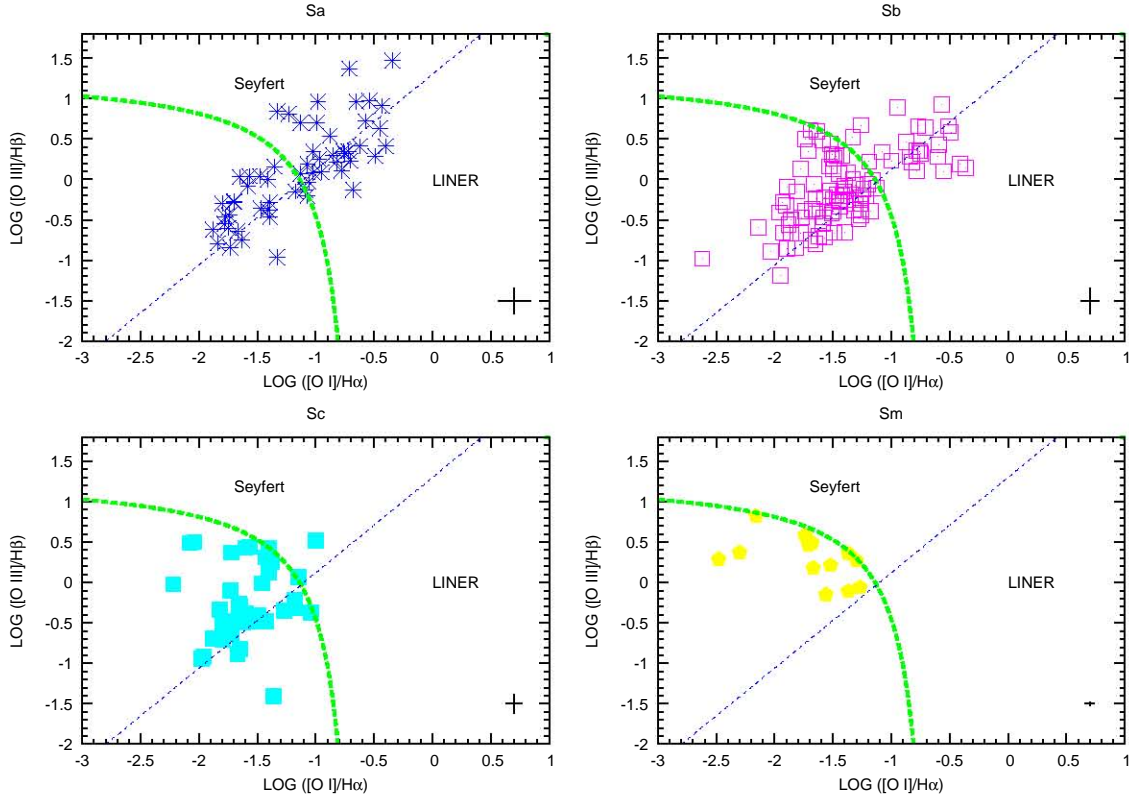
Figure 9. Diagnostic diagram [O I] for galaxies in (S+S) pairs.

Table 5. Incidence type of nuclear activity for different morphologies from [S II] and [O I] diagnostic diagrams for (E+E) sample.

M.T.	[S II] Diagram				[O I] Diagram			
	Total	AGN	Seyfert	LINER	Total	AGN	Seyfert	LINER
E	18	12(67%)	2(11%)	10(56%)	18	10(56%)	5(50%)	5(50%)
S0	7	5(71%)	0(0%)	5(100%)	7	5(71%)	1(20%)	4(80%)
Total	25	17(68%)	2(12%)	15(88%)	25	15(60%)	6(40%)	9(60%)

by error in measurement, and the same thing for LINER-Seyfert (L-S), Seyfert-LINER (S-L) or other combination. (See Tables 8,9 and 10 at the end of this article where we show logarithm intensities ratios and type classification for every object in the three subsamples).

In all the 385 revised spectra, only 4 objects present AGN type 1 activity, which represents ∼ 1% of the sample. This result does not seems to support the unified model at least in its simpler version.

4   DISCUSSION

We have made a comparison of the incidence of nuclear activity in a sample of paired galaxies with the incidence in a sample of isolated galaxies. All our samples were analyzed in a homogeneous and consistent way. This comparison has been done separating according to morphological types.

Our results confirm that there is a link between mor-
phology and nuclear activity. The incidence of AGN activity in Elliptical and Spheroidal galaxies is particularly significant (around ∼75 %, almost all LINERs). This incidence is similar in both isolated and paired galaxies. For spiral galaxies (both paired and isolated) the incidence of AGN activity decreases gradually form early to late type galaxies, in other words, as the size of the bulge decreases. Similar result has been found by Varela et al. (2004); Coziol et al. (2011); Sababater et al. (2012); H-I13)). However, if we include the non-emission line galaxies of the total sample, the incidence of activity shows a flatter distribution from E to Sb morphological types in mixed (E+S) pairs.

The comparison between isolated and pair spirals also yields similar levels of nuclear activity incidence, with one exception: Sb type galaxies in mixed morphology (E+S) pairs present a relevant 17% excess in nuclear activity with respect to isolated Sb galaxies. We calculated that this difference is statistically significant within a 2.6 σ level.

Induced Nuclear Activity in Galaxy Pairs With Differents Morphologies (E+E), (E+S) and (S+S).   9

Table 6. Incidence type of nuclear activity for different morphologies from [S II] and [O I] diagnostic diagrams for (E+S) sample.

M.T.	[S II] Diagram				[O I] Diagram			
	Total	AGN	Seyfert	LINER	Total	AGN	Seyfert	LINER
E	21	16(76%)	5(31%)	11(69%)	21	16(76%)	10(63%)	6(37%)
S0	13	9(69%)	2(22%)	7(78%)	13	8(62%)	5(63%)	3(37%)
Sa	10	4(40%)	1(25%)	3(75%)	10	3(30%)	1(33%)	2(67%)
Sb	21	7(33%)	2(29%)	5(71%)	21	9(43%)	5(56%)	4(44%)
Sc	11	0(0%)	0(0%)	0(0%)	11	0(0%)	0(0%)	0(0%)
Sm	2	0(0%)	0(0%)	0(0%)	2	(0%)	0(0%)	0(0%)
Total	78	36(46%)	10(28%)	26(72%)	78	36(46%)	21(58%)	15(42%)

Table 7. Incidence type of nuclear activity for different morphologies from [S II] and [O I] diagnostic diagrams for (S+S) sample.

M.T.	[S II] Diagram				[O I] Diagram			
	Total	AGN	Seyfert	LINER	Total	AGN	Seyfert	LINER
Sa	60	29(48%)	7(24%)	22(76%)	60	31(52%)	18(58%)	13(42%)
Sb	92	30(33%)	13(43%)	17(57%)	92	23(25%)	10(43%)	13(57%)
Sc	39	5(13%)	4(80%)	1(20%)	39	2(5%)	2(100%)	0(0%)
Sm	12	1(8%)	1(100%)	0(0%)	12	(0%)	0(0%)	0(0%)
Total	203	69(34%)	29(42%)	40(58%)	203	56(28%)	30(54%)	26(46%)

The above results indicate that this type of relatively weak (i.e. tidal) interaction between low luminosity galaxies is not a dominant triggering force of nuclear activity. Stronger gravitational interactions (mergers) are needed for gravitational triggering of activity. The particular case of tidal interaction between a Sb and E galaxy deserves further study and simulations. We point out here only that this is the intermediate case of a so called "wet/dry" type of interaction. With respect to the spiral component in this case, the Sb type is more prone to react because it has both a large bulb and a significant disc. With respect to the other pair component, one can expect an E type galaxy to induce the stronger type of perturbation. On the other hand, a study of the activity in (E+S) pairs of galaxies carried out by Dultzin et al. (2008) shows that the distribution of separations between galaxies with and without an AGN are different. They differ in the sense that Spirals that harbor an AGN tend to be closer to their elliptical neighbor.

Another relevant result from this work is the fact that out of the 150 AGN galaxies in pairs, only 4 have albeit a small broad component: We find one 1.9 Sy, two 1.8 Sy and one 1.5 Sy. Not even one type 1 Sy. This result in not possible to explain with the unified model (UM) (Antonucci 1993), which takes into account orientation and obscuration effects only, but does not address the environment at all.

An evolutionary model was developed by Krongold et al. (2002, 2003). This model may include an obscured phase in the evolution which combined with orientation effects can hide broad lines. However, one of the main predictions of this model is that most Seyfert galaxies that have a nearby physical companion of similar mass, should be type 2 Seyfert's.

REFERENCES

Abazajian K. N. et al., 2009, ApJS, 182, 543

Antonucci R., 1993, Ann. Rev. Ast. & Ast., 31, 473

Baldwin J. A., Phillips M. M., Terlevich R., 1981, Publications of the ASP, 93, 5

Barnes J. E., Hernquist L., 1992, Ann. Rev. Ast. & Ast., 30, 705

Coziol R., Torres-Papaqui J. P., Plauchu-Frayn I., Islas-Islas J. M., Ortega-Minakata R. A., Neri-Larios D. M., Andernach H., 2011, Revista Mexicana de Astronomía y Astrofísica, 47, 361

Dahari O., 1985, ApJS, 57, 643

Dahari O. A., 1984, PhD thesis, California Univ., Santa Cruz.

de Mello D. F., Keel W. C., Sulentic J. W., Rampazzo R., 1995, in van der Kruit P. C., Gilmore G., eds, IAU Symposium Vol. 164, Stellar Populations. p. 434

de Mello D. F., Sulentic J. W., de Souza R. E., Reduzzi L., Rampazzo R., 1996, Astronomy and Astrophysics, 308, 387

Domingue D. L., Sulentic J. W., Durbala A., 2005, Astronomical Journal, 129, 2579

Dultzin D. et al., 2008, ArXiv e-prints

Dultzin-Hacyan D., Krongold Y., Fuentes-Guridi I., Marziani P., 1999, ApJL, 513, L111

Ellison S. L., Patton D. R., Mendel J. T., Scudder J. M., 2011, MNRAS, 418, 2043

Franco-Balderas A., Hernández-Toledo H. M., Dultzin-Hacyan D., 2004, Astronomy and Astrophysics, 417, 411

González-Martín O., Masegosa J., Márquez I., Jiménez-Bailón E., 2007, in Karas V., Matt G., eds, IAU Symposium Vol. 238, IAU Symposium. pp 373–374

Hao L. et al., 2005, Astronomical Journal, 129, 1795

Hernández Toledo H. M., Dultzin-Hacyan D., Gonzalez J. J., Sulentic J. W., 1999, Astronomical Journal, 118, 108

Ho L. C., Filippenko A. V., Sargent W. L. W., 1997, ApJS

Ho L. C., Filippenko A. V., Sargent W. L. W., Peng C. Y., 1997, ApJS

Karachentsev I. D., 1972, Soobshcheniya Spetsial'noj Astrofizicheskoj Observatorii, 7, 1

Kauffmann G. et al., 2003, MNRAS, 346, 1055

Keel W. C., 1993, Astronomical Journal, 106, 1771

Kennicutt Jr. R. C., Keel W. C., 1984, ApJL, 279, L5

Kewley L. J., Dopita M. A., Sutherland R. S., Heisler C. A., Trevena J., 2001, ApJ, 556, 121

Kewley L. J., Groves B., Kauffmann G., Heckman T., 2006, MNRAS, 372, 961

Koulouridis E., Chavushyan V., Plionis M., Krongold Y., Dultzin-Hacyan D., 2006, ApJ, 651, 93

Koulouridis E., Plionis M., Chavushyan V., Dultzin-Hacyan D., Krongold Y., Goudis C., 2006, ApJ, 639, 37

Krongold Y., Dultzin-Hacyan D., Marziani P., 2001, Astronomical Journal, 121, 702

Krongold Y., Dultzin-Hacyan D., Marziani P., 2002, 572, 169

Krongold Y., Dultzin-Hacyan D., Marziani P., 2003, in Collin S., Combes F., Shlosman I., eds, Astronomical Society of the Pacific Conference Series Vol. 290, Active Galactic Nuclei: From Central Engine to Host Galaxy. p. 523

Márquez I., Masegosa J., 2008, in Revista Mexicana de Astronomia y Astrofisica Conference Series. pp 150–154

Perry J. J., Dyson J. E., 1985, MNRAS, 213, 665

Rogers B., Ferreras I., Kaviraj S., Pasquali A., Sarzi M., 2009, MNRAS, 399, 2172

Sabater J., Verdes-Montenegro L., Leon S., Best P., Sulentic J., 2012, Astronomy and Astrophysics, 545, A15

Schmitt H. R., 2001, Astronomical Journal, 122, 2243

Sorrentino G., Radovich M., Rifatto A., 2006, Astronomy and Astrophysics, 451, 809

Stauffer J. R., 1982a, ApJ, 262, 66

Stauffer J. R., 1982b, ApJS, 50, 517

Storchi-Bergmann T., 2008, in Revista Mexicana de Astronomia y Astrofisica Conference Series. pp 139–146

Trouille L., Barger A. J., Tremonti C., 2011, ApJ, 742, 46

Veilleux S., Osterbrock D. E., 1987, ApJS, 63, 295

Winkler H., 1992, MNRAS, 257, 677

Table 8. Logarithm intensities ratios and their errors for (E+E) sample.

Object	M.T. [a]	LOG([N II]/Hα)	LOG([O III]/Hβ)	LOG([S II]/Hα)	LOG([O I]/Hα)	Type
Elliptical						
KPG145B	E	0.1852 ± 0.0233	0.1772 ± 0.0714	0.2792 ± 0.0292	-0.7272 ± 0.0758	LINER
KPG170B	E	0.1994 ± 0.0698	0.0503 ± 0.1249	0.2482 ± 0.0792	-0.8132 ± 0.2803	LINER
KPG192B	E	0.3005 ± 0.0333	0.2032 ± 0.1058	0.2222 ± 0.0445	-0.4733 ± 0.0740	LINER
KPG204A	E	-0.6887 ± 0.0087	-0.2983 ± 0.0685	-0.5590 ± 0.0159	-1.6857 ± 0.0682	H II
KPG223A	E	0.3833 ± 0.0353	-0.0495 ± 0.0947	0.1936 ± 0.0389	-0.5300 ± 0.0684	LINER
KPG235B	E	0.2970 ± 0.0240	-0.0619 ± 0.0803	-0.1959 ± 0.0396	-1.1057 ± 0.1250	Sy2
KPG238A	E	-0.0985 ± 0.0713	-0.1181 ± 0.1809	-0.3106 ± 0.1496	-1.3532 ± 0.6396	AGN
KPG238B	E	-0.2778 ± 0.0091	0.1318 ± 0.0065	-1.0212 ± 0.0210	-1.3708 ± 0.0233	AGN*
KPG361B	E	0.1256 ± 0.0889	0.1128 ± 0.2682	0.0330 ± 0.1426	-1.0029 ± 0.5114	S-L
KPG372B	E	-0.0923 ± 0.0071	-0.4935 ± 0.0085	-0.3473 ± 0.0071	-1.6329 ± 0.0191	H II
KPG373A	E	0.5639 ± 0.0450	0.2682 ± 0.1039	0.1240 ± 0.0695	-0.6585 ± 0.1421	S-L
KPG399A	E	0.6728 ± 0.0459	0.3764 ± 0.2281	0.2738 ± 0.0657	-0.6724 ± 0.1656	S-L
KPG454A	E	-0.7423 ± 0.0065	-0.4240 ± 0.0199	-0.4600 ± 0.0078	-1.8731 ± 0.0401	H II
KPG454B	E	-0.1145 ± 0.0110	-0.4070 ± 0.0196	-0.3490 ± 0.0133	-1.7599 ± 0.0843	H II
KPG489A	E	-0.3270 ± 0.2184	0.1827 ± 0.2343	0.3003 ± 0.2657	-0.1871 ± 0.3307	LINER
KPG489B	E	-0.0934 ± 0.0477	-0.0634 ± 0.1344	-0.0082 ± 0.0654	-1.5781 ± 0.7487	AGN
KPG510B	E	0.1006 ± 0.0070	0.9620 ± 0.0095	-0.2733 ± 0.0095	-1.0261 ± 0.0205	Sy1.8
KPG600B	E	-0.1817 ± 0.0169	-0.4024 ± 0.0415	-0.2919 ± 0.0217	-1.5216 ± 0.1035	H II
Spheroidal						
KPG184B	S0	0.4740 ± 0.0313	0.3984 ± 0.1213	0.2363 ± 0.0469	-0.6619 ± 0.1102	LINER
KPG208A	S0	0.4751 ± 0.0102	-0.3961 ± 0.0124	-0.1139 ± 0.0107	-0.5039 ± 0.0093	Sy1.5
KPG208B	S0	-0.1639 ± 0.0068	-0.6217 ± 0.0095	-0.4434 ± 0.0073	-1.8897 ± 0.0319	H II
KPG277B	SB0	0.1127 ± 0.0388	0.2444 ± 0.1296	0.1511 ± 0.0584	-0.8281 ± 0.1667	LINER
KPG359A	SB0	0.4238 ± 0.0893	-0.2928 ± 0.2166	0.0869 ± 0.0805	-0.7440 ± 0.1854	S-L
KPG431B	S0	-0.4124 ± 0.0725	0.1635 ± 0.3280	0.3248 ± 0.0841	-1.8051 ± 2.5943	AGN
KPG492A	S0	1.6559 ± 0.0812	0.4975 ± -	0.5138 ± 0.0994	-0.3183 ± 0.1803	S-L

[a] M.T.- Morphological Type.

˙AGN classification denotes those galaxies that are AGN according to the [N II] diagrams but not to the [S II] and/or [O I].

[†] L-S classification means that galaxies fall in the separation line for Seyfert and LINER according to [S II] and [O I] diagrams.

[*] Type with weak broad component in permitted lines. Seyfert quiantitative classification according to Winkler (1992).

Table 9.   Logarithm intensities ratios and their errors for (E+S) sample.

Object	M.T.[a]	LOG([N II]/Hα)	LOG([O III]/Hβ)	LOG([S II]/Hα)	LOG([O I]/Hα)	Type
Eliptical						
KPG055A	E	0.4993 ± 0.1027	1.0842 ± 0.8013	0.4597 ± 0.1329	-0.9006 ± 0.9222	S-L
KPG089B	E	0.3029 ± 0.0896	0.7262 ± 0.4881	0.0451 ± 0.1716	-0.4415 ± 0.2174	S-L
KPG091B	E	0.4149 ± 0.0881	0.1889 ± 0.1558	0.3686 ± 0.1197	-1.0699 ± 1.2131	AGN
KPG144B	E	-0.4333 ± 0.0086	-0.7456 ± 0.0294	-0.5566 ± 0.0130	-1.8652 ± 0.0627	H II
KPG155A	E	-0.6479 ± 0.0128	0.0830 ± 0.0188	-0.4416 ± 0.0158	-1.3675 ± 0.0876	H II
KPG167A	E	0.3963 ± 0.0562	0.2965 ± 0.1364	0.2132 ± 0.0893	-0.7086 ± 0.2628	LINER
KPG197B	E	0.1071 ± 0.1254	0.5876 ± 0.5488	-0.0212 ± 0.2225	-1.3599 ± 1.8493	AGN
KPG198B	E	0.2118 ± 0.0666	0.4295 ± 0.1479	0.1489± 0.0988	-1.0428 ± 0.73956	AGN
KPG244A	E	0.2472 ± 0.1071	0.9321 ± 0.5472	0.0682 ± 0.1872	-0.3952 ± 0.2798	S-L
KPG254B	E	0.1830 ± 0.1103	0.7963 ± 0.6008	0.1519 ± 0.1599	-0.5364 ± 0.3098	S-L
KPG260B	E	-0.0098 ± 0.0491	0.5369 ± 0.1214	-0.0516 ± 0.0798	-0.7262 ± 0.1743	S-L
KPG339B	E	0.3400 ± 0.1271	0.4900 ± 0.2531	-0.4000 ± 0.5529	-0.6500 ± 0.7326	S-L
KPG363A	E	-0.1500 ± 0.0048	0.3900 ± 0.0100	-0.2062 ± 0.0053	-1.1900 ± 0.0286	Sy2
KPG383A	E	-0.0589 ± 0.0253	0.1041 ± 0.0549	0.0646 ± 0.0323	-0.6045 ± 0.0432	LINER
KPG394A	E	-0.5482 ± 0.0103	-0.3162 ± 0.0199	-0.4843 ± 0.0135	-1.7759 ± 0.1200	H II
KPG412B	E	0.0100 ± 0.0861	0.3000 ± 0.5584	-0.3400 ± 0.2379	-0.5900 ± 0.1510	AGN
KPG414B	E	-1.0658 ± 0.0064	0.5854 ± 0.0050	-0.8526 ± 0.0075	-1.9263 ± 0.3964	H II
KPG432A	E/S0	0.1500 ± 0.1628	0.6500 ± 0.2518	-0.0800 ± 0.3282	-0.79 ± 1.3913	AGN
KPG466B	E/S0	-0.2432 ± 0.0054	-0.5659 ± 0.0156	-0.5076 ± 0.0082	-1.4698 ± 0.0223	AGN
KPG494B	E	-0.5027 ± 0.0065	0.0234 ± 0.0087	-0.6204 ± 0.0094	-1.7156 ± 0.1363	H II
KPG565A	E	0.0575 ± 0.1217	0.3907± 0.1637	0.1120 ± 0.1654	-1.0119 ± 0.6625	S-L
Spheroidal						
KPG006A	S0	-0.4195 ± 0.0048	-0.7951 ± 0.0234	-0.6294 ± 0.0084	-1.7974 ± 0.0364	H II
KPG062A	S0/a	0.2940 ± 0.0327	0.6557 ± 0.1096	0.1072 ± 0.0540	-0.4205 ± 0.0758	LINER
KPG162A	S0	0.0361 ± 0.0650	0.3679 ± 0.1335	0.1669 ± 0.0810	-0.5131 ± 0.1451	LINER
KPG231A	S0	-0.1258 ± 0.0148	-0.1432 ± 0.0520	-0.3094 ± 0.0275	-1.1732 ± 0.0599	AGN
KPG243B	S0	-0.2481 ± 0.0124	-0.2337 ± 0.0358	-0.4167 ± 0.0220	-1.2459 ± 0.0583	AGN
KPG269A	S0	-0.3083 ± 0.0240	-0.0619 ± 0.0434	-0.1174 ± 0.0289	-0.6155 ± 0.0305	LINER
KPG275B	S0	-0.3729 ± 0.0071	-0.6161 ± 0.0192	-0.5494 ± 0.0106	-1.7735 ± 0.0488	H II
KPG304A	S0	-0.0882 ± 0.0262	0.0342 ± 0.1529	-0.2112 ± 0.0514	-1.5169 ± 0.3948	AGN
KPG317B	S0	-0.1411 ± 0.0318	-0.0846 ± 0.0741	-0.1459 ± 0.0495	-1.1398 ± 0.1709	AGN
KPG345B	S0/a	0.1580 ± 0.0438	0.4055 ± 0.2242	-0.1401 ± 0.0953	-1.0692 ± 0.2704	S-L
KPG374A	S0	0.2022 ± 0.0470	0.8882 ± 0.1197	0.2350 ± 0.0630	-0.5566 ± 0.2465	S-L
KPG392A	S0	0.2696 ± 0.0880	1.0135 ± 0.6311	0.1277 ± 0.1462	-0.6750 ± 0.4153	S-L
KPG402B	S0	-0.0239 ± 0.0353	0.3299 ± 0.0950	-0.0300 ± 0.0542	-1.2199 ± 0.3090	AGN
KPG408A	S0	0.0200 ± 0.0732	0.6000 ± -0.2100	-0.2200 ± 0.1651	-0.9400 ± 0.4780	S-L
KPG436A	S0	-0.4464 ± 0.0115	-0.8387 ± 0.0711	-0.6157 ± 0.0222	-0.9604 ± 0.2130	H II
Sa						
KPG055B	Sa	-0.4164 ± 0.0355	-0.7504 ± 0.2962	-0.8892 ± 0.1335	-1.6462 ± 0.3224	H II
KPG188A	Sa	-0.3864 ± 0.0080	-0.6397 ± 0.0235	-0.5991 ± 0.0130	-2.0507 ± 0.1187	H II
KPG197A	Sa	0.3868 ± 0.1200	0.0900 ± 0.1292	0.3765 ± 0.1596	-0.8110 ± 1.1059	AGN
KPG199B	Sa	-0.3736 ± 0.0231	-0.4916 ± 0.1184	-0.4074 ± 0.0370	-1.6238 ± 0.2468	H II
KPG239B	Sa	0.2471 ± 0.0812	-0.0440 ± 0.1153	0.1137 ± 0.1344	-0.6385 ± 0.3831	LINER
KPG260A	Sa	0.2989 ± 0.0445	0.2197 ± 0.0947	0.2112 ± 0.0657	-0.6162 ± 0.1726	LINER
KPG284A	Sa	-0.0451 ± 0.0223	-0.0490 ± 0.0966	-0.2627 ± 0.0448	-1.1747 ± 0.1157	AGN
KPG303B	Sa	0.2100 ± 0.1207	0.7600 ± -0.6208	-0.2500 ± 0.3488	-0.8100 ± 0.6206	Sy2
KPG317A	Sab	0.0313 ± 0.0566	0.0050 ± -0.2062	-0.6094 ± 0.2568	-0.8377 ± 0.2280	AGN
KPG402A	Sab	-0.5588 ± 0.0195	-0.0488 ± 0.0470	-0.3656 ± 0.0251	-1.3444 ± 0.0987	H II
KPG439B	Sa	-0.2339 ± 0.0068	-0.3203 ± 0.0247	-0.5447 ± 0.0126	-2.0767 ± 0.0270	AGN
KPG548A	Sa	0.1074 ± 0.0315	0.3850 ± 0.0636	0.1196 ± 0.0437	-1.7587 ± 0.0811	AGN
KPG466A	Sa	-0.6200 ± 0.0098	0.6000 ± -0.2100	-0.1500 ± 0.0122	-0.6300 ± 0.0300	S-L
Sb						
KPG089A	Sb	-0.4280 ± 0.0063	-0.3958 ± 0.0129	-0.5371 ± 0.0090	-1.7760 ± 0.0579	H II
KPG148A	Sb	-0.7930 ± 0.0076	0.1195 ± 0.0094	-0.6847 ± 0.0094	-1.9934 ± 0.1879	H II
KPG162B	Sb	-0.2290 ± 0.0278	-0.1913 ± 0.0809	-0.3094 ± 0.0494	-1.7259 ± 0.4955	AGN
KPG202B	Sb	0.3768 ± 0.0374	1.0828 ± 0.2444	0.2005 ± 0.0582	-0.5370 ± 0.1209	S-L
KPG229B	Sb	-0.4275 ± 0.0133	-0.5682 ± 0.0579	-0.6502 ± 0.0274	-1.7358 ± 0.1053	H II

Induced Nuclear Activity in Galaxy Pairs With Differents Morphologies (E+E), (E+S) and (S+S). 13

Table 9 (cont'd)

Object	M.T. [a]	LOG([N II]/Hα)	LOG([O III]/Hβ)	LOG([S II]/Hα)	LOG([O I]/Hα)	Type
KPG243A	Sb	-0.2517 ± 0.0125	0.9063 ± 0.0179	-0.3040 ± 0.0191	-1.2366 ± 0.2450	Sy2
KPG248B	Sb	-0.0132 ± 0.0176	0.2765 ± 0.0935	-0.2094 ± 0.0349	-1.0981 ± 0.1070	S-L
KPG254A	Sbab	0.1189 ± 0.0062	1.0848 ± 0.0092	-0.2198 ± 0.0098	-0.7999 ± 0.0984	Sy2
KPG269B	Sb	-0.5115 ± 0.0073	-0.3156 ± 0.0140	-0.5588 ± 0.0101	-1.7537 ± 0.0710	H II
KPG339A	Sb	-0.5009 ± 0.0144	-0.9664 ± 0.1302	-0.5756 ± 0.0244	-1.5262 ± 0.0801	H II
KPG345A	Sbs(dm)	-0.6208 ± 0.0266	-0.1099 ± 0.0559	-0.2803 ± 0.0271	-1.1642 ± 0.1137	H II
KPG374B	Sbc	-0.4636 ± 0.0162	-0.6559 ± 0.1089	-0.5556 ± 0.0298	-1.6522 ± 0.1230	H II
KPG392B	Sb	-0.1453 ± 0.0412	0.3090 ± 0.0698	-0.1000 ± 0.0604	-0.9476 ± 0.2024	S-L
KPG408B	Sb	-0.5318 ± 0.0276	-0.0493 ± 0.0680	-0.2616 ± 0.0306	-1.2143 ± 0.1363	H II
KPG416A	Sb	-0.4165 ± 0.0079	-0.7686 ± 0.0294	-0.6609 ± 0.0129	-2.0159 ± 0.0828	H II
KPG419A	SBb	-0.0400 ± 0.0073	1.0000 ± -0.2100	-0.1400 ± 0.0082	-0.8800 ± 0.0654	Sy1.9
KPG432B	Sb	-0.5281 ± 0.0183	-0.8646 ± 0.1123	-0.5979 ± 0.0308	-0.8139 ± 0.6375	H II
KPG436B	Sb	-0.3351 ± 0.0260	-0.2282 ± 0.1648	-0.5081 ± 0.0554	-2.3363 ± 0.1890	H II
KPG484B	Sb	-0.4621 ± 0.0242	-0.5690 ± 0.1357	-0.6541 ± 0.0586	-1.3153 ± 0.5506	H II
KPG494A	Sbc	-0.2737 ± 0.0106	-0.4524 ± 0.0416	-0.4959 ± 0.0207	-0.6307 ± 0.1096	AGN
KPG497B	Sb	0.2149 ± 0.0372	0.1282 ± 0.1041	0.2410 ± 0.0495	-1.9189 ± 0.2746	AGN
KPG558A	Sb	-0.3820 ± 0.0216	-0.5685 ± 0.1345	-0.5350 ± 0.0464	-1.8762 ± 2.0941	H II
KPG565B	Sb	-0.5528 ± 0.0163	-0.2266 ± 0.0389	-0.4436 ± 0.0215	-0.5792 ± 0.1180	H II
Sc						
KPG058A	Sc	-0.2334 ± 0.0200	-0.3081 ± 0.1289	-0.3386 ± 0.0395	-1.2968 ± 0.1063	AGN
KPG287A	Sc	-0.4494 ± 0.0290	-0.7093 ± 0.2075	-0.5882 ± 0.0640	-1.7455 ± 0.4297	H II
KPG314B	Sc	-0.4574 ± 0.0225	-0.6110 ± 0.1444	-0.2951 ± 0.0290	-1.2424 ± 0.0949	H II
KPG353A	Sc	-0.6103 ± 0.0155	-0.9310 ± 0.1019	-0.8004 ± 0.0309	-2.1018 ± 0.2166	H II
KPG407A	Sc	-0.1260 ± 0.0093	0.1290 ± 0.0184	-0.4357 ± 0.0173	-1.3858 ± 0.0731	AGN
KPG412A	Sc	-0.3194 ± 0.0167	-0.2700 ± 0.0974	-0.4120 ± 0.0315	-1.3003 ± 0.0892	H II
KPG464B	Sc	-0.3634 ± 0.0338	-0.6033 ± 0.2548	-0.6392 ± 0.0926	-1.4960 ± 0.1895	H II
Sm						
KPG198A	Sm	-0.6659 ± 0.0053	0.0858 ± 0.0066	-0.6191 ± 0.0066	-1.6593 ± 0.0651	H II
KPG414A	Sm	-0.7539 ± 0.0291	0.1398 ± 0.0340	-0.3100 ± 0.0247	-1.4477 ± 0.2577	H II

[a] M.T.- Morphological Type.

˙AGN classification denotes those galaxies that are AGN according to the [N II] diagrams but not to the [S II] and/or [O I].

[†] L-S classification means that galaxies fall in the separation line for Seyfert and LINER according to [S II] and [O I] diagrams.

[*] Type with weak broad component in permitted lines. Seyfert quiantitative classification according to Winkler (1992).

Table 10.   Logarithm intensities ratios and their errors for (S+S) sample.

Object	M.T. [a]	LOG([N II]/Hα)	LOG([O III]/Hβ)	LOG([S II]/Hα)	LOG([O I]/Hα)	Type
Sa						
KPG052B	SBa	-0.0227 ± 0.0390	0.3490 ± 0.0996	0.1075 ± 0.0491	-0.7634 ± 0.1161	LINER
KPG161A	Sa	-0.5634 ± 0.0375	0.0263 ± 0.0066	-0.5587 ± 0.0491	-1.6507 ± 0.0301	H II
KPG174B	Sab	0.2549 ± 0.0612	0.2078 ± 0.0900	0.1152 ± 0.0763	-0.8191 ± 0.1435	LINER
KPG185B	Sab	-0.2759 ± 0.0069	-0.2778 ± 0.0168	-0.5190 ± 0.0130	-1.6973 ± 0.0616	AGN
KPG190B	Sab	0.1749 ± 0.0543	0.3164 ± 0.1391	0.0379 ± 0.0914	-0.7517 ± 0.2010	LINER
KPG201A	Sa	0.4490 ± 0.0698	1.4683 ± 1.8727	0.4423 ± 0.0912	-0.3428 ± 0.1627	S-L
KPG211A	Sa	0.4428 ± 0.0748	0.7200 ± 0.2252	0.1979 ± 0.1218	-0.5703 ± 0.1677	LINER
KPG213B	Sa	0.3444 ± 0.0579	0.2904 ± 0.1466	0.2517 ± 0.0891	-0.4891 ± 0.1528	LINER
KPG215A	Sab	-0.1434 ± 0.0328	0.0360 ± 0.1589	-0.2980 ± 0.0655	-1.4753 ± 0.3560	LINER
KPG220B	SBa	-0.1989 ± 0.0099	-0.2887 ± 0.0302	-0.3935 ± 0.0168	-1.3904 ± 0.0502	AGN
KPG222A	Sa	-0.8551 ± 0.0166	0.2688 ± 0.0138	-0.4264 ± 0.0146	-1.3003 ± 0.0321	H II
KPG226A	Sa	-0.3940 ± 0.0285	-0.4566 ± 0.0566	-0.6650 ± 0.0497	-1.7715 ± 0.1479	H II
KPG228A	Sa	0.6609 ± 0.0571	0.9678 ± 0.4890	0.5192 ± 0.0759	-0.5400 ± 0.1937	LINER
KPG241B	Sab	0.2447 ± 0.0812	0.2500 ± 0.1807	-0.0550 ± 0.1654	-0.9701 ± 0.4729	LINER
KPG246A	Sa	-0.2320 ± 0.0315	-0.1986 ± 0.1405	-0.3219 ± 0.0585	-1.0657 ± 0.1296	AGN
KPG252A	Sa	-0.3869 ± 0.0086	-0.3767 ± 0.0242	-0.4692 ± 0.0130	-1.4058 ± 0.0306	H II
KPG255A	Sab	-0.5744 ± 0.0633	0.0659 ± 0.1759	-0.2047 ± 0.0573	-1.1323 ± 0.2016	H II
KPG257B	Sab	-0.3510 ± 0.0424	-0.4617 ± 0.1430	-0.3507 ± 0.0626	-1.3867 ± 0.1455	H II
KPG265B	Sa	-0.5187 ± 0.0063	-0.2686 ± 0.0157	-0.4742 ± 0.0083	-1.7040 ± 0.0328	H II
KPG266A	Sab	0.2197 ± 0.0233	0.2318 ± 0.0836	0.0383 ± 0.0383	-0.6966 ± 0.0718	LINER
KPG270A	Sab	-0.3889 ± 0.0286	-0.6248 ± 0.1815	-0.5075 ± 0.0526	-1.8829 ± 0.5054	H II
KPG285A	Sab	0.1228 ± 0.0315	0.3531 ± 0.1212	0.0166 ± 0.0511	-1.0220 ± 0.1804	LINER
KPG289B	Sa	-0.5191 ± 0.0108	-0.8371 ± 0.0614	-0.8041 ± 0.0242	-1.7303 ± 0.0709	H II
KPG312B	S0	0.0515 ± 0.0162	-0.0333 ± 0.0438	-0.3137 ± 0.0367	-1.0605 ± 0.0770	AGN
KPG318A	Sa	-0.0607 ± 0.0213	0.1645 ± 0.0371	-0.2907 ± 0.0402	-1.3473 ± 0.1531	S-L
KPG327A	S0/a	0.1601 ± 0.0569	0.5441 ± 0.1769	0.0906 ± 0.0883	-0.8800 ± 0.2621	LINER
KPG327B	S0/a	-0.3217 ± 0.0079	-0.6363 ± 0.0345	-0.5507 ± 0.0141	-1.6678 ± 0.0495	H II
KPG337A	SABa	0.0719 ± 0.0000	1.3675 ± 1.9245	-0.3788 ± 0.0559	-0.7109 ± 0.0000	Sy2
KPG342A	Sa	-0.5285 ± 0.0085	-0.3034 ± 0.0160	-0.5119 ± 0.0118	-1.8031 ± 0.0491	H II
KPG348A	Sa	-0.1799 ± 0.0124	0.0827 ± 0.0168	-0.1113 ± 0.0146	-1.0213 ± 0.0319	AGN*
KPG349B	SABm	-0.2769 ± 0.0287	-0.3732 ± 0.1181	-0.2745 ± 0.0429	-1.0415 ± 0.0947	AGN
KPG355A	S0/a	-0.2799 ± 0.0102	-0.0799 ± 0.0338	-0.3937 ± 0.0173	-1.5822 ± 0.0717	AGN
KPG360A	Sab	0.1978 ± 0.0842	0.6304 ± 0.1412	0.2513 ± 0.1100	-0.4534 ± 0.1876	LINER
KPG366A	S0/a	-0.3838 ± 0.0145	-0.5970 ± 0.0743	-0.5617 ± 0.0291	-1.7457 ± 0.1496	H II
KPG368A	Sa	-0.0668 ± 0.0168	0.7033 ± 0.0284	-0.2514 ± 0.0306	-0.9945 ± 0.0627	Sy2
KPG369B	Sab	-0.3745 ± 0.0043	0.0370 ± 0.0046	-0.6268 ± 0.0061	-1.5678 ± 0.0101	AGN
KPG384A	SABd	-1.2366 ± 0.0395	0.4807 ± 0.0155	-0.6179 ± 0.0234	-1.8310 ± 0.1430	H II
KPG385A	Sab	-0.2753 ± 0.0144	-0.1326 ± 0.0389	-0.3423 ± 0.0224	-1.0884 ± 0.0442	AGN*
KPG395B	Sa	-0.4141 ± 0.0192	-0.5530 ± 0.1063	-0.5156 ± 0.0351	-1.7811 ± 0.2259	H II
KPG400B	Sa	-0.4082 ± 0.0112	-0.7861 ± 0.0539	-0.5737 ± 0.0192	-1.8396 ± 0.1003	H II
KPG413A	Sa	0.1181 ± 0.0441	0.3457 ± 0.0734	0.1669 ± 0.0605	-0.7199 ± 0.1441	LINER
KPG423A	Sab	-0.2772 ± 0.0156	-0.3584 ± 0.0750	-0.6121 ± 0.0392	-1.4676 ± 0.1124	AGN
KPG425A	SBa	-0.4318 ± 0.0080	-0.5628 ± 0.0166	-0.5251 ± 0.0114	-1.8760 ± 0.0501	H II
KPG425B	S0/a	-0.0411 ± 0.0260	0.8092 ± 0.0597	-0.1732 ± 0.0475	-1.2296 ± 0.1709	Sy2
KPG437B	Sab	-0.1406 ± 0.0056	0.8404 ± 0.0079	-0.5234 ± 0.0099	-1.3326 ± 0.0184	Sy2
KPG447A	Sa	-0.3622 ± 0.0120	-0.4357 ± 0.0390	-0.4910 ± 0.0198	-1.7377 ± 0.0999	H II
KPG449B	Sab	-0.1371 ± 0.0189	-0.1516 ± 0.0570	-0.2620 ± 0.0316	-1.1676 ± 0.0897	AGN
KPG455A	Sa	0.3636 ± 0.0750	0.9361 ± 59.0739	0.1912 ± 0.1196	-0.7281 ± 0.3089	LINER
KPG474B	Sa	-0.5031 ± 0.0114	-0.7489 ± 0.0666	-0.6821 ± 0.0237	-1.6340 ± 0.0783	H II
KPG477B	S0	0.2623 ± 0.0419	0.4125 ± 0.1388	0.1872 ± 0.0615	-0.6152 ± 0.1262	LINER
KPG480B	S0a	0.3424 ± 0.0285	0.9104 ± 0.1547	0.0440 ± 0.0531	-0.4339 ± 0.0653	S-L
KPG495B	SBab	-0.3551 ± 0.0309	-0.9646 ± 0.5063	-0.5157 ± 0.0663	-1.3328 ± 0.1772	H II
KPG496A	S0	-0.1891 ± 0.0222	0.0000 ± 0.0976	-0.4839 ± 0.0572	-1.4065 ± 0.1872	AGN
KPG150A	Sa	0.3299 ± 0.0499	0.9581 ± 0.1379	0.1766 ± 0.0791	-0.6516 ± 0.1713	LINER
KPG286B	Sa	0.6966 ± 0.2316	0.0401 ± 0.0193	-0.3559 ± 0.0159	-1.1296 ± 0.0055	AGN
KPG355B	Sa	-0.1845 ± 0.0111	-0.1347 ± 0.0255	0.0186 ± 0.0130	-0.6826 ± 0.0209	LINER
KPG368B	Sa	-0.2844 ± 0.0063	0.3010 ± 0.0084	-0.1928 ± 0.0078	-0.8456 ± 0.0102	LINER

Induced Nuclear Activity in Galaxy Pairs With Differents Morphologies (E+E), (E+S) and (S+S).   15

Table 10 (cont'd)

Object	M.T.[a]	LOG([N II]/Hα)	LOG([O III]/Hβ)	LOG([S II]/Hα)	LOG([O I]/Hα)	Type
KPG378B	SABb	0.2798 ± 0.0172	0.4255 ± 0.0470	0.1171 ± 0.0268	-0.5858 ± 0.0457	LINER
KPG388B	Sab	-0.2007 ± 0.0049	0.0933 ± 0.0058	-0.3396 ± 0.0065	-0.9527 ± 0.0077	AGN
KPG398A	Sab	-0.4541 ± 0.0056	0.9582 ± 0.0055	-0.7017 ± 0.0102	-0.9831 ± 0.0096	Sy2
Sb						
KPG022B	Sbb	-0.1212 ± 0.0147	-0.1473 ± 0.0777	-0.3904 ± 0.0314	-1.4088 ± 0.1171	AGN
KPG049A	Sb	0.1339 ± 0.0282	0.4632 ± 0.0831	-0.1497 ± 0.0587	-0.8720 ± 0.1155	S-L
KPG053B	Sbb	-0.1190 ± 0.0520	0.6112 ± 0.1749	-0.2358 ± 0.1017	-1.6885 ± 0.9768	Sy2
KPG146A	Sb	-0.3627 ± 0.0189	-0.2041 ± 0.0486	-0.5772 ± 0.0351	-1.4183 ± 0.0865	AGN
KPG150B	Sb	0.2416 ± 0.0323	0.2774 ± 0.0938	0.1807 ± 0.0462	-0.6013 ± 0.0887	LINER
KPG159B	Sb	-0.3331 ± 0.0310	-0.1897 ± 0.0773	-0.3514 ± 0.0512	-1.4715 ± 0.2742	H II
KPG163B	Sbc	-0.4105 ± 0.0292	-0.6588 ± 0.2047	-0.5693 ± 0.0666	-1.4852 ± 0.2231	H II
KPG168B	Sc	-0.6883 ± 0.0060	-0.0187 ± 0.0075	-0.8003 ± 0.0078	-2.2243 ± 0.0307	H II
KPG171A	Sbc	-0.7311 ± 0.0115	0.2867 ± 0.0141	-0.5201 ± 0.0135	-1.4738 ± 0.0332	H II
KPG171B	Sb	-0.4419 ± 0.0085	-0.3946 ± 0.0230	-0.5073 ± 0.0125	-1.6458 ± 0.0451	H II
KPG174A	Sbc	-0.5573 ± 0.0201	-0.3020 ± 0.0520	-0.3529 ± 0.0257	-1.3068 ± 0.0740	H II
KPG178B	Sb	-0.7183 ± 0.0142	0.3040 ± 0.0150	-0.4359 ± 0.0157	-1.4182 ± 0.0422	H II
KPG179B	Sb	-0.0412 ± 0.0464	0.2803 ± 0.0994	0.0372 ± 0.0623	-0.8445 ± 0.1574	S-L
KPG193B	Sb	-0.1522 ± 0.0152	0.0000 ± 0.0936	-0.3304 ± 0.0288	-1.3312 ± 0.0911	AGN
KPG200B	Sb	-0.4491 ± 0.0052	-0.1530 ± 0.0080	-0.5813 ± 0.0072	-1.8146 ± 0.0219	H II
KPG205B	Sb	-0.3443 ± 0.0296	-0.4197 ± 0.1369	-0.5707 ± 0.0555	-1.5058 ± 0.0627	H II
KPG206A	Sb	-0.8756 ± 0.0178	0.2553 ± 0.0124	-0.4909 ± 0.0151	-1.4872 ± 0.0417	H II
KPG215B	Sb	-0.2622 ± 0.0239	0.0711 ± 0.0420	-0.5030 ± 0.0453	-1.4455 ± 0.0635	AGN
KPG216B	Sbc	-0.6998 ± 0.0110	0.1614 ± 0.0152	-0.4748 ± 0.0131	-1.5286 ± 0.0489	H II
KPG219B	Sb	-0.3349 ± 0.0352	-0.6951 ± 0.1467	-0.5481 ± 0.0619	-1.6193 ± 0.0652	H II
KPG225A	Sb	-0.3561 ± 0.0392	-0.4868 ± 0.0688	-0.3852 ± 0.0491	-1.2769 ± 0.0931	H II
KPG225B	Sb	-0.2276 ± 0.0130	-0.3010 ± 0.0614	-0.4369 ± 0.0258	-1.2730 ± 0.0656	AGN
KPG226B	Sb	0.2264 ± 0.0506	0.0969 ± 0.0844	0.2264 ± 0.0690	-0.5540 ± 0.1575	LINER
KPG227B	Sb	-0.6104 ± 0.0110	-0.0578 ± 0.0175	-0.3952 ± 0.0128	-1.6618 ± 0.0590	H II
KPG240A	Sbc	0.2991 ± 0.5267	0.9284 ± 0.1415	-0.2885 ± 0.0649	-0.5655 ± 0.1300	Sy2
KPG242A	Sb	-1.1193 ± 0.1114	0.4814 ± 0.0118	-0.6282 ± 0.0363	-1.5874 ± 0.0727	H II
KPG245B	Sb	0.1627 ± 0.0400	0.3357 ± 0.1047	0.0205 ± 0.0660	-1.0810 ± 0.2713	LINER
KPG257A	Sb	-0.4876 ± 0.0266	-0.2314 ± 0.0898	-0.2550 ± 0.0296	-1.2567 ± 0.1024	H II
KPG261A	Sb	-0.3536 ± 0.0225	-0.4393 ± 0.0897	-0.4580 ± 0.0416	-1.2600 ± 0.1160	H II
KPG261B	Sb	-0.4749 ± 0.0354	-0.7247 ± 0.1746	-0.6270 ± 0.0707	-1.5737 ± 0.1622	H II
KPG266B	Sb	-0.5208 ± 0.0195	-0.2194 ± 0.0601	-0.3808 ± 0.0269	-1.5672 ± 0.1464	H II
KPG270B	Sb	0.2372 ± 0.0993	0.1943 ± 0.1247	0.2138 ± 0.1373	-0.4133 ± 0.2153	LINER
KPG283B	Sb	-1.1220 ± 0.0158	0.5031 ± 0.0121	-0.6785 ± 0.0139	-1.7420 ± 0.0507	H II
KPG289A	Sb	-0.2022 ± 0.0161	-0.0746 ± 0.0431	-0.3911 ± 0.0313	-1.3118 ± 0.0922	AGN
KPG291A	Sbc	-0.2478 ± 0.0183	-0.0911 ± 0.0752	-0.3840 ± 0.0363	-1.8866 ± 0.4021	AGN
KPG293A	Sb	-0.3586 ± 0.0095	-0.3903 ± 0.0327	-0.4269 ± 0.0153	-1.5016 ± 0.0569	H II
KPG294A	Sb	-0.3972 ± 0.0191	-0.2596 ± 0.0482	-0.2512 ± 0.0235	-1.4523 ± 0.1082	H II
KPG296A	SBb	-0.0555 ± 0.0299	0.2300 ± 0.0682	-0.1711 ± 0.0515	-1.0046 ± 0.1286	LINER
KPG298A	Sbc	-0.1960 ± 0.0399	-0.3293 ± 0.1168	-0.4070 ± 0.0917	-1.4421 ± 0.3712	AGN
KPG298B	Sbc	0.1259 ± 0.0537	0.8943 ± 0.4159	0.0713 ± 0.0834	-0.9495 ± 0.2633	S-L
KPG299A	Sb	0.3614 ± 0.0275	0.6642 ± 0.0974	0.3055 ± 0.0377	-0.5099 ± 0.0716	LINER
KPG301A	Sb	-0.4259 ± 0.0101	-0.8002 ± 0.0459	-0.7081 ± 0.0211	-1.6543 ± 0.0636	H II
KPG306B	Sb	-0.2486 ± 0.0073	-0.8852 ± 0.0379	-0.6573 ± 0.0147	-2.0341 ± 0.0968	H II
KPG307A	Sb	-0.4932 ± 0.0064	-0.2756 ± 0.0094	-0.6434 ± 0.0099	-1.9298 ± 0.0341	H II
KPG313A	Sbc	-0.4405 ± 0.0205	-0.5497 ± 0.0759	-0.3869 ± 0.0283	-1.5895 ± 0.1532	H II
KPG313B	Sb	-0.0556 ± 0.0158	0.6717 ± 0.0276	-0.3918 ± 0.0340	-1.2583 ± 0.0855	Sy2
KPG319A	Sb	-0.9226 ± 0.0147	0.5866 ± 0.0120	-0.6614 ± 0.0167	-1.6406 ± 0.0467	H II
KPG322B	Sbc	-0.2800 ± 0.0038	-0.6701 ± 0.0083	-0.6007 ± 0.0056	-1.8646 ± 0.0157	H II
KPG323A	SBbc	-0.5878 ± 0.0179	-0.2800 ± 0.0410	-0.3375 ± 0.0221	-1.4370 ± 0.0741	H II
KPG323B	Sbc	-0.4803 ± 0.0239	-0.2004 ± 0.0598	-0.3376 ± 0.0336	-1.2207 ± 0.0834	H II
KPG329B	Sb	-0.3388 ± 0.0082	-0.8493 ± 0.0334	-0.6378 ± 0.0147	-1.8235 ± 0.1893	H II
KPG337B	Sb	-1.0264 ± 0.0152	0.3467 ± 0.0126	-0.6109 ± 0.0139	-1.7134 ± 0.0522	H II
KPG347A	Sbc	-0.5044 ± 0.0196	-1.1862 ± 0.3571	-0.7406 ± 0.0449	-1.9546 ± 0.2896	H II
KPG347B	Sbc	-0.3895 ± 0.0136	-0.4110 ± 0.0496	-0.7557 ± 0.0338	-1.9613 ± 0.1864	H II

16   *F. J. Hernández-Ibarra, D. Dultzin, Y. Krongold, A. Del Olmo, J. Perea, J. González*

Table 10   (cont'd)

Object	M.T. [a]	LOG([N II]/Hα)	LOG([O III]/Hβ)	LOG([S II]/Hα)	LOG([O I]/Hα)	Type
KPG352A	SBb	0.0507 ± 0.0545	0.2041 ± 0.1114	-0.2545 ± 0.1282	-1.7096 ± 1.3149	S-L
KPG360B	Sb	-0.2248 ± 0.0376	-0.3919 ± 0.1875	-0.3567 ± 0.0812	-1.1835 ± 0.1990	H II
KPG366B	SBb	0.3802 ± 0.0669	0.5819 ± 0.1983	0.2094 ± 0.1066	-0.4882 ± 0.1790	LINER
KPG375A	SBbc	-0.2547 ± 0.0074	-0.4952 ± 0.0257	-0.6052 ± 0.0140	-1.8573 ± 0.0695	AGN
KPG378A	Sb	0.0231 ± 0.0197	-0.0637 ± 0.0670	-0.1819 ± 0.0375	-1.2019 ± 0.1338	LINER
KPG381B	Sbc	-0.2224 ± 0.0122	0.2234 ± 0.0205	-0.3702 ± 0.0187	-1.1871 ± 0.0390	Sy1.8
KPG382A	Sbc	-0.5246 ± 0.0182	-0.6493 ± 0.0810	-0.3999 ± 0.0268	-1.3977 ± 0.0793	H II
KPG395A	Sbc	-0.4479 ± 0.0164	-0.7495 ± 0.1079	-0.5490 ± 0.0293	-1.6905 ± 0.1385	H II
KPG400A	Sb	-0.1371 ± 0.0348	-0.0136 ± 0.1297	-0.5150 ± 0.1049	-1.1601 ± 0.1908	AGN
KPG403B	Sb	-0.4262 ± 0.0124	-0.3931 ± 0.0558	-0.4494 ± 0.0202	-1.7366 ± 0.1136	H II
KPG404B	Sb	0.2027 ± 0.0368	0.3643 ± 0.0746	0.0242 ± 0.0627	-0.7755 ± 0.1349	LINER
KPG405A	Sb	-0.5513 ± 0.0106	-0.2386 ± 0.0225	-0.4504 ± 0.0138	-1.6452 ± 0.0503	H II
KPG406A	Sb	-0.5073 ± 0.0170	-0.2486 ± 0.0390	-0.3416 ± 0.0209	-1.5003 ± 0.0891	H II
KPG413B	Sbc	-0.3930 ± 0.0088	-0.8571 ± 0.0582	-0.6651 ± 0.0175	-1.8924 ± 0.0907	H II
KPG426B	Sb	-0.3316 ± 0.0105	-0.6744 ± 0.0464	-0.5643 ± 0.0196	-1.7752 ± 0.0979	H II
KPG427B	Sb	-0.1189 ± 0.0000	-0.0786 ± 0.0981	-0.5960 ± 0.1585	-1.4024 ± 0.0000	AGN
KPG428A	SBb	-0.7162 ± 0.0286	0.0823 ± 0.0445	-0.2671 ± 0.0247	-1.3747 ± 0.0990	H II
KPG430B	Sbc	-0.6538 ± 0.0130	0.1317 ± 0.0136	-0.4513 ± 0.0150	-1.4976 ± 0.0461	H II
KPG433A	Sbc	-0.3162 ± 0.0105	-0.4688 ± 0.0581	-0.4791 ± 0.0196	-1.5846 ± 0.0807	H II
KPG433B	Sbc	-0.4007 ± 0.0088	-0.4745 ± 0.0271	-0.6150 ± 0.0158	-1.7666 ± 0.0749	H II
KPG434A	Sb	-0.1953 ± 0.0084	-0.1419 ± 0.0128	-0.4085 ± 0.0136	-1.5190 ± 0.0470	AGN
KPG440B	Sbc	-0.0786 ± 0.0000	0.5229 ± 0.1657	-0.4296 ± 0.0888	-1.3291 ± 0.0000	Sy2
KPG444A	Sbb	-0.3297 ± 0.0254	-0.3689 ± 0.1314	-0.3151 ± 0.0416	-1.2612 ± 0.1253	H II
KPG453A	Sb	-0.5125 ± 0.0154	-0.9789 ± 0.1342	-0.6406 ± 0.0303	-2.6157 ± 0.9549	H II
KPG455B	Sbb	0.2561 ± 0.0280	0.6353 ± 0.1704	0.0502 ± 0.0480	-0.7091 ± 0.0903	LINER
KPG458A	Sbc	-0.4771 ± 0.0172	-0.2489 ± 0.0535	-0.4462 ± 0.0266	-1.3659 ± 0.0793	H II
KPG472A	Sbc	-0.9767 ± 0.0151	0.4390 ± 0.0128	-0.5645 ± 0.0143	-1.5243 ± 0.0373	H II
KPG472B	Sbc	-0.4078 ± 0.0055	-0.5936 ± 0.0120	-0.6977 ± 0.0081	-2.1438 ± 0.0372	H II
KPG473A	Sb	0.1025 ± 0.0128	0.6555 ± 0.0172	-0.0690 ± 0.0206	-0.7704 ± 0.0355	S-L
KPG474A	Sb	-0.5142 ± 0.0170	-0.6642 ± 0.0698	-0.7027 ± 0.0356	-1.9255 ± 0.2235	H II
KPG477A	Sb	0.4227 ± 0.0844	0.1440 ± 0.1333	0.2329 ± 0.1339	-0.3647 ± 0.1966	LINER
KPG478A	Sb	-0.2775 ± 0.0192	-0.3219 ± 0.1062	-0.6253 ± 0.0499	-1.8999 ± 0.3595	AGN
KPG495A	Sb	-0.0963 ± 0.0343	-0.1120 ± 0.1161	-0.2400 ± 0.0655	-1.1265 ± 0.1882	AGN
KPG496B	Sb	-0.2829 ± 0.0181	-0.3802 ± 0.0969	-0.4329 ± 0.0346	-1.3222 ± 0.0984	AGN
KPG518A	Sb	-0.8578 ± 0.0156	0.3108 ± 0.0140	-0.4839 ± 0.0150	-1.5081 ± 0.0458	H II
KPG557A	Sba	0.3193 ± 0.1119	0.1060 ± 0.1160	0.3521 ± 0.1453	-0.7773 ± 0.4971	LINER
KPG557B	Sb	-0.1795 ± 0.0276	0.1283 ± 0.0775	-0.3771 ± 0.0615	-1.7788 ± 0.5191	AGN
KPG597B	Sbc	-0.3348 ± 0.0244	-0.3667 ± 0.0791	-0.5572 ± 0.0538	-1.6819 ± 0.2660	H II
Sc						
KPG021B	Sc	-0.3770 ± 0.0130	-0.3828 ± 0.0452	-0.5009 ± 0.0222	-1.6011 ± 0.0939	H II
KPG052A	Sc	-0.4884 ± 0.0152	-0.8899 ± 0.1115	-0.6032 ± 0.0291	-1.6722 ± 0.1132	H II
KPG156A	Sc	-0.4170 ± 0.0086	-0.9228 ± 0.0437	-0.6787 ± 0.0148	-1.9553 ± 0.0733	H II
KPG156B	Sbc	-0.4136 ± 0.0665	-0.1190 ± 0.0420	-0.3272 ± 0.0417	-1.2446 ± 0.0832	H II
KPG159A	Sc	-0.6847 ± 0.0131	0.1349 ± 0.0156	-0.3835 ± 0.0148	-1.3963 ± 0.0397	H II
KPG168B	Sc	-0.6883 ± 0.0060	-0.0187 ± 0.0075	-0.8003 ± 0.0078	-2.2243 ± 0.0307	H II
KPG178A	Sc	-0.3970 ± 0.0604	-0.6943 ± 0.2973	-0.5252 ± 0.1315	-1.8832 ± 0.5726	H II
KPG220A	Sc	-0.4434 ± 0.0470	-0.3413 ± 0.0383	-0.7012 ± 0.1023	-1.8214 ± 0.1622	H II
KPG230A	Sc	-0.9396 ± 0.0135	0.3703 ± 0.0124	-0.6510 ± 0.0145	-1.7235 ± 0.0484	H II
KPG230B	Sc	-0.4175 ± 0.0411	-0.4150 ± 0.0402	-0.4549 ± 0.0633	-1.4852 ± 0.0857	H II
KPG236A	Sc	-1.1876 ± 0.0107	0.4876 ± 0.0064	-0.8385 ± 0.0108	-2.0797 ± 0.0350	H II
KPG241A	Sc	-0.4165 ± 0.0726	-1.4075 ± 2.3641	-0.4338 ± 0.1264	-1.3555 ± 0.2458	H II
KPG263A	Sc	-0.1856 ± 0.0000	-0.3118 ± 0.1230	-0.4967 ± 0.0895	-1.1815 ± 0.0000	AGN
KPG272A	Sc	-0.5089 ± 0.0189	-0.2902 ± 0.0607	-0.4501 ± 0.0256	-1.6451 ± 0.1368	H II
KPG272B	Sc	-0.4911 ± 0.0085	-0.6236 ± 0.0293	-0.5440 ± 0.0125	-1.7161 ± 0.0499	H II
KPG280A	Sc	-0.2986 ± 0.0158	0.0736 ± 0.0430	-0.3369 ± 0.0252	-1.1528 ± 0.0542	AGN
KPG292A	Sc	-0.3666 ± 0.0051	-0.4466 ± 0.0170	-0.5041 ± 0.0076	-1.6306 ± 0.0226	H II
KPG293B	Sc	-0.4792 ± 0.0082	-0.4215 ± 0.0229	-0.5214 ± 0.0126	-1.5532 ± 0.0366	H II
KPG309A	Sc	-0.9356 ± 0.0372	0.4175 ± 0.0303	-0.4406 ± 0.0296	-1.3956 ± 0.0995	H II

Induced Nuclear Activity in Galaxy Pairs With Differents Morphologies (E+E), (E+S) and (S+S).   17

Table 10 (cont'd)

Object	M.T. [a]	LOG([N II]/Hα)	LOG([O III]/Hβ)	LOG([S II]/Hα)	LOG([O I]/Hα)	Type
KPG311B	Sc	-1.1629 $\pm$ 0.0067	0.5032 $\pm$ 0.0056	-0.9062 $\pm$ 0.0075	-2.0387 $\pm$ 0.0170	H II
KPG316A	Sc	-0.4852 $\pm$ 0.0133	-0.4773 $\pm$ 0.0349	-0.4391 $\pm$ 0.0179	-1.4281 $\pm$ 0.0662	H II
KPG326B	Sc	-0.8369 $\pm$ 0.0162	0.2645 $\pm$ 0.0162	-0.4116 $\pm$ 0.0164	-1.3800 $\pm$ 0.0402	H II
KPG332A	Sc	-0.4636 $\pm$ 0.0049	-0.7057 $\pm$ 0.0792	-0.5754 $\pm$ 0.0290	-1.8044 $\pm$ 0.1368	H II
KPG340A	Sc	-0.1040 $\pm$ 0.0138	-0.2199 $\pm$ 0.0327	-0.2439 $\pm$ 0.0229	-1.1756 $\pm$ 0.0584	AGN
KPG352B	Sc	-0.5745 $\pm$ 0.0087	-0.2580 $\pm$ 0.0165	-0.4783 $\pm$ 0.0111	-1.6564 $\pm$ 0.0344	H II
KPG354B	Sc	-1.0198 $\pm$ 0.0111	0.4307 $\pm$ 0.0095	-0.6488 $\pm$ 0.0111	-1.6017 $\pm$ 0.0251	H II
KPG375B	Sc	-0.4157 $\pm$ 0.0203	-0.4856 $\pm$ 0.0949	-0.6585 $\pm$ 0.0467	-1.6168 $\pm$ 0.1686	H II
KPG396A	Sc	-0.6008 $\pm$ 0.0120	-0.2880 $\pm$ 0.0282	-0.4628 $\pm$ 0.0151	-1.6624 $\pm$ 0.0616	H II
KPG397A	Sc	-0.8750 $\pm$ 0.0176	0.3096 $\pm$ 0.0148	-0.4922 $\pm$ 0.0159	-1.4277 $\pm$ 0.0493	H II
KPG409A	Sc	-0.1843 $\pm$ 0.0350	-0.1009 $\pm$ 0.1275	-0.3476 $\pm$ 0.0711	-1.7309 $\pm$ 0.6074	AGN
KPG410A	Sc	-0.2192 $\pm$ 0.0430	-0.8206 $\pm$ 0.7114	-0.4261 $\pm$ 0.1021	-1.6475 $\pm$ 0.6513	AGN
KPG415B	Sc	-0.6773 $\pm$ 0.0144	-0.0080 $\pm$ 0.0260	-0.4111 $\pm$ 0.0166	-1.4555 $\pm$ 0.0563	H II
KPG423B	Sc	-0.3710 $\pm$ 0.0097	-0.4824 $\pm$ 0.0339	-0.6073 $\pm$ 0.0173	-1.7118 $\pm$ 0.0670	H II
KPG424A	Sc	-0.3510 $\pm$ 0.0058	-0.9426 $\pm$ 0.0219	-0.7013 $\pm$ 0.0094	-1.9789 $\pm$ 0.0352	H II
KPG440A	Sc	-0.4141 $\pm$ 0.0307	-0.3505 $\pm$ 0.1693	-0.2034 $\pm$ 0.0349	-1.2652 $\pm$ 0.1371	H II
KPG444B	Sc	-0.4339 $\pm$ 0.0117	-0.4837 $\pm$ 0.0294	-0.4150 $\pm$ 0.0167	-1.5429 $\pm$ 0.0592	H II
KPG461A	Sc	-0.9182 $\pm$ 0.0144	0.4357 $\pm$ 0.0122	-0.5501 $\pm$ 0.0147	-1.5747 $\pm$ 0.0404	H II
KPG511A	Sc	-0.2486 $\pm$ 0.0162	-0.5187 $\pm$ 0.1321	-0.3983 $\pm$ 0.0318	-1.8039 $\pm$ 0.2530	AGN
KPG330B	SBc	-0.8000 $\pm$ 0.1290	0.1277 $\pm$ 0.0126	1.5051 $\pm$ 0.1180	0.3939 $\pm$ 0.1383	H II
Sm						
KPG212A	Sd	-1.9482 $\pm$ 0.0085	0.8194 $\pm$ 0.0041	-1.3579 $\pm$ 0.0076	-2.1572 $\pm$ 0.0113	H II
KPG217A	Sd	-1.2775 $\pm$ 0.0541	0.5761 $\pm$ 0.0167	-0.7283 $\pm$ 0.0422	-1.7440 $\pm$ 0.0463	H II
KPG249B	SBm	-0.5904 $\pm$ 0.0164	0.2123 $\pm$ 0.0144	-0.5536 $\pm$ 0.0210	-1.5194 $\pm$ 0.0351	H II
KPG288B	SBm	-0.3851 $\pm$ 0.0048	-0.0627 $\pm$ 0.0060	-0.4600 $\pm$ 0.0064	-1.2651 $\pm$ 0.0089	AGN
KPG294B	SBm	-1.2259 $\pm$ 0.0155	0.4646 $\pm$ 0.0088	-0.6840 $\pm$ 0.0126	-1.7147 $\pm$ 0.0333	H II
KPG330A	Sd	-1.0493 $\pm$ 0.0083	0.3708 $\pm$ 0.0073	-0.9699 $\pm$ 0.0106	-2.2974 $\pm$ 0.0525	H II
KPG344A	Sd	-1.0957 $\pm$ 0.0093	0.2902 $\pm$ 0.0080	-0.9707 $\pm$ 0.0112	-2.4805 $\pm$ 0.0869	H II
KPG349A	SBm	-0.7375 $\pm$ 0.0095	0.1800 $\pm$ 0.0082	-0.5429 $\pm$ 0.0109	-1.6739 $\pm$ 0.0325	H II
KPG406B	Irr	-0.8857 $\pm$ 0.0257	0.3590 $\pm$ 0.0253	-0.4545 $\pm$ 0.0224	-1.3702 $\pm$ 0.0635	H II
KPG430A	Irr	-0.4817 $\pm$ 0.0124	-0.1523 $\pm$ 0.0265	-0.4120 $\pm$ 0.0159	-1.5648 $\pm$ 0.0612	H II
KPG438B	Sd	-0.9974 $\pm$ 0.0162	0.4950 $\pm$ 0.0129	-0.6597 $\pm$ 0.0161	-1.6763 $\pm$ 0.0507	H II
KPG511B	Sd	-0.5686 $\pm$ 0.0141	-0.1076 $\pm$ 0.0275	-0.3915 $\pm$ 0.0182	-1.3732 $\pm$ 0.0548	H II

[a] M.T.- Morphological Type.

˙AGN classification denotes those galaxies that are AGN according to the [N II] diagrams but not to the [S II] and/or [O I].

[†]L-S classification means that galaxies fall in the separation line for Seyfert and LINER according to [S II] and [O I] diagrams.

[*]Type with weak broad component in permitted lines. Seyfert quiantitative classification according to Winkler (1992).

Capítulo 5

The Transition from "Normal" to "Broad Absorption Line Quasar" of TON 34

Estuve involucrado en buscar relaciones entre líneas de emisión e inflecciones en el ajuste espectral para longitudes de onda del ultravioleta. Al compararse los espectros de un objeto en particular (TON 34) con diferencia de alrededor de 26 años, se observo que una línea en absorción estaba predominantemente más intensa en el espectro del SLOAN de 2006 que en el de las campanas y el observatorio de palomar en 1981.

El cuásar TON 34 a z $\approx$1.928, representa uno de los casos más extremos en cuanto al quiebre o inflexión que presentan los cuásares alrededor de los 1100 Å. Si el continuo en el lejano UV de estos cuasares puede ajustarse con una ley de potencia del tipo $F_\nu \propto \nu^\alpha$, para TON 34, α = -5.3 en el quiebre o inflexión que es considerablemente más pronunciado que el promedio de α = -1.76 en otros cuasares.

La línea en absorción se extiende desde 5000 hasta 25,000 kms^{-1} y es considerada como una línea de absorción ancha típica de cuasares (BALQSOs).

La posible explicación radica en un denominado "outflow" que es un viento atravesando nuestra línea de visión hacia la fuente del AGN como la principal explicación después de considerar otros escenarios.

THE TRANSITION FROM "NORMAL" TO "BROAD ABSORPTION LINE QUASAR" OF TON 34

Y. KRONGOLD, L. BINETTE, AND F. HERNÁNDEZ-IBARRA
Instituto de Astronomia, Universidad Nacional Autonoma de Mexico, Apartado Postal 70-264, 04510 Mexico DF, Mexico

ABSTRACT

We report the emergence of a high-velocity, broad absorption line outflow in the luminous quasar Ton 34, at $z_q = 1.928$. The outflow is detected through an ultraviolet C IV broad absorption line, in a spectrum obtained in 2006 January by the Sloan Digital Sky Survey. No absorption trough was present in two different spectra acquired in 1981 at Las Campanas and Palomar observatories, indicating the emergence of the outflow in less than ∼8 yr (rest frame). The absorption line spans a velocity range from ∼5000 to 25,000 km s^{-1}, and resembles typical troughs found in broad absorption line quasars (BALQSOs). We measure a balnicity index $\gtrsim$600 (though this value might be an underestimation due to a conservative placing of the continuum). The absorption trough is likely saturated, with the absorbing gas covering ∼25% of the emitting region. We explore different scenarios for the emergence of this outflow, and find an existing wind moving across our line of sight to the source as the most likely explanation. This indicates that high-velocity outflows (producing broad absorption troughs in BALQSOs) might be ubiquitous in quasars, yet only become observable when the wind accidentally crosses our line of vision to the central source.

Key words: quasars: absorption lines – quasars: individual (Ton 34)

Online-only material: color figures

1. INTRODUCTION

More than 50% of active galaxies and quasars display clear signatures of outflows, easily identified in the form of absorption lines (e.g., Crenshaw et al. 2003; Ganguly & Brotherton 2008). These lines appear in active galactic nuclei (AGNs) spectra in different forms, either as broad absorption lines (BALs; FWHM ∼ 10,000 km s^{-1}), narrow absorption lines (NALs; FWHM ∼ 100 km s^{-1}), or intermediate mini-BALs.

Understanding these winds is essential to understanding the structure and dynamics of quasars (Elvis 2000). Since they carry mass and kinetic energy outside the central region of the host galaxy, it has been suggested that they may also be essential for galaxy evolution, being responsible for the relation between the mass of the supermassive black hole in the center of galaxies and their bulge velocity dispersion (Scannapieco & Oh 2004; Hopkins et al. 2005; King 2010; Ostriker et al. 2010). They may also pollute the intergalactic medium with metals and heat, stopping structure formation. However, before these outflows can be used as cosmic probes, it is imperative to understand their nature. Unfortunately, there is little understanding so far on their origin, geometry and physical properties. In addition, we still do not know the relation among the systems with different FWHMs in their absorption lines, the exact relation between the UV and X-ray absorbers, and any possible connection between the absorbing and emitting gas in the central regions of AGNs.

It has been suggested that the different UV and X-ray absorption lines with different FWHMs correspond to a single phenomenon, viewed at different angles, and that the same gas may be responsible for absorption and emission (e.g., Elvis 2000; Krongold et al. 2007; Andrade-Velázquez et al. 2010). Other ideas suggest that mini-BALs and BALs may represent the same outflow but at different evolutionary stages (Hamann & Sabra 2004). These ideas are not opposed to each other, as they describe different parts of the global picture.

Given that absorption lines provide information on the material located only in our line of sight to the source, and that the presence of outflowing material is not always evident in emission lines, one must rely on a different diagnostic to understand the true nature of these winds. Line variability has proven to be an effective method for the study of AGN of winds. However, the variations can be produced by different effects, such as changing in the ionization state of the gas, changes in column density, or changes in covering factor, and these effects are not always straightforward to differentiate. Line variations in broad absorption line quasars (BALQSOs) are generally small, indicating that BAL winds are long-lived stable flows (Barlow 1994; Lundgren et al. 2007; Gibson et al. 2008). However, in two cases, strong variations have been found, showing the emergence of BAL (or BAL-like) outflows. Leighly et al. (2009) reported the appearance of BAL troughs in the narrow-line Seyfert 1 galaxy WVPS 007, an object where a BAL outflow is not expected given its intrinsic low luminosity. Hamann et al. (2008) reported the appearance of broad absorption lines in the spectra of quasar J105400.40+034801.2. The lines, though typical of BALQSOs, presented a velocity shift of 26,300 km s^{-1}, which resulted in a balnicity index of zero,[1] excluding them from the standard BAL definition (Weymann et al. 1991).

In this Letter, we report the emergence of a BAL outflow in the luminous quasar Ton 34 (PG 1017+280). Ton 34, at $z_q = 1.928$, represents an extreme case of the continuum decline (or UV-break) that takes place in quasar spectra shortward of ≈1100 Å (Telfer et al. 2002, hereafter TZ02), contrasted by a "normal" spectrum redward of this break. If the far UV decline is fitted by a power law ($F_\nu \propto \nu^{+\alpha}$), the index value in Ton 34 is $\alpha = -5.3$, remarkably steeper than the "average" spectral energy distribution (SED) derived by TZ02, which behaves as $\nu^{-1.76}$ (in fact, among the 77 far UV indices measured by TZ02, only in 3 objects was there an ionizing continuum steeper than ν^{-3}). Binette & Krongold (2008a) suggested that the extreme

---

[1] The balnicity index (which is to be applied to C IV) measures the equivalent width of strong absorption features (expressed in km s^{-1}), but requires that each absorption feature contributing to the index spans at least 2000 km s^{-1} (to exclude intervening systems) and only includes in the calculation absorption regions dipping 10% or more below the normalized continuum. In addition, the first 3000 km s^{-1} blueward of the emission peak are excluded to distinguish "associated absorption" from broad absorption. For further details see Appendix A in Weymann et al. (1991).
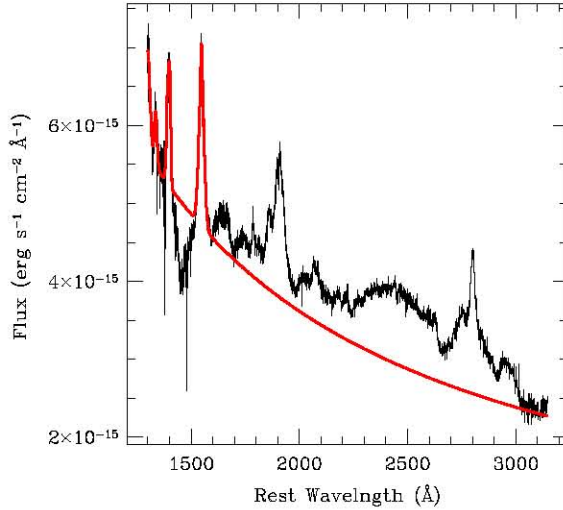
Figure 1. Full band rest-frame SDSS spectrum of quasar Ton 34. The red line corresponds to the continuum plus emission lines (in the blue part of the spectrum) adopted in this Letter.

(A color version of this figure is available in the online journal.)

UV flux might undergo a recovery shortward of 450 Å (as hinted by *International Ultraviolet Explorer* data), and studied the possibility that the particular shape of the SED could be the result of carbon crystalline dust absorption (Binette et al. 2005; Haro-Corzo et al. 2007). They found that moderate columns of dust could indeed reproduce the UV-break. However, due to the observational limits on atomic gas absorption, they hypothesized the possibility that the dust was part of an ionized high-velocity flow in this system. Given the lack of UV ionizing photons in the SED of Ton 34, Binette & Krongold (2008b) further analyzed the emission line spectrum of this quasar. They find evidence of an unusual strength (relative to Lyα) of low to intermediate excitation lines (such as O II + O III $\lambda\lambda835$, N III + O III $\lambda\lambda686$–703, and N III + N IV $\lambda\lambda765$), which could not be explained by photoionization processes in the emitting gas, but rather by shock excitation.

2. MULTI-TIME SPECTRA OF THE QUASAR TON 34

The Sloan Digital Sky Survey (SDSS) carried spectroscopic observations of the quasar Ton 34 on 2006 January 30. The fully reduced spectrum was retrieved from the SDSS data release 7 (Abazajian et al. 2009). The spectrum covers the spectral range between 3808 and 9215 Å (1335 to 3147 Å in the rest frame of Ton 34), with a resolving power $\sim$2000 (130 km s^{-1}). According to the SDSS data release, an uncertainty of less than 3% is expected in the flux calibration. The signal-to-noise ratio (S/N) ranges from 45 in the blue end to 39 in the red one. A detailed analysis of the full range spectrum will be presented in a forth coming paper (L. Binette et al. 2011, in preparation). To study the spectral variability in Ton 34, we refer to the published optical spectrum obtained by Sargent et al. (1988). Only for illustrative purposes, we present here the digitized data presented by Binette & Krongold (2008a, 2008b). Briefly, we describe the properties of the data, as reported by Sargent et al. (1988). The spectrum was taken at the Palomar 5.08 m Hale Telescope (we focus on the red arm spectrum, covering the C IV region of interest), between 1981 November 19–21. The total

Table 1
Emission Lines in the SDSS Data

| Species	λ (Å)	FWHM (km s^{-1})	Flux (10^{-14} erg s^{-1} cm^{-2})
Broad components			
C IV	1549	5600	16.0
Si IV	1402	3400	7.0
C II	1335	3300	2.8
O I	1302	5800	6.0
Narrow components			
C IV	1549	1700	1.4
Si IV	1402	1900	2.9

exposure time was 13,500 s. The resulting spectrum covers the spectral range between 3600 and 4810 Å (1229 to 1642 Å in the rest frame of Ton 34) with a resolution $\sim$100 km s^{-1}. The S/N is $\sim$75 in the region between the Lyα and C IV emission lines. The data was acquired with the sole purpose of detecting broad and narrow absorption lines, and thus, only a relative flux calibration was carried out.

The spectra was corrected for Galactic reddening assuming the Cardelli et al. (1989) extinction curve corresponding to $R_V = 3.1$ and $E_{B-V} = 0.13$. The latter value corresponds to the mean extinction inferred from the 100μ maps of Schlegel et al. (1998) near Ton 34. We note however, that this correction has no effect on the results presented here. Throughout this paper we assume a cosmology consisting of $H_o = 71$ km s^{-1} Mpc^{-1}, $\Omega_M = 0.27$, and $\Omega_\lambda = 0.73$.

3. THE EMERGENCE OF A BAL FLOW

Figure 1 presents the full band SDSS rest-frame spectrum of Ton 34. A visual inspection hints at the presence of a strong broad absorption line blueward of the C IVλ1549 emission line region. However, given the numerous emission features present in the region covered by the spectrum redward of this emission line (including strong blends of Fe II transitions), a full band continuum determination is not straightforward (for a detailed analysis of the full band spectrum see L. Binette et al. 2011, in preparation). Since our goal is to test the presence of a C IV BAL trough, we defined the most conservative continuum level, as shown in Figure 1. To define this continuum, we fit a simple power law to the "line free regions" in the full band spectrum, particularly, we forced this simple power law to fit the regions around 3000–3100 Å (assumed to be a "good continuum representation" given the lack of Fe II emission) and the line free regions between 1320 and 1380 Å (so that in the continuum determination we are assuming no absorption by Si IV). This simple fit also provides a good continuum description of the two line free regions close to 1600 Å and 1700 Å. We note that other representations of the continuum (including local fits to the C IV–Si IV region or broken power laws) are possible, though all of them would place the continuum at higher flux levels, making the absorption trough stronger. The emission lines in the blue part of the spectrum were fit using up to two different Gaussian components. These lines are reported in Table 1.

Figure 2 presents the same fit on the 1300–1600 Å spectral region, along with the normalized spectra (in velocity space). The spectral fit to the SDSS spectrum clearly shows the presence of a strong broad absorption line consistent with absorption by C IVλ1549 with velocities ranging from $\sim$5000 to 25,000 km s^{-1} with respect to the rest frame of the source. This feature was
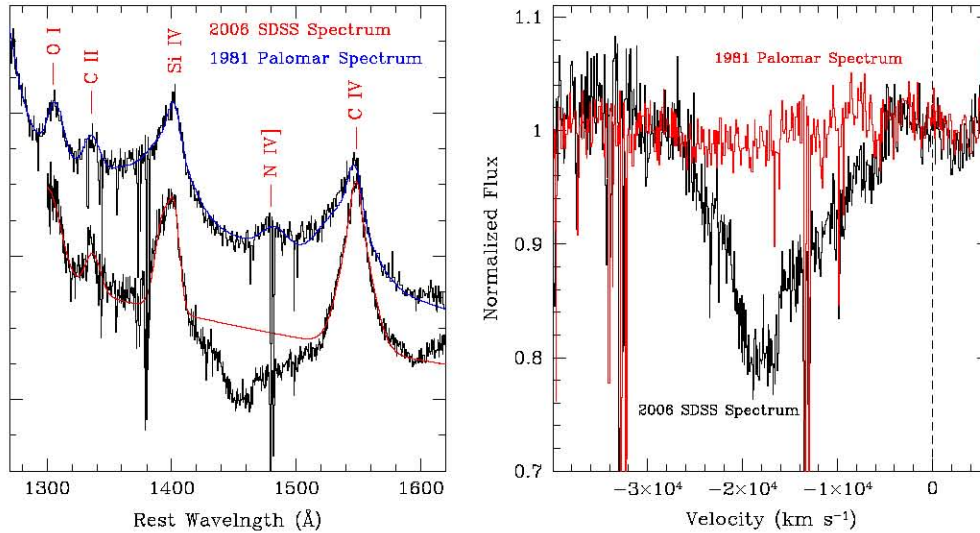
Figure 2. Left: 2006 SDSS spectrum of Ton 34 in the 1300–1600 Å range (rest frame). The red line represents the (full range) continuum plus emission lines fit. For illustrative purposes, the 1981 Palomar digitized spectrum (Sargent et al. 1988) is also shown, along with the best continuum plus lines fit (blue line). The spectra is presented in arbitrary flux units. Right: normalized SDSS and Palomar spectra in velocity space. The emergence of a C IV BAL is evident in the data.

(A color version of this figure is available in the online journal.)

not present during the Palomar observation ≈24.2 years before (≈8.3 years in the rest frame). We note, however, that other narrow absorption features present in the Palomar spectrum (probably intervening systems from the inter-galactic medium) are also present in the SDSS spectrum. It should be stressed that the Palomar data was obtained with the sole purpose of discovering absorption lines (both narrow and broad) in the spectrum of Ton 34. Yet, no BAL line was reported by Sargent et al (1988). Additional confirmation of the lack of the BAL comes from a former spectrum taken at Las Campanas (100 inch telescope) in 1981 March 11 (Young et al. 1982), obtained also with the sole purpose of detecting absorption lines.

To further illustrate the emergence of the BAL, we present in Figure 2 the earlier Palomar spectrum, digitized. This plot also shows the Palomar normalized spectrum, after performing a continuum plus emission line fit, similar to the one applied to the SDSS data.

4. DISCUSSION

The absorption feature present in the SDSS spectrum of Ton 34 resembles typical C IV troughs found in BALQSOs. This feature spans velocities ranging from ∼5000 to 25,000 km s^{-1}, with an FWHM ∼ 9000 km s^{-1}. Following the standard BAL definition (Weymann et al., 1991), we calculate a balnicity index ≳600, but note that this index strongly depends on the continuum determination, thus, it could easily be much larger. Given our continuum determination, no absorption by Si IV was detected, although the possible presence of this line is strongly dependent on the actual continuum level. We note however, that Si IV absorption is not always observed in the spectra of BALQSOs.

The spectral shape of the absorption feature cannot be adjusted with two Gaussians, shifted by ∼300 km s^{-1} to account for the C IVλλ1548, 1550 doublet. Rather, a velocity structure is evident (suggesting a velocity-dependent covering factor), with the absorption becoming more prominent between 18,000 and

20,000 km s^{-1}. We estimate the column density directly from the normalized data using Equation (9) by Savage & Sembach (1991). We integrate the column density over the line profile assuming the 2:1 ratio in the oscillator strengths of the C IV doublet, i.e., we assume that the line is optically thin. Doing this we measure a C IV column density $>2 \times 10^{15}$ cm^{-2}. However, we consider this a very uncertain lower limit given that the lines might be highly saturated and the covering fraction might be much smaller than one. We have no means to measure the saturation level of the lines with the current data, however, saturation and partial covering have been observed in other UV outflows (e.g., Arav et al. 2001; Hamann & Sabra 2004; Gabel et al. 2005). If the line was indeed highly saturated (optical depth $\tau_o > 3$ in the center of the line), then the C IV column density would be larger than 10^{16} cm^{-2}, and from the residual flux in the core of the line the covering factor would be ∼25%.

Following Hamann et al. (2008) we can compare different time-scales relevant to the system to the timescale in which the outflow appeared in the spectrum of Ton 34 (<8.3 years, rest frame of the source), to test different processes responsible for the emergence of the flow. Assuming that the wind originates in the accretion disk, then a characteristic time-scale for the flow is simply $t_{\rm wind} \sim R_{\rm wind}/v_{\rm wind}$, where $R_{\rm wind}$ is the distance from the wind to the central source, and $v_{\rm wind}$ the wind velocity. For accretion-disk winds $R_{\rm wind}$ is expected to lie just beyond the C IV emission line region (e.g., Everett 2005; Proga 2007). Using Equation (3) from Kaspi et al. (2007), and the 1350 Å luminosity of Ton 34, we estimate $R_{\rm C\,IV} \sim 2 \times 10^{18}$ cm, which along with $v_{\rm wind} \sim 19,000$ km s^{-1} yields a flow timescale $t_{\rm wind} \sim 33$ yr. This is a factor ≳4 larger than the elapsed time between the observations, making the hypothesis of an arising flow unlikely.

On the other hand, the crossing time of absorbing clouds through the continuum source is generally smaller than the flow time. A typical crossing timescale can be obtained from the ratio between the size of the emitting region and the transverse velocity of the clouds, $t_{\rm cross} \sim R_{\rm em}/v_{\rm tr}$. Assuming $v_{\rm tr}$ is similar to the rotational speed in the BLR, we can estimate this quantity

from the width of the C IV emission line, thus $v_{tr} \sim 2500$ km s^{-1}. Since the size of the emitting region is constrained by the variability timescale of the source, from variability studies we can estimate $R_{em}(1500 \text{ Å}) \sim$ few $\times 10^{16}$ (e.g., Kaspi et al. 2007). Thus $t_{cross} \sim 4$ yr, making the possibility that an existing flow got into our line of sight consistent with the observations.

We further consider the hypothesis that changes in ionization state may have produced the appearance of the absorption line. We only consider the possibility of a decrease in ionization as no broad absorption by H I was observed in the Palomar spectra (Sargent et al. 1988). Thus, if the wind was already present during the earlier observation, its ionization level would have to be much larger than during the SDSS one. We do not have accurate physical properties (i.e., ionization parameter and temperature) of the absorbing gas to calculate the photoionization equilibrium timescale (e.g., Krongold et al. 2005, 2007). However, we can calculate the recombination time (defined as the inverse of the recombination coefficient times the electron density of the gas) for C v, which is an upper limit to this timescale (Nicastro et al. 1999). We draw the recombination coefficient from Shull & Van Steenberg (1982) and assume a temperature of few $\times 10^4$ K. In order for the gas to recombine and the trough to emerge in the spectrum of Ton 34 in the 8.3 yr interval between the observations, the number density of the absorber need to be >100 cm^{-3}. Thus, the possibility of a decrease in ionization state is also consistent with the observations. Nevertheless, we consider this alternate possibility less likely, given that a large change in the ionizing flux would be required to produce such a large change in the ionization state of the gas, which is not typically observed in quasars. On the other hand, the unusual SED of Ton 34 and the lack of recent extreme UV observations prevents us from ruling out this idea.

Finally, we stress that the extreme far UV break observed in the spectrum of Ton 34 is difficult to explain in terms of accretion disk models. This break can be explained (see review by Binette et al. 2008c) in terms of atomic absorption by an ionized, nearly relativistic outflow (Eastman et al. 1983), or in terms of absorption by an intervening carbon crystalline dust component close to the quasar. In the case of Ton 34, Binette & Krongold (2008a) concluded that the dust component should be part of an ionized medium, and hypothesized that it could be part of a (moderate velocity) outflow. If the emission line region is located closer to the ionization source than this outflow, this would also bring the required SED by photoionization models to a much better agreement with the intrinsic SED of the central source. In the case of three AGNs, namely quasar Ton 34, NLSy1 galaxy WVPS 007 (Leighly et al. 2009), and quasar J105400.40+034801.2 (Hamann et al. 2008), the emergence of a BAL outflow has been reported. For the two quasars the most likely explanation is that the outflow was already present and simply intersected our line of sight (also possible for WVPS 007). This may imply that such outflows are ubiquitous in quasars, yet only become observable when the absorbing material accidentally crosses our line of vision to the central

source. In the case of Ton 34, a subject that deserves further attention is the fact that an outflow emerged in a quasar with such an extreme SED.

REFERENCES

Abazajian, K. N., et al. 2009, ApJS, 182, 543
Andrade-Velázquez, M., Krongold, Y., Elvis, M., Nicastro, F., Brickhouse, N., Binette, L., Mathur, S., & Jiménez-Bailón, E. 2010, ApJ, 711, 888
Arav, N., et al. 2001, ApJ, 561, 118
Barlow, T. A. 1994, PASP, 106, 548
Binette, L., Haro-Corzo, S., Krongold, Y., & Andersen, A. C. 2008, RevMexAA, Conf. Ser., 32, 115
Binette, L., & Krongold, Y. 2008a, A&A, 478, 739
Binette, L., & Krongold, Y. 2008b, A&A, 477, 413
Binette, L., Magris, C. G., Krongold, Y., Morisset, C., Haro-Corzo, S., de Diego, J. A., Mutschke, H., & Andersen, A. C. 2005, ApJ, 631, 661
Cardelli, J. A., Clayton, G. C., & Mathis, J. S. 1989, ApJ, 345, 245
Crenshaw, D. M., Kraemer, S. B., & George, I. M. 2003, ARA&A, 41, 117
Eastman, R. G., MacAlpine, G. M., & Richstone, D. O. 1983, ApJ, 275, 53
Elvis, M. 2000, ApJ, 545, 63
Everett, J. E. 2005, ApJ, 631, 689
Gabel, J. R., et al. 2005, ApJ, 623, 85
Ganguly, R., & Brotherton, M. S. 2008, ApJ, 672, 102
Gibson, R. R., Brandt, W. N., Schneider, D. P., & Gallagher, S. C. 2008, ApJ, 675, 985
Hamann, F., Kaplan, K. F., Rodríguez Hidalgo, P., Prochaska, J. X., & Herbert-Fort, S. 2008, MNRAS, 391, L39
Hamann, F., & Sabra, B. 2004, in ASP Conf. Ser. 311, AGN Physics with the Sloan Digital Sky Survey, ed. G. T. Richards & P. B. Hall (San Francisco, CA: ASP), 203
Haro-Corzo, S. A. R., Binette, L., Krongold, Y., Benitez, E., Humphrey, A., Nicastro, F., & Rodríguez-Martínez, M. 2007, ApJ, 662, 145
Hopkins, P. F., Hernquist, L., Cox, T. J., Di Matteo, T., Martini, P., Robertson, B., & Springel, V. 2005, ApJ, 630, 705
Kaspi, S., Brandt, W. N., Maoz, D., Netzer, H., Schneider, D. P., & Shemmer, O. 2007, ApJ, 659, 997
King, A. R. 2010, MNRAS, 402, 1516
Krongold, Y., Nicastro, F., Brickhouse, N. S., Elvis, M., & Mathur, S. 2005, ApJ, 622, 842
Krongold, Y., Nicastro, F., Elvis, M., Brickhouse, N., Binette, L., Mathur, S., & Jiménez-Bailón, E. 2007, ApJ, 659, 1022
Leighly, K. M., Hamann, F., Casebeer, D. A., & Grupe, D. 2009, ApJ, 701, 176
Lundgren, B. F., Wilhite, B. C., Brunner, R. J., Hall, P. B., Schneider, D. P., York, D. G., Vanden Berk, D. E., & Brinkmann, J. 2007, ApJ, 656, 73
Nicastro, F., Fiore, F., & Matt, G. 1999, ApJ, 517, 108
Ostriker, J. P., Choi, E., Ciotti, L., Novak, G. S., & Proga, D. 2010, ApJ, 722, 642
Proga, D. 2007, ApJ, 661, 693
Sargent, W. L. W., Boksenberg, A., & Steidel, C. C. 1988, ApJS, 68, 539
Savage, B. D., & Sembach, K. R. 1991, ApJ, 379, 245
Scannapieco, E., & Oh, S. P. 2004, ApJ, 608, 62
Schlegel, D. J., Finkbeiner, D. P., & Davis, M. 1998, ApJ, 500, 525
Shull, J. M., & van Steenberg, M. 1982, ApJS, 48, 95
Telfer, R. C., Zheng, W., Kriss, G. A., & Davidsen, A. F. 2002, ApJ, 565, 773
Weymann, R. J., Morris, S. L., Foltz, C. B., & Hewett, P. C. 1991, ApJ, 373, 23
Young, P., Sargent, W. L. W., & Boksenberg, A. 1982, ApJS, 48, 455

Capítulo 6

Conclusiones Generales

Durante el trabajo realizado en esta tesis doctoral hemos estudiado y analizado como se relaciona la actividad nuclear AGN con el medio ambiente circumgaláctico de la galaxia anfitriona. Uno de los resultados más importantes es que la actividad nuclear o AGN esta presente con la misma incidencia entre galaxias aisladas y galaxias pares para muestras comparables en número total y por tipo morfológico. De lo cual se desprende que la evolución secular en galaxias puede detonar un AGN sin necesidad de una colisión o fusión de galaxias en por lo menos los últimos 3 Gaños. Las características que sobresalen en nuestras galaxias con actividad nuclear de baja luminosidad son tasas de acreción bajas y ausencia o inexistencia de líneas anchas.

La relación entre AGN y el tipo morfológico es una realidad que ya se conoce y que nosotros en este trabajo confirmamos para galaxias aisladas y pares. El hecho de que la actividad AGN sea mucho más incidente entre las galaxias con bulbo y espirales tempranas nos muestra que los posibles mecanismos para llevar material al hoyo negro pueden ser más eficientes a medida que las galaxias posean bulbos más grandes. Esta relación puede verse afectada cuando se incluyen las galaxias con no emisiones entre las tempranas. La incidencia se aplana cuando consideramos la muestra completa entre galaxias elípticas y esferoidales. Esto puede deberse al hecho de que en estos sistemas en particular se clasifican como de tipo LINER y están en el extremo de baja luminosidad de los AGN. Si la galaxia es de tipo temprano se le atribuye poco gas y estrellas evolucionadas, algunos autores han propuesto que la emisión de sus líneas no es debido a la acreción del hoyo negro sino a grandes cantidades de estrellas post-AGB junto con enanas blancas las que pueden ionizar el medio y provocar lo que denominan como "falsos" AGN.

La ausencia de la actividad nuclear de tipo 1 en nuestras muestras no parece estar rela-

cionada con la explicación de un modelo unificado de galaxias únicamente. Más bien parece que se debe tomar en cuenta los factores de llenado, tasas de acreción y la historia de fusión que haya tenido una galaxia para completar un esquema más general. Todo esto con la finalidad de explicar a fondo el fenómeno de la actividad nuclear o AGN.

A lo largo de este trabajo hemos sido testigos de que simulaciones númericas entre fusiones de galaxias con diferentes razones de masa pueden cerrar la brecha en cuanto a la explicación de la evolución galáctica. La relación encontrada entre la separación de galaxias y los núcleos activos de galaxias que han presentado algunos autores puede verse como episodios de colisiones directas entre galaxias que detonan un Starburst o AGN.

Considerando todos los ingredientes que forman parte de la actividad AGN. La historia de evolución galáctica estaría realmente asociada a los eventos de fusiones entre ellas. Las galaxias con una historia rica en fusiones tienden a ser más grandes, más energéticas, con una incidencia alta de AGN. Por otro lado, las galaxias con un historial pobre de fusiones tienden a ser de tipo espiral, menos masivas, menos energéticas, con menor incidencia de AGN y con colores más azules dado la gran cantidad de gas para formar población estelar joven y seguir produciendo estrellas.

Bibliografía

[1] Abazajian, K. N., Adelman-McCarthy, J. K., Agüeros, M. A., et al. 2009, ApJS, 182, 543

[2] Alexander, T. 1997, MNRAS, 285, 891

[3] Alexander, T. & Netzer, H. 1997, MNRAS, 284, 967

[4] Alonso-Herrero, A., Quillen, A. C., Rieke, G. H., Ivanov, V. D., & Efstathiou, A. 2003, Astronomical Journal, 126, 81

[5] Andrade-Velázquez, M., Krongold, Y., Elvis, M., Nicastro, F., Brickhouse, N., Binette, L., Mathur, S., & Jiménez-Bailón, E. 2010, ApJ, 711, 888

[6] Antonucci, R. 1993, Ann. Rev. Ast. & Ast., 31, 473

[7] Antonucci, R. R. J., & Miller, J. S. 1985, ApJ, 297, 621

[8] Arav, N., et al. 2001, ApJ, 561, 118

[9] Bahcall, J. N., Kirhakos, S., Saxe, D. H., & Schneider, D. P. 1997, ApJ, 479, 642

[10] Baldwin, J. A., Phillips, M. M., & Terlevich, R. 1981, Publications of the ASP, 93, 5

[11] Barlow, T. A. 1994, Publications of the ASP, 106, 548

[12] Barnes, J. E. & Hernquist, L. 1992, Ann. Rev. Ast. & Ast., 30, 705

[13] Barth, A. J., Filippenko, A. V., & Moran, E. C. 1999a, ApJ, 525, 673

[14] Barth, A. J., Filippenko, A. V., & Moran, E. C. 1999b, ApJL, 515, L61

[15] Barton, E. J., Geller, M. J., & Kenyon, S. J. 2000, ApJ, 530, 660

[16] Bertola, F., Buson, L. M., & Zeilinger, W. W. 1992, ApJL, 401, L79

[17] Binette, L., Magris, C. G., Stasińska, G., & Bruzual, A. G. 1994, Astronomy and Astrophysics, 292, 13

[18] Binette, L., Magris C., G., Krongold, Y., Morisset, C., Haro-Corzo, S., de Diego, J. A., Mutschke, H., & Andersen, A. C. 2005, ApJ, 631, 661

[19] Binette, L., & Krongold, Y. 2008a, Astronomy and Astrophysics, 478, 739

[20] Binette, L., & Krongold, Y. 2008b, Astronomy and Astrophysics, 477, 413

[21] Binette, L., Haro-Corzo, S., Krongold, Y., & Andersen, A. C. 2008c, Revista Mexicana de Astronomia y Astrofisica Conference Series, 32, 115

[22] Binette, L., Drissen, L., Ubeda, L., et al. 2009, Astronomy and Astrophysics, 500, 817

[23] 1987, Nature, 326, 219

[24] Caon, N., Macchetto, D., & Pastoriza, M. 2000, ApJS, 127, 39

[25] Cardelli, J. A., Clayton, G. C., & Mathis, J. S. 1989, ApJ, 345, 245

[26] Carroll, B. W., & Ostlie, D. A. 1996, Institute for Mathematics and Its Applications,

[27] Cid Fernandes, R., Stasińska, G., Mateus, A., & Vale Asari, N. 2011, MNRAS, 413, 1687

[28] Crenshaw, D. M., Kraemer, S. B., & George, I. M. 2003, Ann. Rev. Ast. & Ast., 41, 117

[29] Dahari, O. 1985, ApJS, 57, 643

[30] Dahari, O. A. 1984, PhD thesis, California Univ., Santa Cruz.

[31] Disney, M. J., Boyce, P. J., Blades, J. C., et al. 1995, Nature, 376, 150

[32] de Mello, D. F., Keel, W. C., Sulentic, J. W., & Rampazzo, R. 1995, in IAU Symposium, Vol. 164, Stellar Populations, ed. P. C. van der Kruit & G. Gilmore, 434

[33] de Mello, D. F., Sulentic, J. W., de Souza, R. E., Reduzzi, L., & Rampazzo, R. 1996, Astronomy and Astrophysics, 308, 387

[34] Domingue, D. L., Sulentic, J. W., & Durbala, A. 2005, Astronomical Journal, 129, 2579

[35] Dultzin-Hacyan, D., & Ruano, C. 1996, Astronomy and Astrophysics, 305, 719

[36] Dultzin-Hacyan, D. 1997, Revista Mexicana de Astronomia y Astrofisica Conference Series, 6, 132

[37] Dultzin-Hacyan, D., Krongold, Y., Fuentes-Guridi, I., & Marziani, P. 1999, ApJL, 513, L111

[38] Dultzin, D., Gonzalez, J. J., Krongold, Y., et al. 2008, ArXiv e-prints

[39] Eastman, R. G., MacAlpine, G. M., & Richstone, D. O. 1983, ApJ, 275, 53

[40] Elitzur, M. & Ho, L. C. 2009, ApJL, 701, L91

[41] Ellison, S. L., Patton, D. R., Simard, L., et al. 2010, MNRAS, 407, 1514

[42] Ellison, S. L., Patton, D. R., Mendel, J. T., & Scudder, J. M. 2011, MNRAS, 418, 2043

[43] Elvis, M., Maccacaro, T., Wilson, A. S., et al. 1978, MNRAS, 183, 129

[44] Elvis, M. 2000, ApJ, 545, 63

[45] Everett, J. E. 2005, ApJ, 631, 689

[46] Fabian, A. C. 2005, Astrophysics and Space Science, 300, 97

[47] Ferrarese, L., & Ford, H. C. 1999, ApJ, 515, 583

[48] Filippenko, A. V., & Terlevich, R. 1992, ApJL, 397, L79

[49] Fosbury, R. A. E., Mebold, U., Goss, W. M., & Dopita, M. A. 1978, MNRAS, 183, 549

[50] Franco-Balderas, A., Hernández-Toledo, H. M., & Dultzin-Hacyan, D. 2004, Astronomy and Astrophysics, 417, 411

[51] Gabel, J. R., et al. 2005, ApJ, 623, 85

[52] Ganguly, R., & Brotherton, M. S. 2008, ApJ, 672, 102

[53] Gebhardt, K., Kormendy, J., Ho, L. C., et al. 2000, ApJL, 543, L5

[54] Gibson, R. R., Brandt, W. N., Schneider, D. P., & Gallagher, S. C. 2008, ApJ, 675, 985

[55] González-Martín, O., Masegosa, J., Márquez, I., & Jiménez-Bailón, E. 2007, in IAU Symposium, Vol. 238, IAU Symposium, ed. V. Karas & G. Matt, 373–374

[56] Gu, Q., Dultzin-Hacyan, D., & de Diego, J. A. 2001, Revista Mexicana de Astronomía y Astrofísica, 37, 3

[57] Gu, Q., Maiolino, R., & Dultzin-Hacyan, D. 2001, Astronomy and Astrophysics, 366, 765

[58] Halpern, J. P., & Filippenko, A. V. 1986, Astronomical Journal, 91, 1019

[59] Hamann, F., & Sabra, B. 2004, AGN Physics with the Sloan Digital Sky Survey, 311, 203

[60] Hamann, F., Kaplan, K. F., Rodríguez Hidalgo, P., Prochaska, J. X., & Herbert-Fort, S. 2008, MNRAS, 391, L39

[61] Harms R. J., et al., 1994, ApJ, 435, L35

[62] Haro-Corzo, S. A. R., Binette, L., Krongold, Y., Benitez, E., Humphrey, A., Nicastro, F., & Rodríguez-Martínez, M. 2007, ApJ, 662, 145

[63] Heckman, T. M. 1980, Highlights of Astronomy, 5, 185

[64] Hernández-Ibarra, F. J., Dultzin, D., Krongold, Y., Del Olmo, A., & Perea, J. 2011, Revista Mexicana de Astronomia y Astrofisica Conference Series, 40, 58

[65] Hernandez-Ibarra, F., Dultzin, D., Krongold, Y., et al. 2012, arXiv:1206.6777

[66] Hernandez, X. & Lee, W. H. 2010, MNRAS, 404, L6

[67] Hernández Toledo, H. M., Dultzin-Hacyan, D., Gonzalez, J. J., & Sulentic, J. W. 1999, Astronomical Journal, 118, 108

[68] Hernández Toledo, H. M. 2000, Mapping the Hidden Universe: The Universe behind the Mily Way - The Universe in HI, 218, 387

[69] Hernández-Toledo, H. M., Vázquez-Mata, J. A., Martínez-Vázquez, L. A., Choi, Y.-Y., & Park, C. 2010, Astronomical Journal, 139, 2525

[70] Ho, L. C., Filippenko, A. V., & Sargent, W. L. W. 1997a, ApJS, 112, 315

[71] Ho, L. C., Filippenko, A. V., & Sargent, W. L. W. 1997b, ApJ, 487, 568

[72] Ho, L. C., Filippenko, A. V., & Sargent, W. L. W. 1997c, ApJ, 487, 591

[73] Ho, L. C., Filippenko, A. V., Sargent, W. L. W., & Peng, C. Y. 1997d, ApJS, 112, 391

[74] Ho, L. C. 2002, in Astronomical Society of the Pacific Conference Series, Vol. 284, IAU Colloq. 184: AGN Surveys, ed. R. F. Green, E. Y. Khachikian, & D. B. Sanders, 13

[75] Ho, L. C. 2003, in Astronomical Society of the Pacific Conference Series, Vol. 290, Active Galactic Nuclei: From Central Engine to Host Galaxy, ed. S. Collin, F. Combes, & I. Shlosman, 379

[76] Hopkins, P. F., Hernquist, L., Cox, T. J., Di Matteo, T., Martini, P., Robertson, B., & Springel, V. 2005, ApJ, 630, 705

[77] Hutchings, J. B. 1987, ApJ, 320, 122

[78] Karachentsev, I. D. 1972, Soobshcheniya Spetsialñoj Astrofizicheskoj Observatorii, 7, 1

[79] Karachentsev, I. D., Makarov, D. I., Karachentseva, V. E., & Melnyk, O. V. 2011, Astrophysical Bulletin, 66, 1

[80] Karachentseva, V. E. 1973, Soobshcheniya Spetsialñoj Astrofizicheskoj Observatorii, 8, 3

[81] Karachentseva, V. E., Mitronova, S. N., Melnyk, O. V., & Karachentsev, I. D. 2010, in Astronomical Society of the Pacific Conference Series, Vol. 421, Galaxies in Isolation: Exploring Nature Versus Nurture, ed. L. Verdes-Montenegro, A. Del Olmo, & J. Sulentic, 11

[82] Kaspi, S., Brandt, W. N., Maoz, D., Netzer, H., Schneider, D. P., & Shemmer, O. 2007, ApJ, 659, 997

[83] Kauffmann, G., Heckman, T. M., Tremonti, C., et al. 2003, MNRAS, 346, 1055

[84] Keel, W. C. 1983, ApJ, 269, 466

[85] Keel, W. C. 1993, Astronomical Journal, 106, 1771

[86] Kennicutt, Jr., R. C. & Keel, W. C. 1984, ApJL, 279, L5

[87] Kennicutt, Jr., R. C., Roettiger, K. A., Keel, W. C., van der Hulst, J. M., & Hummel, E. 1987, Astronomical Journal, 93, 1011

[88] Kewley, L. J., Dopita, M. A., Sutherland, R. S., Heisler, C. A., & Trevena, J. 2001, ApJ, 556, 121

[89] Kewley, L. J., Groves, B., Kauffmann, G., & Heckman, T. 2006, MNRAS, 372, 961

[90] King, A. R. 2010, MNRAS, 402, 1516

[91] Kirhakos, S., Bahcall, J. N., Schneider, D. P., & Kristian, J. 1999, ApJ, 520, 67

[92] Kormendy J., Richstone D., 1995, ARA&A, 33, 581

[93] Koulouridis, E., Chavushyan, V., Plionis, M., Krongold, Y., & Dultzin-Hacyan, D. 2006, ApJ, 651, 93

[94] Koulouridis, E., Plionis, M., Chavushyan, V., et al. 2006, ApJ, 639, 37

[95] Krongold, Y., Dultzin-Hacyan, D., & Marziani, P. 2001, Astronomical Journal, 121, 702

[96] Krongold, Y., Dultzin-Hacyan, D., & Marziani, P. 2002, ApJ, 572, 169

[97] Krongold, Y., Dultzin-Hacyan, D., & Marziani, P. 2003, in Astronomical Society of the Pacific Conference Series, Vol. 290, Active Galactic Nuclei: From Central Engine to Host Galaxy, ed. S. Collin, F. Combes, & I. Shlosman, 523

[98] Krongold, Y., Nicastro, F., Brickhouse, N. S., Elvis, M., & Mathur, S. 2005, ApJ, 622, 842

[99] Krongold, Y., Nicastro, F., Elvis, M., et al. 2007, ApJ, 659, 1022

[100] Laurikainen, E. & Salo, H. 1995, Astronomy and Astrophysics, 293, 683

[101] Lee, G.-H., Woo, J.-H., Lee, M. G., et al. 2012, ApJ, 750, 141

[102] Leighly, K. M., Hamann, F., Casebeer, D. A., & Grupe, D. 2009, ApJ, 701, 176

[103] Lin, L., Koo, D. C., Weiner, B. J., et al. 2007, ApJL, 660, L51

[104] Lonsdale, C. J., Persson, S. E., & Matthews, K. 1984, ApJ, 287, 95

[105] Lundgren, B. F., Wilhite, B. C., Brunner, R. J., Hall, P. B., Schneider, D. P., York, D. G., Vanden Berk, D. E., & Brinkmann, J. 2007, ApJ, 656, 73

[106] Márquez, I. & Masegosa, J. 2008, in Revista Mexicana de Astronomia y Astrofisica, vol. 27, Vol. 32, Revista Mexicana de Astronomia y Astrofisica Conference Series, 150–154

[107] Martínez, M. A., Del Olmo, A., Coziol, R., & Perea, J. 2010, Astronomical Journal, 139, 1199

[108] Miller, C. J., Nichol, R. C., Gómez, P. L., Hopkins, A. M., & Bernardi, M. 2003, ApJ, 597, 142

[109] Moles, M., Marquez, I., & Perez, E. 1995, ApJ, 438, 604

[110] Narayan, R. & McClintock, J. E. 2008, New Astronomy Reviews, 51, 733

[111] Netzer, H. 2006, in Lecture Notes in Physics, Berlin Springer Verlag, Vol. 693, Physics of Active Galactic Nuclei at all Scales, ed. D. Alloin, 1

[112] Nicastro, F., Fiore, F., & Matt, G. 1999, ApJ, 517, 108

[113] Nicastro, F. 2000, ApJL, 530, L65

[114] Osterbrock, D. E. 1978, Bulletin of the AAS, 10, 387

[115] Osterbrock, D. E. 1984, Quarterly Journal of the RAS, 25, 1

[116] Ostriker, J. P., Choi, E., Ciotti, L., Novak, G. S., & Proga, D. 2010, arXiv:1004.2923

[117] Pérez-González, P. G., Alonso-Herrero, A., Donley, J., et al. 2010, in Highlights of Spanish Astrophysics V, ed. J. M. Diego, L. J. Goicoechea, J. I. González-Serrano, & J. Gorgas, 337

[118] Proga, D. 2007, ApJ, 661, 693

[119] Rogers, B., Ferreras, I., Kaviraj, S., Pasquali, A., & Sarzi, M. 2009, MNRAS, 399, 2172

[120] Sabater, J., Verdes-Montenegro, L., Leon, S., Best, P., & Sulentic, J. 2012, Astronomy and Astrophysics, 545, A15

[121] Sargent, W. L. W., Boksenberg, A., & Steidel, C. C. 1988, ApJS, 68, 539

[122] Sarzi, M., Falcón-Barroso, J., Davies, R. L., et al. 2006, MNRAS, 366, 1151

[123] Savage, B. D., & Sembach, K. R. 1991, ApJ, 379, 245

[124] Scannapieco, E., & Oh, S. P. 2004, ApJ, 608, 62

[125] Schlegel, D. J., Finkbeiner, D. P., & Davis, M. 1998, ApJ, 500, 525

[126] Schmitt, H. R. 2001, Astronomical Journal, 122, 2243

[127] Shakura, N. I. & Sunyaev, R. A. 1973, Astronomy and Astrophysics, 24, 337

[128] Shapovalova, A. I., Popović, L. Č., Burenkov, A. N., et al. 2012, ApJS, 202, 10

[129] Shapovalova, A. I., Popović, L. Č., Collin, S., et al. 2008, Astronomy and Astrophysics, 486, 99

[130] Sorrentino, G., Radovich, M., & Rifatto, A. 2006, Astronomy and Astrophysics, 451, 809

[131] Stasińska, G., Cid Fernandes, R., Mateus, A., Sodré, L., & Asari, N. V. 2006, MNRAS, 371, 972

[132] Stauffer, J. R. 1982, ApJ, 262, 66

[133] Stauffer, J. R. 1982, ApJS, 50, 517

[134] Storchi-Bergmann, T. 2008, in Revista Mexicana de Astronomia y Astrofisica, vol. 27, Vol. 32, Revista Mexicana de Astronomia y Astrofisica Conference Series, 139–146

[135] Sulentic, J. W., Verdes-Montenegro, L., Bergond, G., et al. 2006, Astronomy and Astrophysics, 449, 937

[136] Shull, J. M. & van Steenberg, M. 1982, ApJS, 48, 95

[137] Telfer, R. C., Zheng, W., Kriss, G. A., & Davidsen, A. F. 2002, ApJ, 565, 773

[138] Tran, H. D. 2003a, ApJ, 583, 632

[139] Tran, H. D. 2003b, in Astronomical Society of the Pacific Conference Series, Vol. 290, Active Galactic Nuclei: From Central Engine to Host Galaxy, ed. S. Collin, F. Combes, & I. Shlosman, 31

[140] Trouille, L., Barger, A. J., & Tremonti, C. 2011, ApJ, 742, 46

[141] van der Marel, R. P., & van den Bosch, F. C. 1998, Astronomical Journal, 116, 2220

[142] Varela, J., Moles, M., Márquez, I., et al. 2004, Astronomy and Astrophysics, 420, 873

[143] Veilleux, S., Bland-Hawthorn, J., & Cecil, G. 1999, Astronomical Journal, 118, 2108

[144] Veilleux, S. & Osterbrock, D. E. 1987, ApJS, 63, 295

[145] Verdes-Montenegro, L., Sulentic, J., Lisenfeld, U., et al. 2005, Astronomy and Astrophysics, 436, 443

[146] Verley, S., Leon, S., Verdes-Montenegro, L., et al. 2007, Astronomy and Astrophysics, 472, 121

[147] Weymann, R. J., Morris, S. L., Foltz, C. B., & Hewett, P. C. 1991, ApJ, 373, 23

[148] Winkler, H. 1992, MNRAS, 257, 677

[149] Woods, D. F. & Geller, M. J. 2007, Astronomical Journal, 134, 527

[150] Yates, M. G., & Longair, M. S. 1989, MNRAS, 241, 29

[151] Young, P., Sargent, W. L. W., & Boksenberg, A. 1982, ApJS, 48, 455